Dup

Interaction Notes

Note 152

November 1973

Parametric Study of an L-Shaped Wire Using the Singularity Expansion Method

D.R. Wilton and K.R. Umashankar

University of Mississippi

University, Mississippi

Abstract

A Hallén-type integral equation is developed for an L-shaped wire and the singularity expansion method is used to numerically calculate the natural frequencies, modal current and charge distributions, and coupling coefficients for plane wave excitation.

Transient and sinusoidal steady state responses are constructed from the singularity expansion of the current and the time-domain convergence of the solution is illustrated.

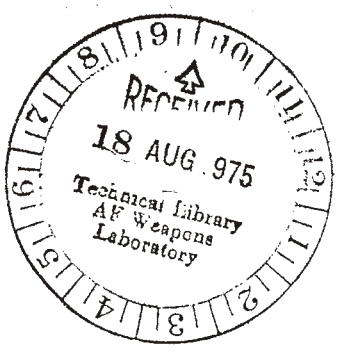

I. INTRODUCTION

The singularity expansion method (SEM) was introduced by Baum [1] as a tool for treating electromagnetic transient scattering problems. One of the primary advantages of the method is that it permits a systematic description of the transient response of an object in terms of a relatively small number of parameters, viz., a set of natural resonant frequencies, a corresponding set of modal currents which are the source free currents that can exist on the object at the resonant frequencies, and a set of coupling coefficients which describe how the object "couples" to the spatial and temporal distribution of the incident field. In principle, this information enables one to construct the transient response of a finite object due to an illumination which is arbitrary in both space and time. The frequency domain response of the object due to a time-harmonic illumination may also be readily constructed simply as a special case.

In addition to the original description of the method of Baum [1], Marin and Latham [2] have considered some of the theoretical aspects of the SEM using an H-field integral equation formulation for scattering by a perfectly conducting object. Tesche applied the method to the calculation of the transient response of a dipole scatterer [3]. His work included calculation of the natural resonant frequencies, modal currents and time domain current and charge distributions due to a step function plane wave illumination. Martinez et.al. treated a conduct-

ing sphere excited by a step function plane wave [4]. Because most of the manipulations could be done analytically for the sphere, thus eliminating errors due to numerical approximations, the sphere problem provided a good test of the representation compared with conventional techniques. Lee and Leung also considered a dipole scatterer and calculated approximate pole locations from a Weiner-Hopf formulation [5]. Marin later considered some aspects of applying SEM to scattering by imperfectly conducting objects and perfectly conducting bodies in a parallel plate region [6]. A parametric study of prolate spheroids was also undertaken by Marin [7]. Wilton and Umashankar have calculated natural resonant frequencies for prolate spheroids, a dipole above a conducting ground, and a wire loop [8].

In this note, we consider the scattering of an L-shaped wire using the SEM. The numerical problem is formulated by applying the method of moments [9] and SEM (Sections III and IV) to the set of coupled Hallén-type integral equations derived in Section II. In Section V is presented the results of a parametric study to determine the influence of the location of the bend and the two wire radii on the scattering characteristics of the object. The complex natural resonant frequencies, modal current and charge distributions, and relevant coupling coefficients are given for each case considered. Sample calculations are carried out for the step function response of an L-wire and the results are compared with those obtained by the

conventional inverse Fourier transform of frequency domain data. The appendices describe some of the numerical procedures employed which are pertinent to the SEM calculations and give a derivation of the reduction of a double integral appearing in the Hallen formulation to a single integral.

II. FORMULATION OF THE COUPLED INTEGRAL EQUATIONS FOR THE L-WIRE STRUCTURE

In this section, Hallen-type integral equations for the induced current on a perfectly conducting L-wire structure, Fig. 1, are developed for illumination by an arbitrary incident electromagnetic field in a linear, homogeneous, isotropic medium. The L-wire structure is in the xz-plane with lengths, r,h and radii a_1, a_2 corresponding to x and z directed elements. The currents i_x and i_z reside on the surfaces of the perfectly conducting wire elements and hence give rise to only x and z components of the magnetic vector potential $\overline{A} = A_x\hat{x} + A_z\hat{z}$. The wire element radii are assumed small compared to the wavelength and the current density is assumed to be uniform around the periphery of the elements.

In the formulation of the Hallen-type coupled integral equations, two expressions are independently established for a given component of the magnetic vector potential. These expressions are obtained as follows:

(a) One expression arises from the solution of an inhomogeneous differential equation.

(b) The second is obtained from the solution vector for the potential in terms of the induced current. These two expressions are equated and the condition that the tangential component of the electric field on the conducting surface is zero is then enforced. The constants of integration should be in compliance with the following

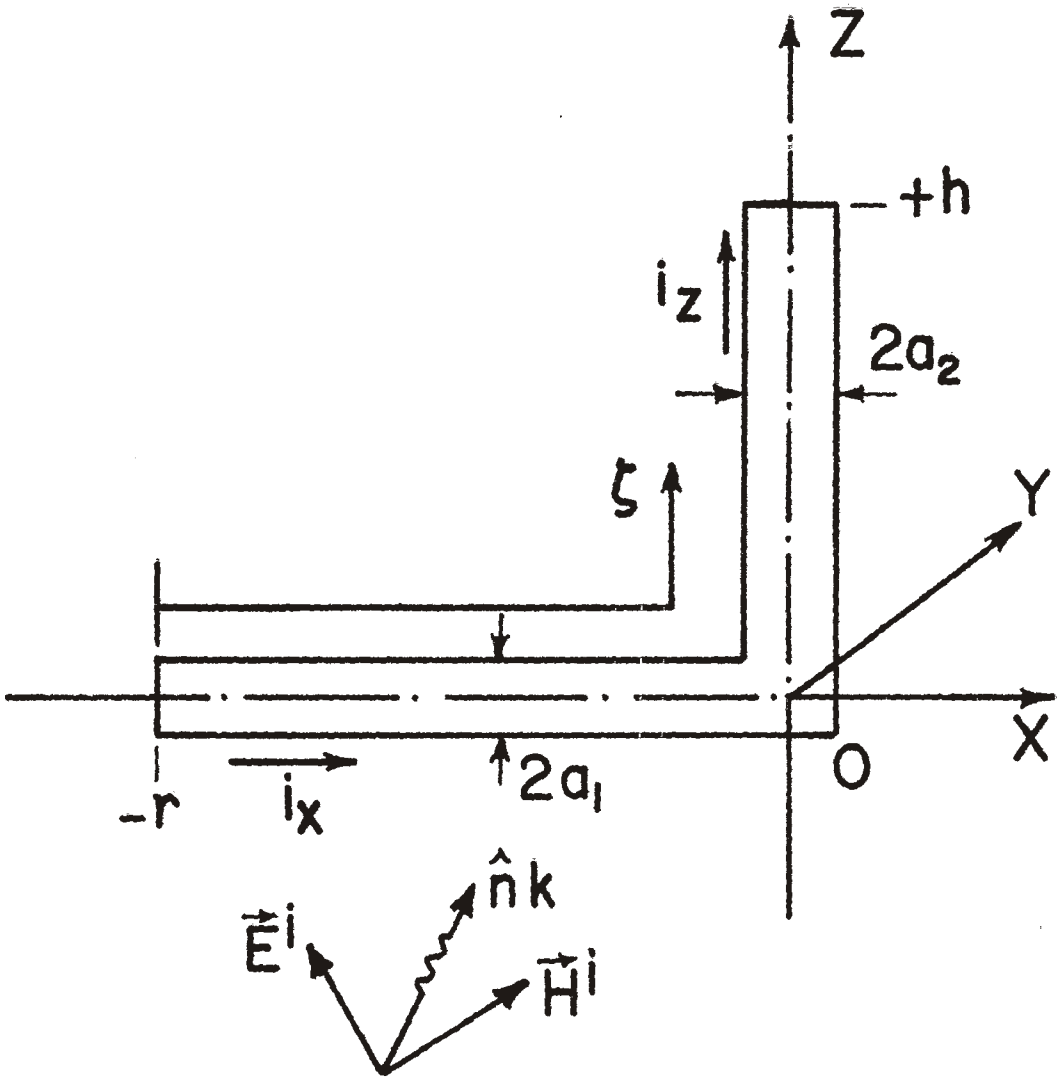

Figure 1. Geometry of the L-wire structure.

conditions:

1. the scalar potential is continuous at the wire junction
2. $i_x = i_z$ at the wire junction
3. $i_x(-r) = 0$ and $i_z(h) = 0$, the currents must be zero at the free ends.

The z and x components of the magnetic vector potential satisfy the partial differential equations

$$\frac{\partial^2 A_z}{\partial z^2} + k^2 A_z = j\frac{k^2}{\omega} E_z - \frac{\partial}{\partial z}\left(\frac{\partial A_x}{\partial x}\right) \tag{2.1}$$

$$\frac{\partial^2 A_x}{\partial x^2} + k^2 A_x = j\frac{k^2}{\omega} E_x - \frac{\partial}{\partial x}\left(\frac{\partial A_z}{\partial z}\right) \tag{2.2}$$

where E_z and E_x are the z and x components of the electric field resulting from currents induced on the scatterer, ω is the angular frequency and k is the free space wave number $2\pi/\lambda$. The complete solution [10] to the above differential equation valid along the surface of the wire may be written as

$$A_z(0,a_2,z) = C_z \cos kz + B_z' \sin kz + v_z(0,a_2,z)$$

$$- \frac{1}{k}\int_{\zeta=0}^{z} \frac{\partial}{\partial \zeta}\left\{\frac{\partial A_x}{\partial x}(0,a_2,\zeta)\right\} \sin k(z-\zeta)\,d\zeta, \quad z\varepsilon(0,+h) \tag{2.3}$$

and

$$A_x(x,a_1,0) = C_x \cos kz + B_x' \sin kx + v_x(x,a_1,0)$$

$$- \frac{1}{k} \int_{\xi=0}^{x} \frac{\partial}{\partial \xi} \left(\frac{\partial A_z(\xi,a_1,0)}{\partial z} \right) \sin k(x-\xi) d\xi, \quad x \varepsilon (-r,0) \qquad (2.4)$$

where C_z, B_z' and C_x, B_x' are arbitrary constants and the forcing functions are

$$v_z(z) = j\frac{k}{\omega} \int_{\zeta=0}^{z} E_z(0,a_2,\zeta) \sin k(z-\zeta) d\zeta \qquad (2.5)$$

and $$v_x(x) = j\frac{k}{\omega} \int_{\xi=0}^{x} E_x(\xi,a_1,0) \sin k(x-\xi) d\xi \qquad (2.6)$$

Integrating once the last term in (2.3) and (2.4) yields the following expressions for the vector potentials along the wire surfaces:

$$A_z(0,a_2,z) = C_z \cos kz + B_z \sin kz + v_z(z)$$

$$- \int_{\zeta=0}^{z} \frac{\partial A_x(0,a_2,\zeta)}{\partial x} \cos k(z-\zeta) d\zeta, \quad z \varepsilon (0,+h) \qquad (2.7)$$

$$A_x(x,a_1,0) = C_x \cos kx + B_x \sin kx + v_x(x)$$

$$- \int_{\xi=0}^{x} \frac{\partial A_z(\xi,a_1,0)}{\partial z} \cos k(x-\xi)d\xi, \quad x\varepsilon(-r,0) \qquad (2.8)$$

where B_z and B_x are constants which simply absorb B_x' and B_z' and terms arising from the integration by parts.

Differentiating (2.7) with respect to z and rearranging terms, in view of the Lorentz gauge, we obtain the scalar potential,

$$-j\frac{k^2}{\omega}\phi(0,a_2,z) = -kC_z \sin kz + kB_z \cos kz + \frac{\partial v_z(z)}{\partial z}$$

$$+ k\int_{\zeta=0}^{z} \frac{\partial A_x}{\partial x}(\zeta) \sin k(z-\zeta)d\zeta, \quad z\varepsilon(0,+h) \qquad (2.9)$$

At z = 0, i.e. at the wire junction,

$$B_z = -j\frac{k}{\omega}\phi(0,a_2,0); \quad \text{similarly} \quad B_x = -j\frac{k}{\omega}\phi(0,a_1,0)$$

Requiring the continuity of scalar potential, we have

$$B_z = B_x = B \qquad (2.10)$$

The magnetic vector potentials A_z and A_x can also be written in terms of potential integrals involving line current distributions $i_z(z)$ and $i_x(x)$. Using the usual reduced kernel approximations [11], we have

$$A_z(0,a_2,z) = \frac{\mu}{4\pi} \int_{z'=0}^{h} i_z(z')\ K(0,x',a_2,z,z')dz' \qquad (2.11)$$

$$A_x(x,a_1,0) = \frac{\mu}{4\pi} \int_{x'=-r}^{0} i_x(x')\ K(x,x',a_1,0,z')dz' \qquad (2.12)$$

and from (2.7), (2.8), (2.11) and (2.12) the coupled integral equations of the Hallen'-type are obtained:

$$\int_{x'=-r}^{0} i_x(x')\ K_x(x,x',a_1)dx' + \int_{z'=0}^{h} i_z(z') \left\{ \int_{\xi=0}^{x} \left[\frac{\partial}{\partial z} K_z'(\xi,a_1,0,z')\right] \cos k(x-\xi)d\xi \right\} dz'$$

$$= c_x \cos kx + b \sin kx - j\frac{4\pi}{\eta} \int_{\xi=0}^{x} E_x(\xi) \sin k(x-\xi)d\xi, \quad x\varepsilon(-r,0) \qquad (2.13)$$

$$\int_{x'=-r}^{0} i_x(x') \left\{ \int_{\zeta=0}^{z} \left[\frac{\partial}{\partial x} K'_x(0,x',a_2,\zeta) \right] \cos k(z-\zeta) d\zeta \right\} dx'$$

$$+ \int_{z'=0}^{h} i_z(z')\, K_z(a_2,z,z') dz' = c_z \cos kz + b \sin kz$$

$$-j\frac{4\pi}{\eta} \int_{\zeta=0}^{z} E_z^i(\zeta) \sin k(z-\zeta) d\zeta, \quad z\varepsilon(0,+h) \tag{2.14}$$

where $\eta = 120$, $c_z = \frac{4\pi}{\mu} C_z$, $c_x = \frac{4\pi}{\mu} C_x$, $b = \frac{4\pi}{\mu} B$ and μ is the permeability of the medium and the various kernels in the integrals are given by

$$K_x(x,x',a_1) = \frac{e^{-jkR_x}}{R_x}, \quad R_x^2 = a_1^2 + (x-x')^2$$

$$K'_z(\xi,a_1,0,z') = \frac{e^{-jkr_z}}{r_z}, \quad r_z^2 = a_1^2 + \xi^2 + z'^2$$

$$K_z(a_2,z,z') = \frac{e^{-jkR_z}}{R_z}, \quad R_z = a_2^2 + (z-z')^2$$

$$K'_x(0,x',a_2,\zeta) = \frac{e^{-jkr_x}}{r_x}, \quad r_x^2 = a_2^2 + x'^2 + \zeta^2$$

and

$$E_x(x) = -E_x^i(x)$$

$$E_z(z) = -E_z^i(z) \tag{2.15}$$

The latter two substitutions arise from the boundary condition that

the field produced by currents flowing on the surface of the L-wire must cancel the incident field $\overline{E}^i$.

In the integral equations (2.13) and (2.14), the internal integrals of the double integral terms can be analytically evaluated (see Appendix A) and the resulting expressions are used in the further development of the matrix equation from the integral equations.

In the coupled integral equations (2.13) and (2.14), k is the wave number of the medium and in the steady state analysis it is real and given by $2\pi/\lambda$ or $\omega\sqrt{\mu\varepsilon}$. We can conveniently write the derived integral equations in terms of the Laplace variable $s=\sigma+j\omega$, which is more suitable for the SEM, by substituting

$$k = -j\frac{s}{c} \tag{2.16}$$

where c is the velocity of light in the medium.

III. NUMERICAL ANALYSIS AND APPLICATION OF THE SINGULARITY EXPANSION METHOD TO THE L-WIRE COUPLED INTEGRAL EQUATIONS

The coupled integral equations derived in the preceding section may be solved numerically by using the so-called method of moments [9]. The currents $i_x(x)$ and $i_z(z)$ are represented by piecewise sinusoidal sub-domain expansion functions (Fig. 2):

$$i_x(x) = i_1^x(x)\, u(x_2-x) + \sum_{q=2}^{Q-1} i_q^x(x)\left\{u(x-x_q) - u(x-x_{q+1})\right\} + i_q^x(x)\, u(x-x_Q)$$

where

$$i_q^x(x) = \frac{1}{\sin k\Delta_x}\left[I_q^x \sin k(x_{q+1}-x) + I_{q+1}^x \sin k(x-x_q)\right],\quad x\in[x_q,x_{q+1}] \tag{3.1}$$

and

$$i_z(z) = i_1^z(z)\, u(z_2-z) + \sum_{n=2}^{N-1} i_n^z(z)\left\{u(z-z_n) - u(z-z_{n+1})\right\} + i_N^z(z)\, u(z-z_N)$$

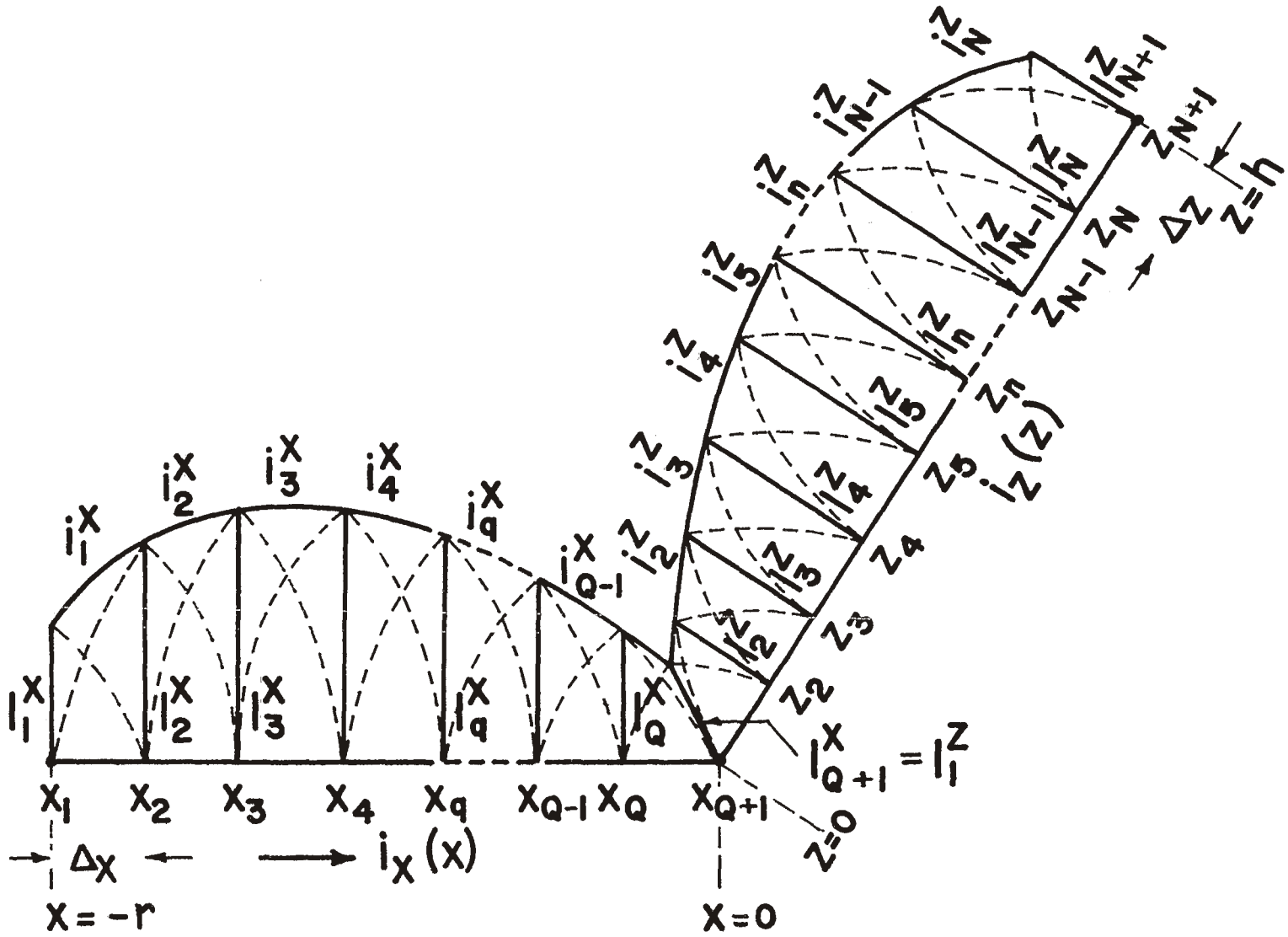

Figure 2. Piecewise sinusoidal basis set and position of match points used in the Hallen-type coupled integral equations.

where

$$i_n^z(z) = \frac{1}{\sin k\Delta_z}\left[I_n^z \sin k(z_{n+1}-z) + I_{n+1}^z \sin k(z-z_n)\right],\ z\varepsilon[z_n,z_{N+1}] \tag{3.2}$$

In the above two expressions u(x) is the familiar unit step function defined by

$$u(x) = \begin{cases} 0, & x < 0 \\ 1, & x > 0 \end{cases}$$

and I_n^z, I_q^x are unknown complex constants which are the values of the current at the points z_n and x_q, respectively.

According to the method of moments, the above current expansions are substituted into the coupled integral equations (2.13) and (2.14) and results in an expression involving the unknown complex coefficients I_n^z and I_q^x. These two functional equations are "tested" at the various match points x_q and z_n (Fig. 2) and result in the following matrix equation:

$$I_1^x U_m^x + \sum_{q=2}^{Q} I_q^x S_{mq}^x + I_{Q+1}^x T_m^x + I_1^z R_m^{xz} + \sum_{n=2}^{N} I_n^z M_{mn}^{xz} + I_{N+1}^z D^{xz} + P_m^x c_x + Q_m^x b = F_m^x,$$

$$m = 1,2,3 \ldots\ Q,Q+1 \tag{3.3}$$

$$I_1^x R_\ell^{zx} + \sum_{q=2}^{Q} I_q^x M_{\ell q}^{zx} + I_{Q+1}^x D_\ell^{zx} + I_1^z U_\ell z + \sum_{n=2}^{N} I_n^z S_{\ell n}^z + I_{N+1}^z T_\ell^z + Q_\ell^z b + P_\ell^z c_z = F_\ell^z,$$

$$\ell = 1,2,3 \ldots\ N, N+1 \tag{3.4}$$

where $$I_1^x = 0,\ I_{Q+1}^x = I_1^z,\ I_{N+1}^z = 0,$$

and the elements of the matrix equation are given by the following single integrals:

$$U_m^x = \int_{x=x_1}^{x_2} K_x(x_m,x,a_1)\frac{\sin k(x_2-x)}{\sin k\Delta_x}\,dx$$

$$S_{mq}^x = \int_{x=x_{q-1}}^{x_q} K_x(x_m,x,a_1)\frac{\sin k(x-x_{q-1})}{\sin k\Delta_x}dx - \int_{x=x_q}^{x_{q+1}} K_x(x_m,x,a_1)\frac{\sin k(x-x_{q+1})}{\sin k\Delta_x}dx$$

$$T_m^x = \int_{x=x_Q}^{x_{Q+1}} K_x(x_m,x,a_1)\frac{\sin k(x-x_Q)}{\sin k\Delta_x}dx$$

$$R_m^{xz} = \int_{z=z_1}^{z_2} K_z'(x_m,z,a_1)\frac{\sin k(z_2-z)}{\sin k\Delta_z}dz$$

$$M_{mn}^{xz} = \int_{z=z_{n-1}}^{z_n} K_z'(x_m,z,a_1)\,\frac{\sin k(z-z_{n-1})}{\sin k\Delta_z}dz - \int_{z=z_n}^{z_{n+1}} K_z'(x_m,z,a_1)\frac{\sin k(z-z_{n+1})}{\sin k\Delta_z}dz$$

$$D_m^{xz} = \int_{z=z_N}^{z_{N+1}} K_z'(x_m,z,a_1)\frac{\sin k(z-z_N)}{\sin k\Delta_z}dz$$

$$P_m^x = -\cos k x_m,\quad Q_m^x = -\sin kx_m$$

and the kernel functions are given by

$$K_x(x_m,x,a_1) = \frac{\exp\left[-jk\left\{a_1^2+(x_m-x)^2\right\}^{1/2}\right]}{\left\{a_1^2+(x_m-x)^2\right\}^{1/2}}$$

$$K_z'(x_m,z,a_1) = \left[\frac{z\,\exp\left[-jk\left\{\xi^2+a_1^2+z^2\right\}^{1/2}\right]}{(a_1^2+z^2)\left\{\xi^2+a_1^2+z^2\right\}^{1/2}}\left\{\xi\cos k(x_m-\xi) - j\left\{\xi^2+a_1^2+z^2\right\}^{1/2}\sin k(x_m-\xi)\right\}\right]_{\xi=0}^{\xi=x_m}$$

Similarly, the remaining elements of the matrix corresponding to the z-directed wire are obtained by interchanging the variables x,x_n,a_1, N with the variables z,z_n,a_2,Q, respectively, in the above expressions. The forcing function terms are given by

$$F_m^x = \frac{-j}{30}\int_{\xi=0}^{x_m} E_x^i(\xi)\sin k(x_m-\xi)d\xi$$

$$F_\ell^z = \frac{-j}{30}\int_{\zeta=0}^{z_\ell} E_z^i(\zeta)\sin k(z_\ell-\zeta)d\zeta$$

In view of the boundary condition on the currents at the ends of the wire and continuity of the current at the junction, the equations (3.3) and (3.4) can be written in a compact form as a

partitioned matrix

$$\left[\begin{array}{c|c} \overline{\overline{A}} & \overline{\overline{B}} \\ \hline \overline{\overline{C}} & \overline{\overline{F}} \end{array}\right] \left[\begin{array}{c} \overline{J} \\ \hline \overline{I} \end{array}\right] = [\overline{F}] \tag{3.5}$$

where $\overline{\overline{A}}$ consists of self and mutual terms corresponding to x and z directed wire elements and $\overline{\overline{B}}$ contains the coefficients of the constants of integration. Explicitly, we have

$$\overline{\overline{A}} = \begin{bmatrix} S^x_{12} & \cdots & S^x_{1Q} & (T^x_1+R^{xz}_1) & M^{xz}_{12} & \cdots & M^{xz}_{1N} \\ \vdots & & \vdots & \vdots & \vdots & & \vdots \\ S^x_{Q+1,2} & \cdots & S^x_{Q+1,Q} & (T^x_{Q+1}R^{xz}_{Q+1}) & M^{xz}_{Q+1,2} & \cdots & M^{xz}_{Q+1,N} \\ M^{zx}_{12} & \cdots & M^{zx}_{1Q} & (D^{zx}_1+U^z_1) & S^z_{12} & \cdots & S^z_{1N} \\ \vdots & & \vdots & \vdots & \vdots & & \vdots \\ M^{zx}_{N+1,2} & \cdots & M^{zx}_{N+1,Q} & (D^{zx}_{N+1}+U^z_{N+1}) & S^z_{N+1,2} & \cdots & S^z_{N+1,N} \end{bmatrix}$$

$$\overline{J} = \begin{bmatrix} I^x_2 \\ \vdots \\ I^x_{Q+1} \ (=I^z_1) \\ I^z_2 \\ \vdots \\ I^z_N \end{bmatrix} \qquad \overline{F} = \begin{bmatrix} F^x_1 \\ \vdots \\ F^x_{Q+1} \\ F^z_1 \\ \vdots \\ F^z_{N+1} \end{bmatrix}$$

$$\overline{C} = \begin{bmatrix} C_x \\ b \\ C_z \\ \\ \end{bmatrix} \qquad \overline{\overline{B}} = \begin{bmatrix} \cos kx_1 & \sin kx_1 & 0 \\ \vdots & \vdots & \vdots \\ \cos kx_{Q+1} & \sin kx_{Q+1} & 0 \\ 0 & \sin kz_1 & \cos kz_1 \\ \vdots & \vdots & \vdots \\ 0 & \sin kz_{N+1} & \cos kz_{N+1} \end{bmatrix}$$

The partitioned matrix equation (3.5) assumes that the current expansion and testing functions have been truncated so that the resulting matrix in (3.5) is of order (N+Q+2) and is a linear system of equations for the unknown current coefficients (only N+Q-1 unknown current coefficients are solved in $\overline{J}$ of expression (3.5) because of the boundary conditions, (3.3) and (3.4)). Without the partioning, (3.5) takes the matrix form

$$\overline{\overline{Z}}(s) \quad \overline{I}(s) = \overline{V}(s) \tag{3.6}$$

Equation (3.6) is the same as the form employed by Tesche [3], who used the generalized impedance matrix interpretation of Harrington [9]. To emphasize the similarity of the approach here, we use similar notation. However, one notes that the form (3.6) has elements with the dimensions of vector potentials, not impedance, because the matrix representation resulted from Hallén-type equations. With $k = -j\frac{s}{c}$ we identify the terms in (3.6) with the corresponding ones in (3.5) and obtain

$$\bar{\bar{Z}}(s) = \left[\bar{\bar{A}} \,\vdots\, \bar{\bar{B}}\right]$$

$$\bar{I}(s) = \begin{bmatrix} \bar{J} \\ \cdots \\ \bar{C} \end{bmatrix}$$

and

$$\bar{V}(s) = \bar{F}$$

The solution of the matrix equation (3.6) is

$$\bar{I}(s) = \bar{\bar{Z}}^{-1}(s)\bar{V}(s) = \bar{\bar{Y}}(s)\bar{V}(s) \tag{3.7}$$

where the elements of $\bar{\bar{Y}}(s)$ are given by

$$\bar{\bar{Y}}(s) = [Y_{nm}(s)] = \left[\frac{(-1)^{m+n}\Delta_{mn}(s)}{\Delta(s)}\right] \tag{3.8}$$

and Δ_{mn} is a minor determinant of $\bar{\bar{Z}}$ formed by deleting the m-th row and the n-th column, and Δ is the determinant of $\bar{\bar{Z}}$.

One can examine the analytic properties of the various quantities in (3.8) in the complex $s = \sigma+j\omega$ plane and observe that every element of the matrix $\bar{\bar{Z}}$ in the expression (3.3) and (3.4) is analytic throughout the finite complex s-plane. We should note that the terms $\Delta_{mn}(s)$, and $\Delta(s)$ are formed by taking various combinations of product factors of the elements in $\bar{\bar{Z}}$; hence they are also analytic everywhere in the finite complex s-plane. Therefore the only possible singularities of $\bar{\bar{Y}}(s)$ are the zeros of the determinant $\Delta(s)$.

Writing $\Delta(s)$ in terms of a partial fraction expansion,

$$\bar{I}(s) = \sum_i \frac{\bar{\bar{Y}}_i^r}{s-s_i} \bar{V}(s) + \bar{W}_e(s) \tag{3.9}$$

where $s = s_i$ are the poles of $\bar{\bar{Y}}(s)$ (the natural frequencies of the structure), and $\bar{\bar{Y}}_i^r$ denotes the corresponding residue matrix of $\bar{\bar{Y}}(s)$ given by

$$\bar{\bar{Y}}_i^r = \lim_{s \to s_i} (s-s_i)\bar{\bar{Y}}(s) \tag{3.10}$$

$\bar{W}_e(s)$ is a vector whose elements are entire functions, that is, they have singularities only at $s = \infty$. For convenience in mathematical notation, it has been assumed that all the poles are of first order. For higher order poles, the following development must be suitably modified [1].

In the following analysis the vector $\bar{W}_e(s)$ is assumed to be zero. This has been found to be the case in a number of exactly solvable geometries. We shall take the point of view that the singularities at $s = \infty$, if they do exist, seem to have negligible effect on numerical results from SEM when compared with those calculated from the inverse Fourier transform of frequency domain data. However, it is cautioned that entire functions generally correspond to time delays and the exclusion of such a term may possibly lead to erroneous results. It is shown in Appendix B, that the residue matrix given by the expression (3.10) can be conveniently written

in the form

$$\overline{\overline{Y}}_i^r = \beta_i \overline{I}_i \overline{H}_i^\dagger \tag{3.11}$$

where $\overline{I}_i$ is called the modal current distribution (together with the constants present in the Hallén formulation) corresponding to a natural frequency of oscillation $s = s_i$ and is the homogeneous solution of the matrix equation (3.6) at $s = s_i$, that is,

$$\overline{\overline{Z}}(s_i)\overline{I}_i = 0 \tag{3.12}$$

and similarly $\overline{H}_i$ is the homogeneous solution of the adjoint matrix equation

$$\overline{\overline{Z}}^\dagger(s_i)\overline{H}_i = 0 \tag{3.13}$$

where the dagger implies the transpose complex conjugate operation. The constant β_i is just a proportionality constant which is determined numerically after the normalization of $\overline{I}_i$ and $\overline{H}_i$. Hence the current solution can be written in the convenient form

$$\overline{I}(s) = \sum_i \frac{\beta_i \overline{I}_i \overline{H}_i^\dagger}{s - s_i} \overline{V}(s) \tag{3.14}$$

In Appendix B, various methods are discussed for the determination of the natural frequencies of oscillation s_i, the natural modal current distribution $\overline{I}_i$, the natural coupling vector $\overline{H}_i$, and the proportionality constant β_i. Alternatively, β_i may be written in a

form independent of the normalization of $\bar{I}_i$ and $\bar{H}_i$ as

$$\beta_i = \frac{1}{\bar{H}_i^t \bar{\bar{Z}}_i' \bar{I}_i} \tag{3.15}$$

where $\bar{\bar{Z}}_i'$ is the first derivative with respect to s of the matrix $\bar{\bar{Z}}(s)$ evaluated at $s = s_i$.

IV. FREQUENCY AND TIME DOMAIN SOLUTIONS

In the expression (3.14), $\overline{I}(s)$ and $\overline{I}_i$ are the partitioned column vectors

$$\overline{I} = \begin{bmatrix} \overline{J} \\ \hline \overline{C} \end{bmatrix} \quad \text{and} \quad \overline{I}_i = \begin{bmatrix} \overline{J}_i \\ \hline \overline{C}_i \end{bmatrix}$$

and hence the actual induced current distribution on the structure is obtained from the upper partition column vector $\overline{J}$

$$\overline{J}(s) = \sum_i \frac{\beta_i \overline{J}_i \overline{H}_i^{\dagger}}{s - s_i} \overline{V}(s) \tag{4.1}$$

This is the most important expression in the SEM from which either the frequency domain or the time domain solution can be determined. Note that because of the Hallen formulation employed here, the matrix $\overline{J}_i \overline{H}_i^{\dagger}$ is not a square matrix as it is in the E-field approach. Furthermore, $\overline{I}_i$ is not equal to $\overline{H}_i^*$, in contrast to the E-field formulation [3].

In the expression (4.1)

$$\overline{V}(s) = \begin{bmatrix} F_m^x \\ \hline F_\ell^z \end{bmatrix}$$

and F_m^x and F_ℓ^z are given by the integrals

$$F_m^x = \frac{-1}{30} \int_{\xi=0}^{x_m} E_x^i(\xi) \sinh \frac{s}{c}(x_m - \xi) d\xi$$

and

$$F_{\ell}^{z} = \frac{-1}{30} \int_{\zeta=0}^{x_m} E_z^i(\zeta) \sinh \frac{s}{c}(z_{\ell}-\zeta)d\zeta \tag{4.2}$$

In the above integrals, $E_x^i(x)$ and $E_z^i(z)$ are the components of the incident field along the x and z directions respectively, evaluated on the scattering structure.

For an incident plane wave with θ-polarization,

$$E_x^i(x) = E_\theta(s) \cos\theta \cos\phi \, e^{-\frac{s}{c} \sin\theta \cos\phi \, x}$$

$$E_z^i(z) = -E_\theta(s) \sin\theta \, e^{-\frac{s}{c} \cos\theta \, z} \tag{4.3}$$

and for ϕ-polarization:

$$E_x^i(x) = -E_\phi(s) \sin\phi \, e^{-\frac{s}{c} \sin\theta \cos\phi \, x}$$

$$E_z^i(z) = 0 \tag{4.4}$$

where θ and ϕ are the angles (Fig. 3) of the direction of propagation of the plane wave. Since the factors $\sin\theta\cos\phi$ and $\cos\theta$ are just direction cosines α and β with respect to x and z axis (Fig. 3), it is possible to decompose a given plane wave into the following two

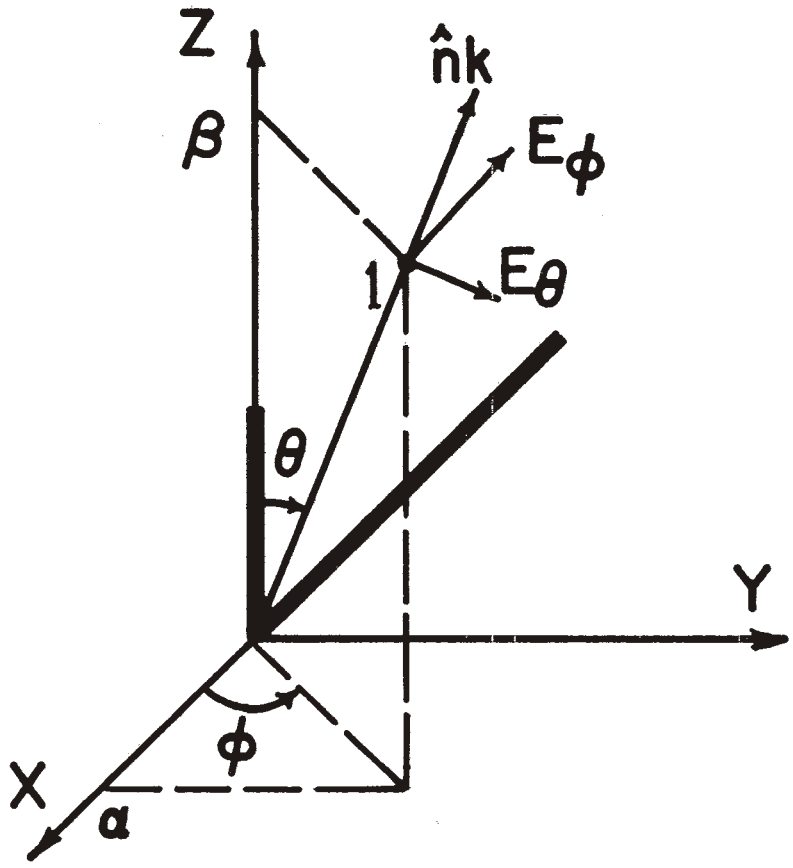

Figure 3. Resolution of the incident plane wave field into E_θ and E_ϕ components.

linearly independent excitations:

a) horizontal wire excitation

$$E^i_{x\alpha}(x) = A(s)e^{-\frac{s}{c}\alpha x}$$

$$E^i_{z\alpha}(z) = 0, \qquad \text{for } -1 < \alpha < 1 \tag{4.5a}$$

and

b) vertical wire excitation

$$E^i_{x\beta}(x) = 0$$

$$E^i_{z\beta}(z) = B(s)e^{-\frac{s}{c}\beta z}, \qquad \text{for } -1 < \beta < 1 \tag{4.5b}$$

Hence, for a given θ and ϕ one may appropriately superpose two solutions obtained from the excitation functions (4.5a) and (4.5b). For the case of plane wave incidence, by substituting (4.5a) and (4.5b), the forcing function integrals (4.2) reduce to

$$F^{x\alpha}_m = \frac{A(s)}{60\frac{s}{c}(1-\alpha^2)}\left\{2e^{-\frac{s}{c}\alpha x_m} - (1-\alpha)e^{+\frac{s}{c}x_m} - (1+\alpha)e^{+\frac{s}{c}x_m}\right\}$$

$$F^{z\alpha}_\ell = 0 \tag{4.5c}$$

and

$$F^{x\beta}_m = 0$$

$$F_{\ell}^{z\beta} = \frac{B(s)}{60\frac{s}{c}(1-\beta^2)} \left\{ 2e^{-\frac{s}{c}\beta z_{\ell}} - (1-\beta)e^{+\frac{s}{c}z_{\ell}} - (1+\beta)e^{-\frac{s}{c}z_{\ell}} \right\} \tag{4.5d}$$

The above excitation terms have a removable singularity at $s = 0$ and therefore the only singularities arise from singularities in either $A(s)$ or $B(s)$.

Frequency Domain Solution

By substituting for the Laplace variable $s = j\omega$, the time harmonic steady state response can be obtained. Hence the expression (4.1) takes the form

$$\overline{J}(j\omega) = \sum_i \frac{\beta_i \overline{J}_i \overline{H}_i^{\dagger}}{j\omega - s_i} \overline{V}(j\omega) \tag{4.6}$$

where the summation is over all the pole locations in the complex s-plane. This expression illustrates that the cause of the "resonances" one customarily observes in scattering or antenna problems in the frequency domain is due to the proximity of a pole of the structure to the $j\omega$ axis. However, one notes that at certain positions on the structure, the modal current corresponding to a particular pole may vanish and the frequency domain behavior of the current at that point will not exhibit the resonance. Nevertheless, the resonance would still be in evidence if one considered, for example, the charge at the same point.

Time Domain Solution

The time domain solution is obtained by taking the Laplace inverse transform of expression (4.1),

$$\bar{i}(t) = L^{-1}\bar{J}(s) = \frac{1}{2\pi j}\int_{C_B} \sum_i \frac{\beta_i \bar{J}_i \bar{H}_i^\dagger}{s-s_i}\bar{V}(s)e^{st}ds$$

$$= \frac{1}{2\pi j}\sum_i \beta_i \bar{J}_i \bar{H}_i^\dagger \int_{C_B} \frac{\bar{V}(s)e^{st}}{s-s_i}ds \qquad (4.7)$$

where C_B is the Bromwich contour in the complex s-plane (Fig. 4), and

$$\bar{V}(s) = [V_m(s)] = \begin{bmatrix} F_1^x \\ \cdot \\ \cdot \\ \cdot \\ F_{Q+1}^x \\ \hline F_1^z \\ \cdot \\ \cdot \\ \cdot \\ F_{N+1}^z \end{bmatrix}$$

The expression (4.7) can be written as

$$\bar{i}(t) = \sum_i \beta_i \bar{J}_i \bar{H}_i^\dagger \bar{v}_i(t) \qquad (4.8)$$

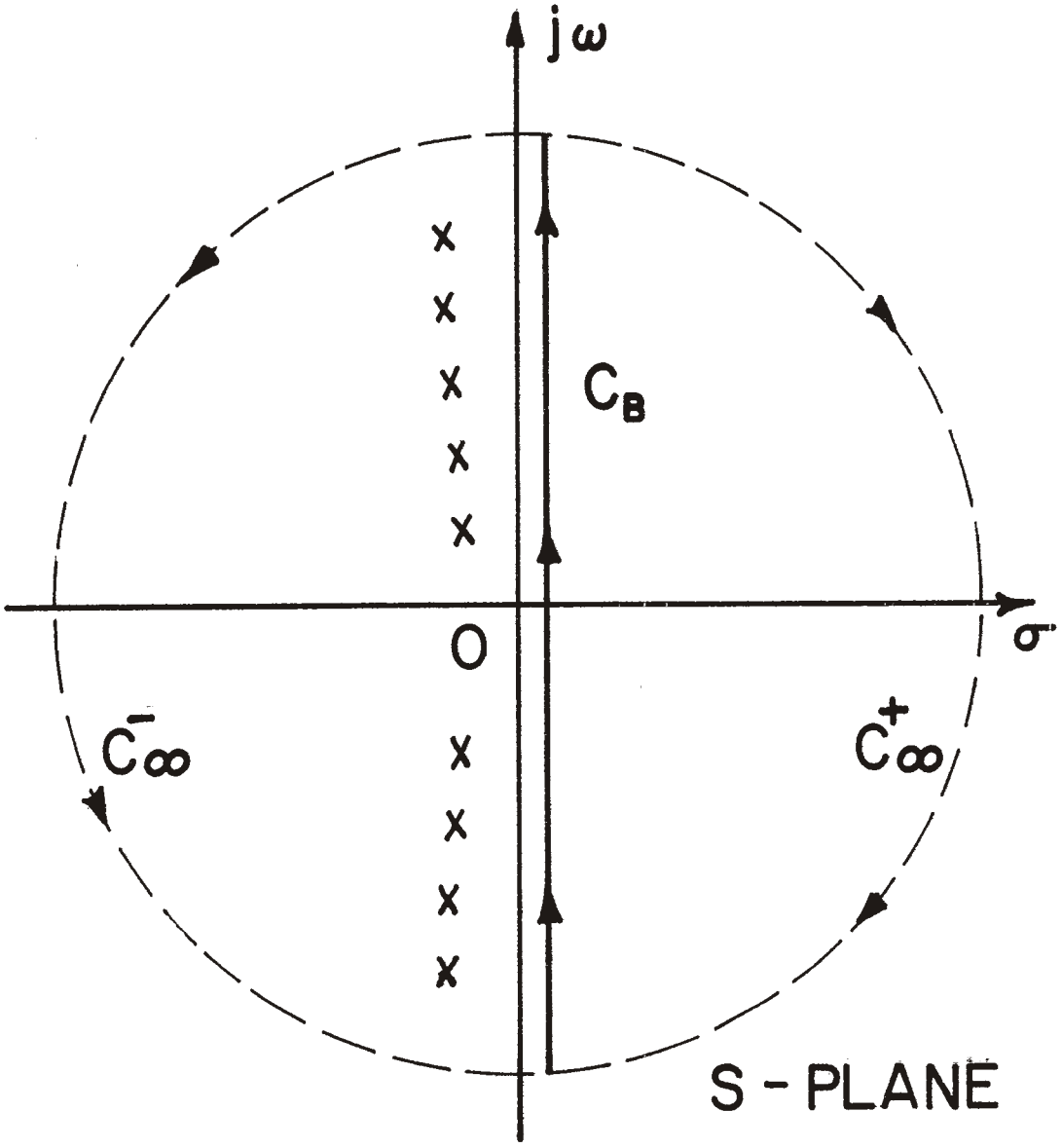

Figure 4. Illustration of the closure of the Bromwich contour in s-plane.

where

$$\bar{v}_i(t) = [v_{mi}(t)] = \frac{1}{2\pi j}\int_{C_B} \frac{V_m(s)e^{st}}{s-s_i}\,ds \tag{4.9}$$

and in the above column vector

$$V_m(s) = \frac{-1}{30}\int_{\xi=0}^{d_m} E_d^i(\xi,s)\ \sinh\frac{s}{c}(d_m-\xi)d\xi,$$

where

$$d = \begin{cases} x, & m = 1,2, \ldots, Q+1 \\ y, & m = Q+2, Q+3, \ldots, N+Q+2 \end{cases}$$

and

$$d_m = x_1, x_2, \ldots x_{Q+1}, z_1, z_2, \ldots z_{N+1}$$

for $m = 1,2, \ldots, N+Q+2$, respectively. Hence we are concerned with the element $v_{mi}(t)$ of the column vector in (4.9)

$$v_{mi}(t) = -\frac{1}{30}\int_{\xi=}^{d_m}\left[\frac{1}{2\pi j}\int_{C_B} E_d^i(\xi,s)\frac{\sinh\frac{s}{c}(d_m-\xi)}{s-s_i}\,e^{st}ds\right]d\xi \tag{4.10}$$

According to the convolution theorem,

$$\frac{1}{2\pi j}\int_{C_B} F(s)G(s)e^{st}ds = f(t) * g(t) = \int_{-\infty}^{+\infty} f(\tau)\, g(t-\tau)d\tau \qquad (4.11)$$

where the lower case letters denote quantities in the time domain and capital letters denote their corresponding Laplace transforms. Hence $v_{mi}(t)$ becomes

$$v_{mi}(t) = \frac{-1}{30}\int_{\xi=0}^{d_m} e_d^i(\xi,t) * L^{-1}\left[\frac{\sinh \frac{s}{c}(d_m-\xi)}{s-s_i}\right]d\xi \qquad (4.12)$$

where the asterisk denotes convolution and the bracketed term may be expanded as

$$L^{-1}\left[\frac{\sinh \frac{s}{c}(d_m-\xi)}{s-s_i}\right] = \frac{1}{2\pi j}\int_{C_B}\left[\frac{e^{\frac{s}{c}\left[ct+(d_m-\xi)\right]}}{2(s-s_i)} - \frac{e^{\frac{s}{c}\left[ct-(d_m-\xi)\right]}}{2(s-s_i)}\right]d\xi$$

$$= \frac{1}{2}\, u[ct+(d_m-\xi)]e^{\frac{s_i}{c}[ct+(d_m-\xi)]}$$

$$- \frac{1}{2}\, u[ct-(d_m-\xi)]e^{\frac{s_i}{c}[ct-(d_m-\xi)]} \qquad (4.13)$$

This result is found by closing the Bromwich contour either by C_∞^+ or C_∞^- (Fig. 4) and the integral is evaluated using the residue

theorem. Because of the fact that all the poles are located in the left half plane, the integral involving $C_B + C_\infty^+$ is identically zero. The above time-space function is shown in Fig. 5. It is seen that if the excitation function $e_d^i(\xi,t)$ is a delta function in both space and time (the antenna problem),

$$e_d^i(\xi,t) = \delta(t)\ \delta(\xi-d_n) \tag{4.14}$$

then the expression (4.12) reduces to the form given in the expression (4.13) with the variable ξ replaced by d_n whenever $|d_n|<|d_m|$ and is zero otherwise. For more general excitation functions, according to the expression (4.12), a convolution in both space and time is required. Alternatively, a coupling coefficient can be defined, as is done later in this Section, which does not require the convolution in time. However, the representation given here converges more rapidly in practice.

For a step function plane wave incident, the electric field has the general form,

$$E_d^i(\xi,s) = \frac{e^{-\frac{s}{c}\gamma\xi}}{s}, \qquad -1 < \gamma < 1 \tag{4.15}$$

and

$$e_d^i(\xi,t) = u[t-\tfrac{\gamma\xi}{c}] \tag{4.16}$$

Substituting the expression (4.15) into (4.10)

$$v_{mi}(t) = \frac{-1}{30}\int_{\xi=0}^{d_m}\left[\frac{1}{2\pi j}\int_{C_B}\frac{e^{-\frac{s}{c}\gamma\xi}\sinh\frac{s}{c}(d_m-\xi)}{s(s-s_i)}e^{st}\,ds\right]$$

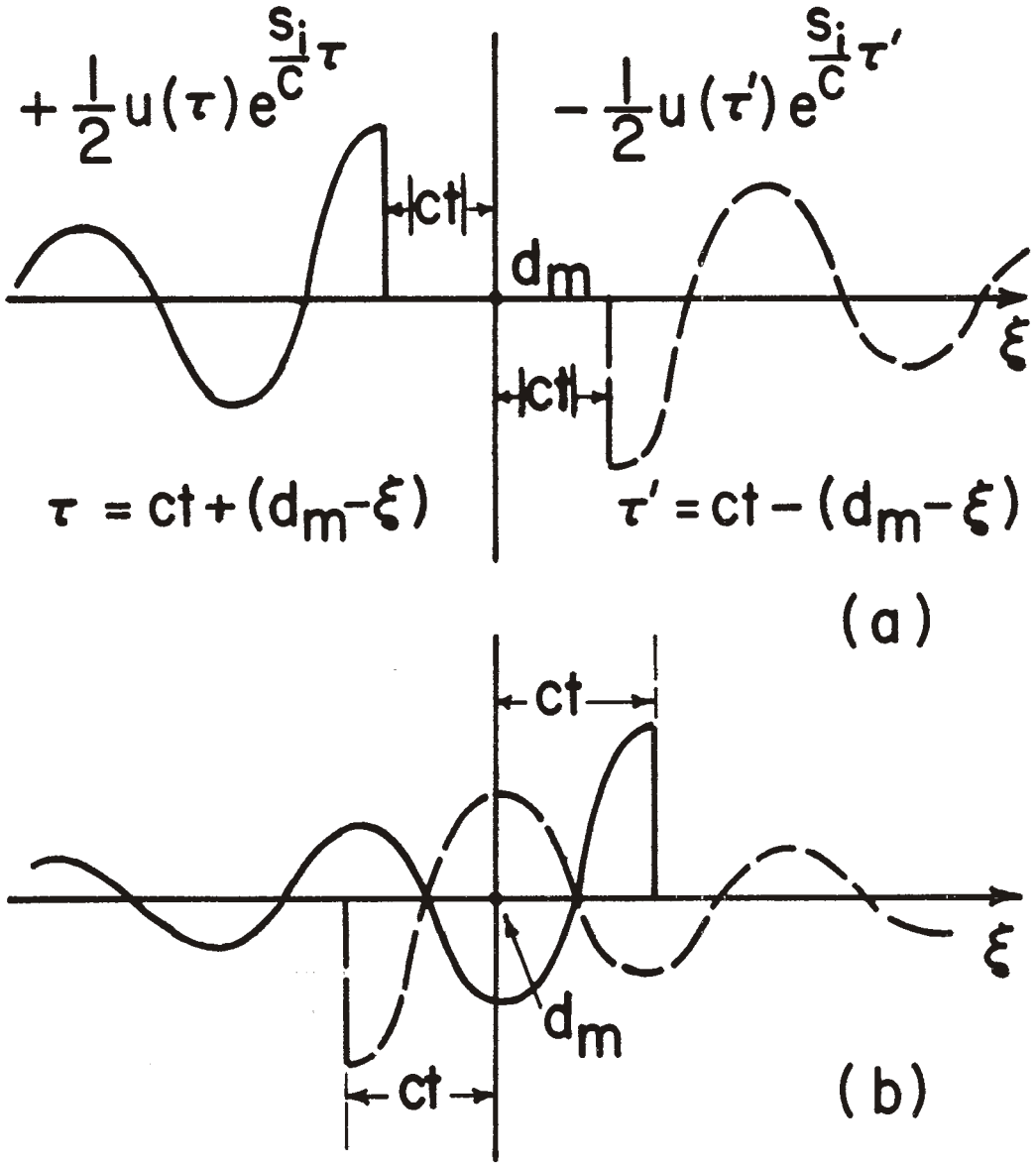

Figure 5. Integrand of the forcing function (equation 4.13) for (a) $t < 0$, (b) $t > 0$.

$$= \frac{-1}{30}\int_{\xi=0}^{d_m} \frac{1}{2\pi j}\left(\int_{C_B} \sinh\frac{s}{c}(d_m-\xi)\, e^{\frac{s}{c}(ct-\gamma\xi)}\left[\frac{1}{s_i(s-s_i)} - \frac{1}{s_i s}\right] ds\right) d\xi \tag{4.17}$$

Hence

$$v_{mi}(t) = \frac{1}{30}\int_{\xi=0}^{d_m}\left(\frac{1}{2s_i}u\left[ct-\gamma\xi+(d_m-\xi)\right]\left[e^{\frac{s_i}{c}\left[ct-\gamma\xi+(d_m-\xi)\right]}-1\right]\right.$$

$$\left. - \frac{1}{2s_i}u\left[ct-\gamma\xi-(d_m-\xi)\right]\left[e^{\frac{s_i}{c}\left[\{ct-\gamma\xi-(d_m-\xi)\}\right]}-1\right]\right) \tag{4.18}$$

With a change in the variable of integration, the above becomes

$$v_{mi}(t) = \frac{1}{60s_i(\alpha+1)}\int_{\tau=ct+d_m}^{ct-\gamma d_m} u(\tau)\left[e^{\frac{s_i}{c}\tau}-1\right]d\tau - \frac{1}{60s_i(\alpha+1)}\int_{\tau=ct-d_m}^{ct-\gamma d_m} u(\tau)\left[e^{\frac{s_i}{c}\tau}-1\right]d\tau \tag{4.19}$$

indicating that the integration is performed for $\tau > 0$ and whenever at least one of the limits of integration is positive. Hence the time domain solution is obtain by substituting the expression (4.19) for $v_{mi}(t)$ into (4.8).

Linear Charge Density

The current-charge continuity equation gives the relationship

$$\bar{\rho}(s) = -\frac{1}{s}\frac{d\bar{J}(s)}{d\zeta} \tag{4.20}$$

where ζ is the coordinate variable along either the x or the z axis. Hence in the time domain, substituting equation (4.7) into (4.20), we have

$$\bar{\rho}(t) = L^{-1}\bar{\rho}(s)$$

$$= \frac{-1}{2\pi j}\sum_i \beta_i \frac{d\bar{J}_i}{d\zeta}\bar{H}_i^{\dagger}\int_{C_B}\frac{\bar{V}(s)e^{st}}{s(s-s_i)}\,ds$$

$$= \sum_i \beta_i \bar{Q}_i \bar{H}_i^{\dagger}\,\bar{v}_i^{q}(t) \tag{4.21}$$

where $\bar{Q}_i = \frac{d\bar{J}_i}{d\zeta}$ is the modal distribution of charge density which is obtained in practice by replacing the derivative operation by a difference approximation,

$$\bar{Q}_i = \left[\frac{J_{n+1,i} - J_{n-1,i}}{2\Delta\zeta}\right]$$

where $J_{n,i}$ is an element of $\bar{J}_i$ and the column vector

$$\bar{v}_i^q(t) = [v_{mi}^q(t)]$$

$$= \left[-\frac{1}{2\pi j} \int_{C_B} \frac{V_m(s)e^{st}}{s(s-s_i)}\, ds \right]$$

Hence the element $v_{mi}^q(t)$ takes the form

$$v_{mi}^q(t) = \frac{-1}{30} \int_{\xi=0}^{d_m} \left[\frac{-1}{2\pi j} \int_{C_B} E_d^i(\xi,s)\, \frac{\sinh \frac{s}{c}(d_m-\xi)}{(s-s_i)s}\, e^{st}\, ds \right] d\xi \qquad (4.22)$$

For a step function plane wave incident, using equation (4.15),

$$v_{mi}^q(t) = \frac{-1}{30} \int_{\xi=0}^{d_m} \left[\frac{-1}{2\pi j} \int_{C_B} \frac{\sinh \frac{s}{c}(d_m-\xi)\, e^{\frac{s}{c}(ct-\gamma\xi)}}{s^2(s-s_i)}\, ds \right] d\xi$$

Rewriting the above expression in terms of a partial fraction expansion, we have

$$v_{mi}^q(t) = \frac{-1}{30} \int_{\xi=0}^{d_m} \frac{1}{2\pi j} \int_{C_B} \left\{ \sinh \frac{s}{c}(d_m-\xi)\, e^{\frac{s}{c}(ct-\gamma\xi)} \right.$$

$$\left. \left[\frac{-1}{s_i^2(s-s_i)} + \frac{1}{s_i s^2} + \frac{1}{s_i^2 s} \right] ds \right\} d\xi$$

and upon taking the inverse Laplace transform, $v^q_{mi}(t)$ reduces to the following form:

$$v^q_{mi}(t) = \frac{-1}{30} \int_{\xi=0}^{d_m} \left\{ \frac{1}{2} u\left[ct-\gamma\xi+(d_m-\xi)\right] \left[\frac{-1}{s_i^2} e^{\frac{s_i}{c}\left[ct-\gamma\xi+(d_m-\xi)\right]} \right.\right.$$

$$\left. + \frac{1}{s_i c}\left[ct-\gamma\xi+(d_m-\xi)\right] + \frac{1}{s_i^2} \right]$$

$$- \frac{1}{2} u\left[ct-\gamma\xi-(d_m-\xi)\right] \left[\frac{-1}{s_i^2} e^{\frac{s_i}{c}\left[ct-\gamma\xi-(d_m-\xi)\right]} \right.$$

$$\left.\left. \frac{1}{s_i c}\left[ct-\gamma\xi-(d_m-\xi)\right] + \frac{1}{s_i^2} \right] \right\} d\xi \qquad (4.23)$$

In the limit as $t \to \infty$, the expression (4.23) gives the constant linear charge distribution corresponding to the static response $s = 0$. This can also be obtained by applying the final value theorem to the expression (4.20) or to (4.22):

$$\lim_{t\to\infty} \bar{\rho}(t) = \lim_{s\to 0} s\bar{\rho}(s) \qquad (4.24)$$

By substituting expressions (3.6) and (4.20) into (4.24), we obtain the result

$$\lim_{t\to\infty} \bar{\rho}(t) = - \lim_{s\to 0} \frac{d}{d\zeta} [\bar{\bar{Z}}^{-1}(s)\bar{V}(s)] \tag{4.25}$$

which with the aid of (4.22) yields

$$\lim_{t\to\infty} \bar{\rho}(t) = \sum_i \beta_i \bar{Q}_i \bar{H}_i \bar{v}_i^q(t\to\infty) \tag{4.26}$$

where

$$\bar{v}_i^q(t\to\infty) = \frac{-1}{60} \frac{d_m^2}{s_i}$$

Coupling Coefficients

The time domain solution of the induced current distribution is given by the expression (4.7)

$$\bar{i}(t) = \frac{1}{2\pi j} \int_{C_B} \sum_i \beta_i \bar{I}_i \bar{H}_i^t \bar{V}(s) \frac{e^{st}}{s-s_i} ds$$

The treatment of the previous sections regarding the closure of the Bromwich contour yields a time-domain current representation which appears to converge favorably as a function of the number of singularities included in the residue series. Another form of the

time domain representation is available, however, which is more convenient for tabulation of the characteristic scattering properties of the structure. This representation is simply

$$\bar{i}(t) = \sum_i C_i \bar{J}_i \, e^{s_i t} \tag{4.27}$$

where

$$C_i = \beta_i \bar{H}_i^{\dagger} \, \bar{V}(s_i) \tag{4.28}$$

and we assume $\bar{V}(s)$ has no singularities in the finite complex s-plane. If V(s) is due to a plane wave with a more general time dependence, the time dependence may be factored from the plane wave dependence and an expression similar to (4.27) with additional terms to account for the waveform singularities results [1]. The quantity C_i is the coupling coefficient corresponding to the natural frequency s_i and depends only on the geometry-dependent factors β_i and $\bar{H}_i$, and the transform of the incident field evaluated at the natural frequency. Hence, if the incident field is a step function plane wave, for example, the coupling coefficients C_i depend only on the angle of incidence.

Corresponding to the two types of incident fields as defined in (4.5a) and (4.5b), coupling coefficients $C_{\alpha i}$ and $C_{\beta i}$ may be defined as

$$C_{\alpha i} = \beta_i \bar{H}_i^{\dagger} \, \bar{V}_{\alpha}(s_i) \tag{4.29}$$

where

$$\overline{V}_{\alpha}(s_i) = \begin{bmatrix} F_1^{x\alpha} \\ \vdots \\ F_{Q+1}^{x\alpha} \\ \hline 0 \\ \vdots \\ 0 \end{bmatrix} \qquad \text{for } -1 < \alpha < 1$$

and

$$C_{\beta i} = \beta_i \overline{H}_i^{\dagger}\, \overline{V}_{\beta}(s_i) \tag{4.30}$$

where

$$\overline{V}_{\beta}(s_i) \qquad \begin{bmatrix} 0 \\ \vdots \\ 0 \\ \hline F_1^{z\beta} \\ \vdots \\ F_{N+1}^{z\beta} \end{bmatrix} \qquad \text{for } -1 < \beta < 1$$

and $F_m^{x\alpha}$, $F_{\ell}^{z\beta}$ are defined in (4.5c) and (4.5d).

V. NUMERICAL CALCULATIONS

In this section is presented the results of a parameter study of the L-wire structure using the SEM. Referring to Fig. 1, where all geometric parameters are normalized to the total wire length $L = r + h$, only three parameters are required to specify the geometry. The parameters are the radius ratios a_1/L and a_2/L, and the length r/L, which is taken to be the longer arm of the L. The length of the shorter arm is simply $h/L = 1 - r/L$.

The natural frequencies, modal current and modal charge distributions, and coupling coefficients are given in the following for various combinations of the structure parameters. Sample time and frequency domain current responses are presented and the convergence behavior of the time domain current representation is illustrated. The time domain response of the charge is also presented.

Natural Frequencies

Tables 1, 2, and 3 give the calculated natural resonant frequencies for an L-wire with the longer arm having length $r/L = 0.9$, 0.7, and 0.5, respectively. As in the case of the straight wire, the poles appear in layers which lie roughly parallel to the $j\omega$ axis [3]. In the tables and following figures, the layer nearest the axis is denoted as the $\ell = 1$ layer and the index n labels poles in that layer according to their distance from the σ axis. The location of a pole in the s-plane is then given by the complex number $s_{\ell n}$

ℓ	n	$\frac{a_1}{L} = 0.001$, $\frac{a_2}{L} = 0.001$		$\frac{a_1}{L} = 0.001$ $\frac{a_2}{L} = 0.01$		$\frac{a_1}{L} = 0.01$ $\frac{a_2}{L} = 0.001$		$\frac{a_1}{L} = 0.01$ $\frac{a_2}{L} = 0.01$	
		$\frac{\sigma L}{2c}$	$\frac{\omega L}{2c}$	$\frac{\sigma L}{2c}$	$\frac{\omega L}{2c}$	$\frac{\sigma L}{2c}$	$\frac{\omega L}{2c}$	$\frac{\sigma L}{2c}$	$\frac{\omega L}{2c}$
1	1	-0.0943	1.5049	-0.0809	1.3729	-0.1589	1.4991	-0.1472	1.4368
	2	-0.1269	3.0782	-0.1098	2.8947	-0.2343	3.1117	-0.2122	2.9861
	3	-0.1327	4.6554	-0.1350	4.5008	-0.2778	4.7204	-0.2549	4.5614
	4	-0.1440	6.2417	-0.1633	6.1525	-0.2978	6.2864	-0.2984	6.1458
	5	-0.1665	7.8291	-0.1993	7.8262	-0.3193	7.7572	-0.3631	7.7367
	6	-0.2073	9.4169	-0.2523	9.5140	-0.4042	9.1522	-0.4654	9.3427
	7	-0.2679	11.0046	-0.3400	11.2276	-0.5188	10.6023	-0.6179	10.9799
	8	-0.3454	12.5872	-0.4456	13.0427	-0.5974	12.1500	-0.8551	12.6841
	9	-0.4295	14.1497	--	--	--	--	--	--
	10	-0.4929	15.6809	--	--	--	--	--	--
2	0	-3.9069	0.0	-3.8381	0.0	-3.3398	0.0	-3.2963	0.0
	1	-4.4159	2.3928	-4.3634	2.3608	-3.9904	2.6976	-4.1364	2.2898

Table 1. Natural frequencies of L-wire structure, r/L = 0.9.

ℓ	n	$\frac{a_1}{L} = 0.001$ $\frac{a_2}{L} = 0.001$		$\frac{a_1}{L} = 0.001$ $\frac{a_2}{L} = 0.01$		$\frac{a_1}{L} = 0.01$ $\frac{a_2}{L} = 0.001$		$\frac{a_1}{L} = 0.01$ $\frac{a_2}{L} = 0.01$	
		$\frac{\sigma L}{2c}$	$\frac{\omega L}{2c}$	$\frac{\sigma L}{2c}$	$\frac{\omega L}{2c}$	$\frac{\sigma L}{2c}$	$\frac{\omega L}{2c}$	$\frac{\sigma L}{2c}$	$\frac{\omega L}{2c}$
1	1	-0.0759	1.5326	-0.0666	1.3962	-0.1404	1.6133	-0.1233	1.4801
	2	-0.1275	3.1248	-0.1629	3.1952	-0.1707	2.9866	-0.2293	3.0676
	3	-0.2580	4.7215	-0.4749	4.6837	-0.3747	4.4813	-0.5104	4.6109
	4	-0.2831	6.2206	-0.3589	5.9087	-0.4806	6.3022	-0.5902	6.0905
	5	-0.2204	7.8251	-0.3172	7.8114	-0.4337	7.7698	-0.5528	7.6846
	6	-0.3786	9.4183	-0.8752	9.4471	-0.5719	8.9414	-0.8936	9.1639
	7	-0.4358	10.8581	-0.4747	10.3155	-0.6739	10.7761	-0.8542	10.4894
	8	-0.2741	12.4592	-0.3333	12.3323	-0.5996	12.5301	-0.6424	12.2332
	9	--	--	--	--	--	--	--	--
	10	--	--	--	--	--	--	--	--
2	0	-4.6492	0.0	-4.4498	0.0	-4.2687	0.0	-4.1219	0.0
	1	-4.9128	2.1697	-4.6373	2.1726	-4.8196	2.1545	-4.5321	2.1290

Table 2. Natural frequencies of L-wire structure, r/L = 0.7.

ℓ	n	$\frac{a_1}{L} = 0.001$ $\frac{a_2}{L} = 0.001$		$\frac{a_1}{L} = 0.01$ $\frac{a_2}{L} = 0.001$†		$\frac{a_1}{L} = 0.01$ $\frac{a_2}{L} = 0.01$	
		$\frac{\sigma L}{2c}$	$\frac{\omega L}{2c}$	$\frac{\sigma L}{2c}$	$\frac{\omega L}{2c}$	$\frac{\sigma L}{2c}$	$\frac{\omega L}{2c}$
1	1	-0.0531	1.5439	-0.1022	1.4997	-0.1028	1.5001
	2	-0.2085	3.1212	-0.3762	3.0389	-0.3763	3.0390
	3	-0.1969	4.7047	-0.3763	4.6178	-0.3794	4.6211
	4	-0.3632	6.2440	-0.7251	6.0605	-0.7251	6.0607
	5	-0.2885	7.8016	-0.5502	7.6231	-0.5587	7.6312
	6	-0.4243	9.3316	-0.8610	9.0290	-0.8612	9.0293
	7	-0.3086	10.9217	-0.5934	10.7067	-0.6081	10.7212
	8	-0.4528	12.4781	-0.9864	12.1681	-0.9867	12.1685
	9	-0.3438	14.0815	-0.7015	13.8544	-0.7244	13.8820
	10	-0.5191	15.6308	--	--	-1.2394	15.2280
2	1	-4.8121	0.0	-2.9787	0.0	-4.3075	0.0
	1	-5.3886	2.2573	-3.8876	2.8260	-5.1622	2.1316

†Natural frequencies are the same for $a_1/L = 0.001$ and $a_2/L = 0.01$

Table 3. Natural frequencies of L-wire structure, r/L = 0.5.

Only a few poles in the second layer are given in the tables.

Figures 6-9 show the location of the natural frequencies in the s-plane for the four radius combinations considered here. In each figure, the complex natural frequencies in the $\ell = 1$ layer are plotted for three ratios of r/L. To some degree, the pole distributions are similar to those found by Tesche for the straight wire [3]. However, the bend tends to increase the damping constants, particularly when the bend is toward the center of the wire. Furthermore, the poles associated with a layer no longer appear to lie along a smooth arc, but seem to be distributed along a zigzag path curving slightly away from the $j\omega$ axis.

In Figures 10-12, the data above are again displayed, but with the ratio r/L held fixed for the various radii combinations in each figure. These figures show an increase in the damping constant whenever one of the arms of the L-wire is increased in radius, the largest effect arising when the radius of the longer arm is increased. An important observation is that the figures indicate that poles at $s = s_{1p}$, where

$$p = m\left[\frac{L}{h}\right], \quad m = 1,2,\ldots, \tag{5.1}$$

(i.e., p is an integral multiple of the integer closest to the quantity in brackets), are shifted to the left relative to neighboring

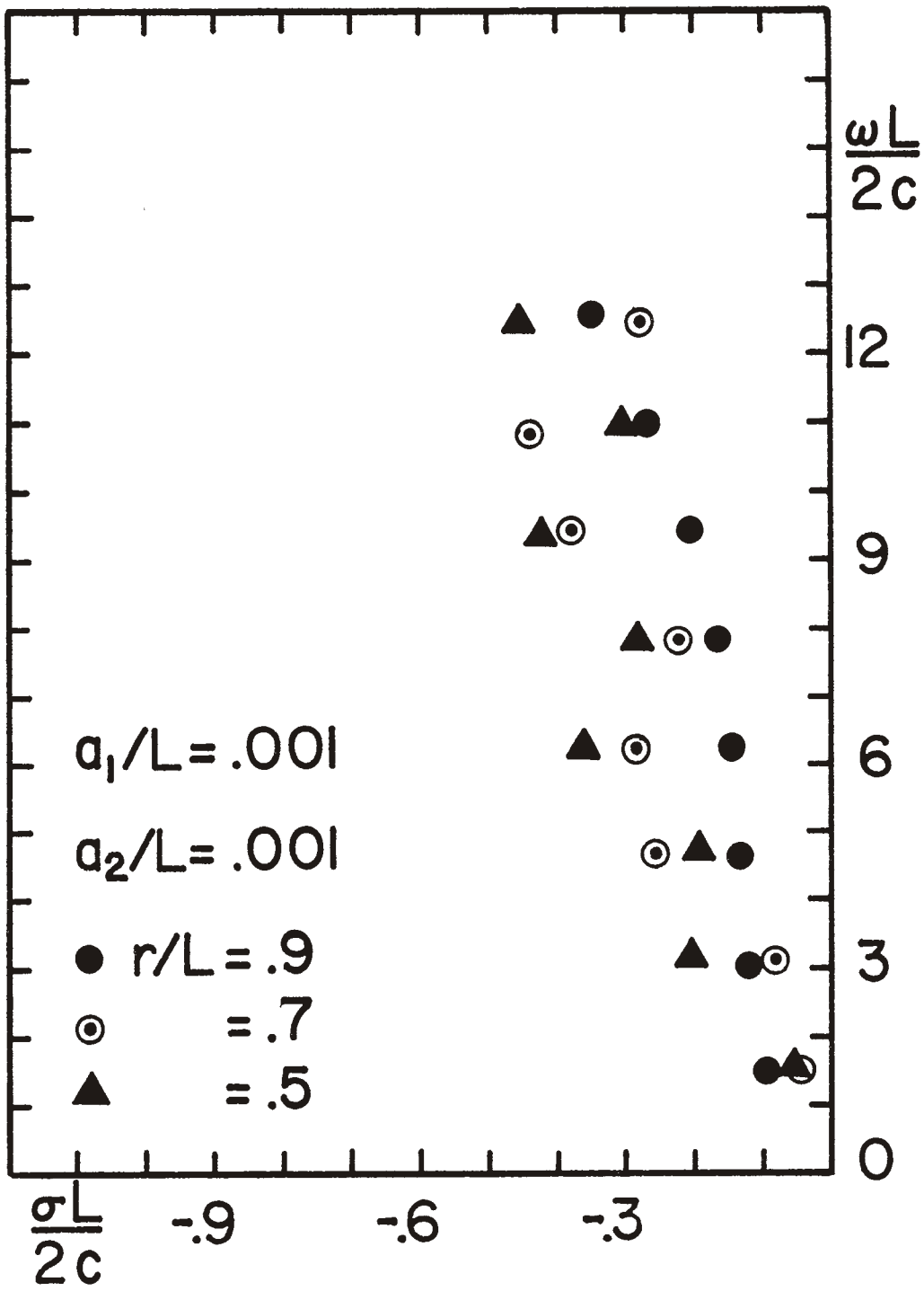

Figure 6. Natural frequencies of L-wire, $a_1/L = 0.001$, $a_2/L = 0.001$.

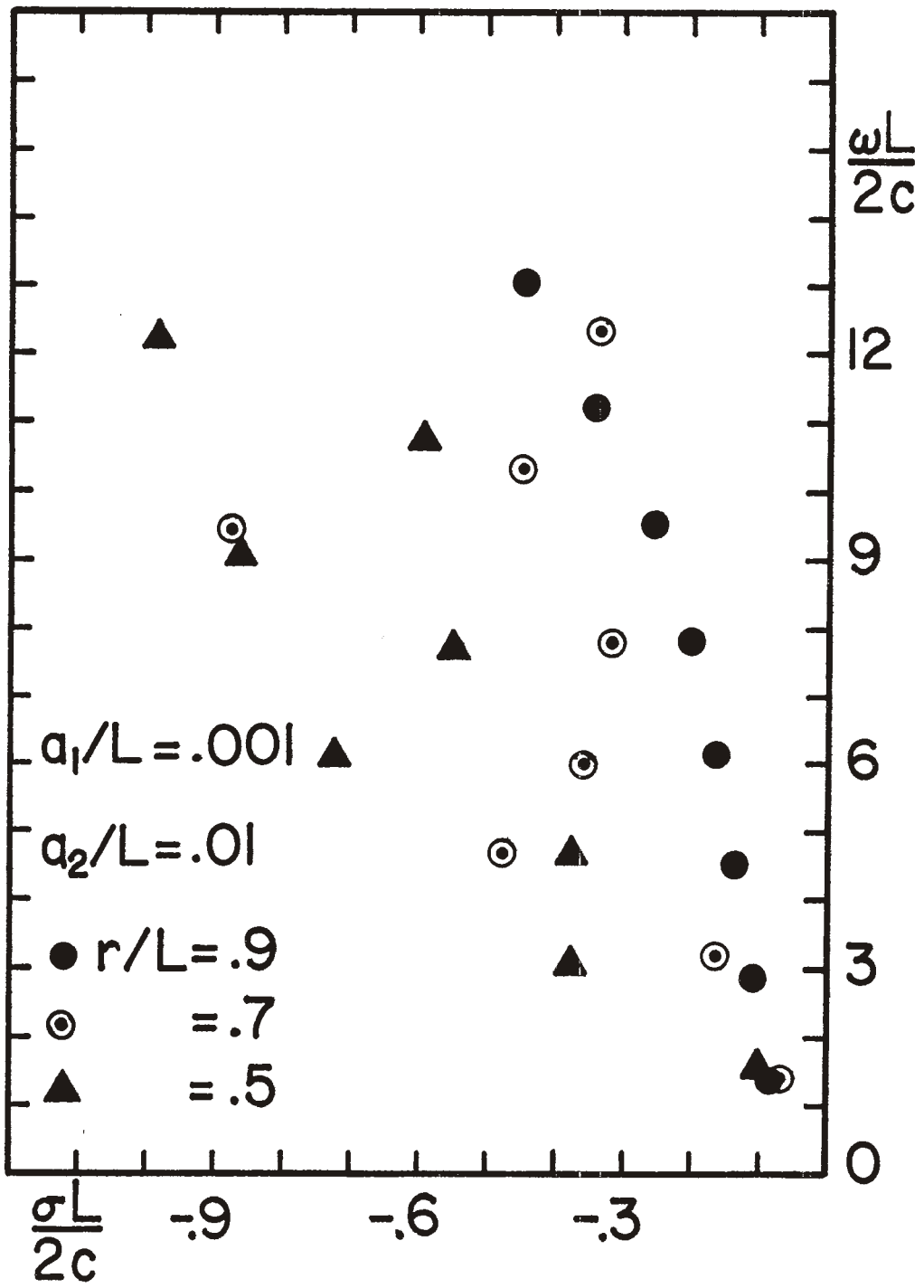

Figure 7. Natural frequencies of L-wire, $a_1/L = 0.001$, $a_2/L = 0.01$.

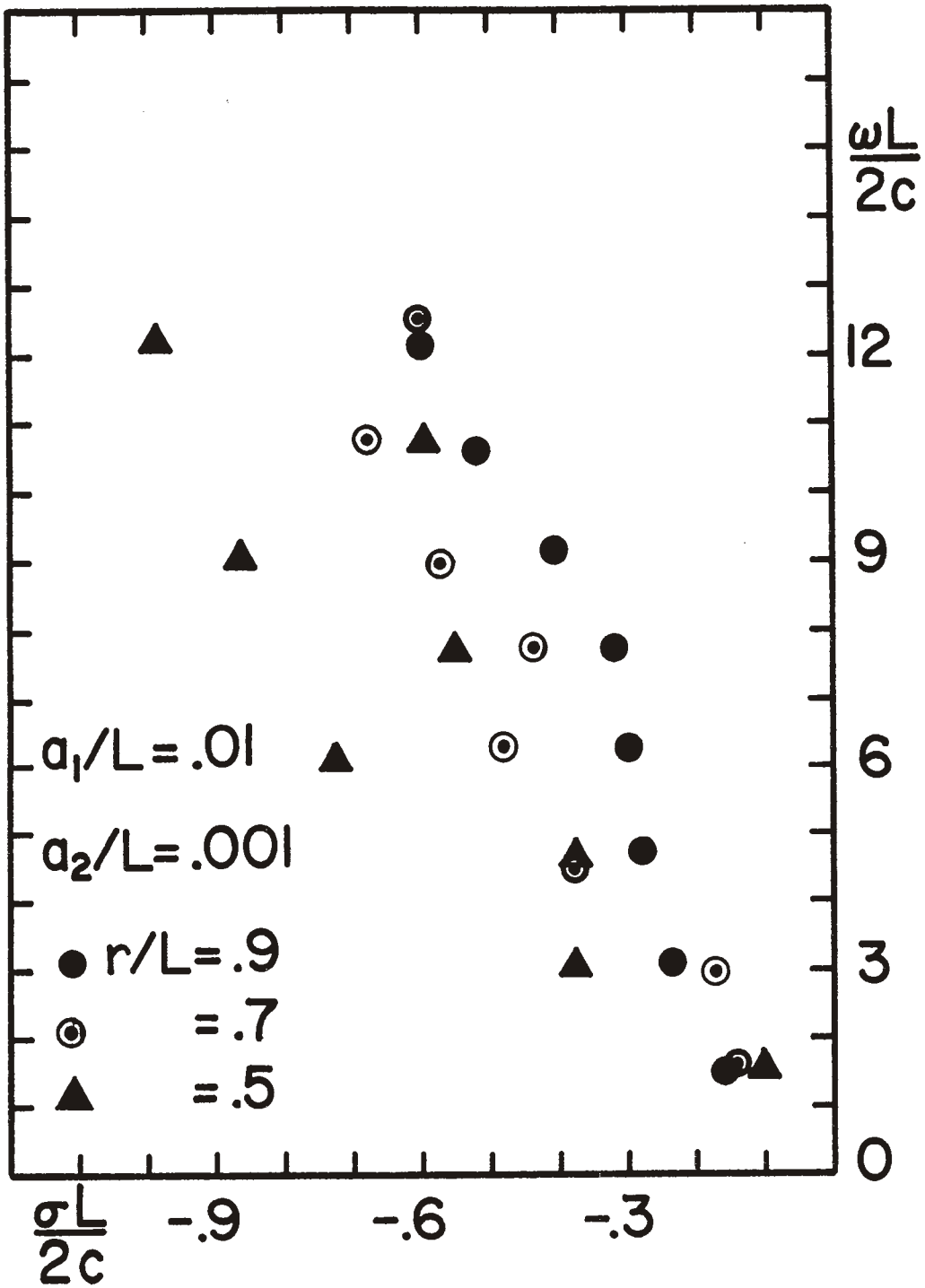

Figure 8. Natural frequencies of L-wire, $a_1/L = 0.01$, $a_2/L = 0.001$.

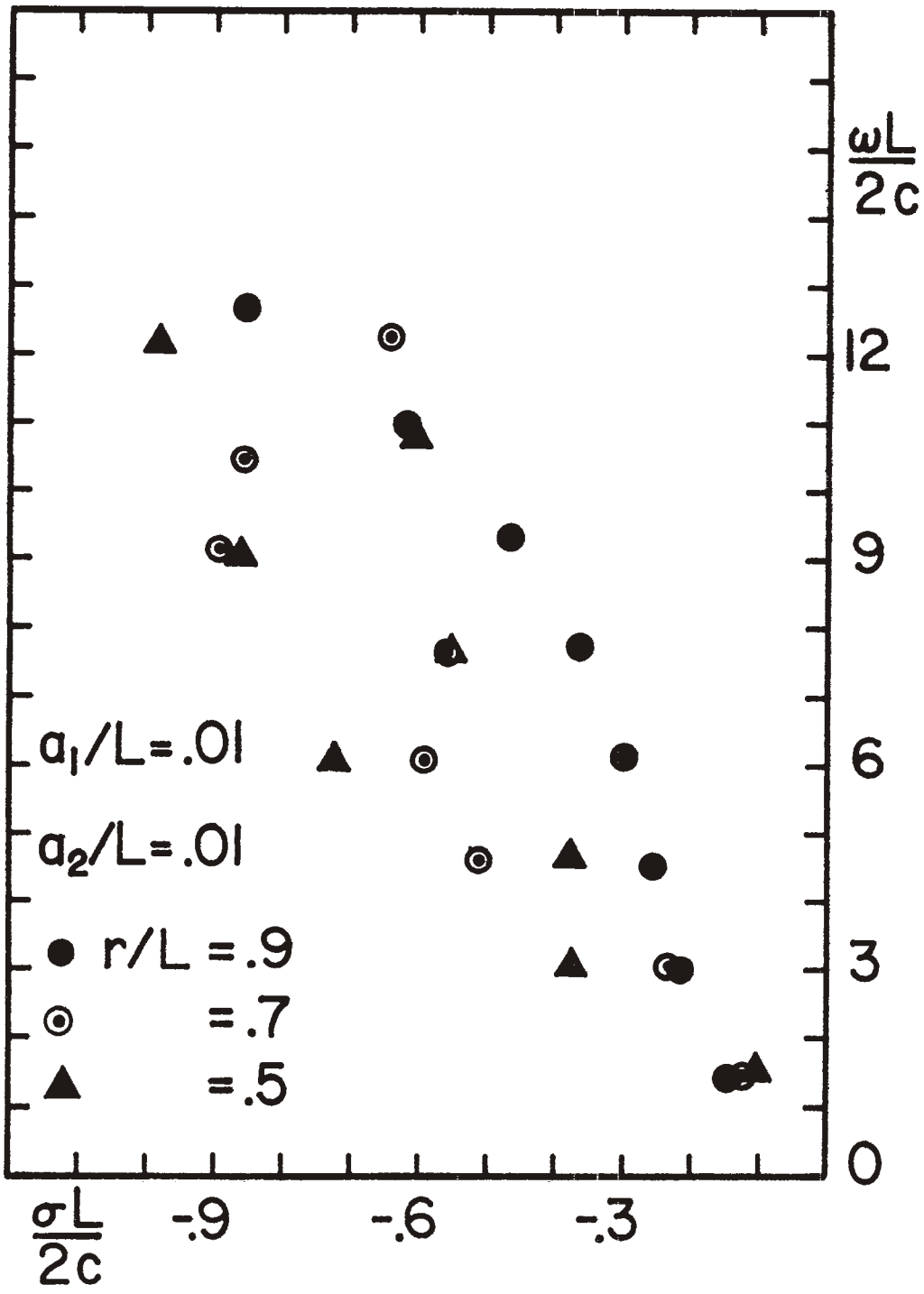

Figure 9. Natural frequencies of L-wire, $a_1/L = 0.01$, $a_2/L = 0.01$.

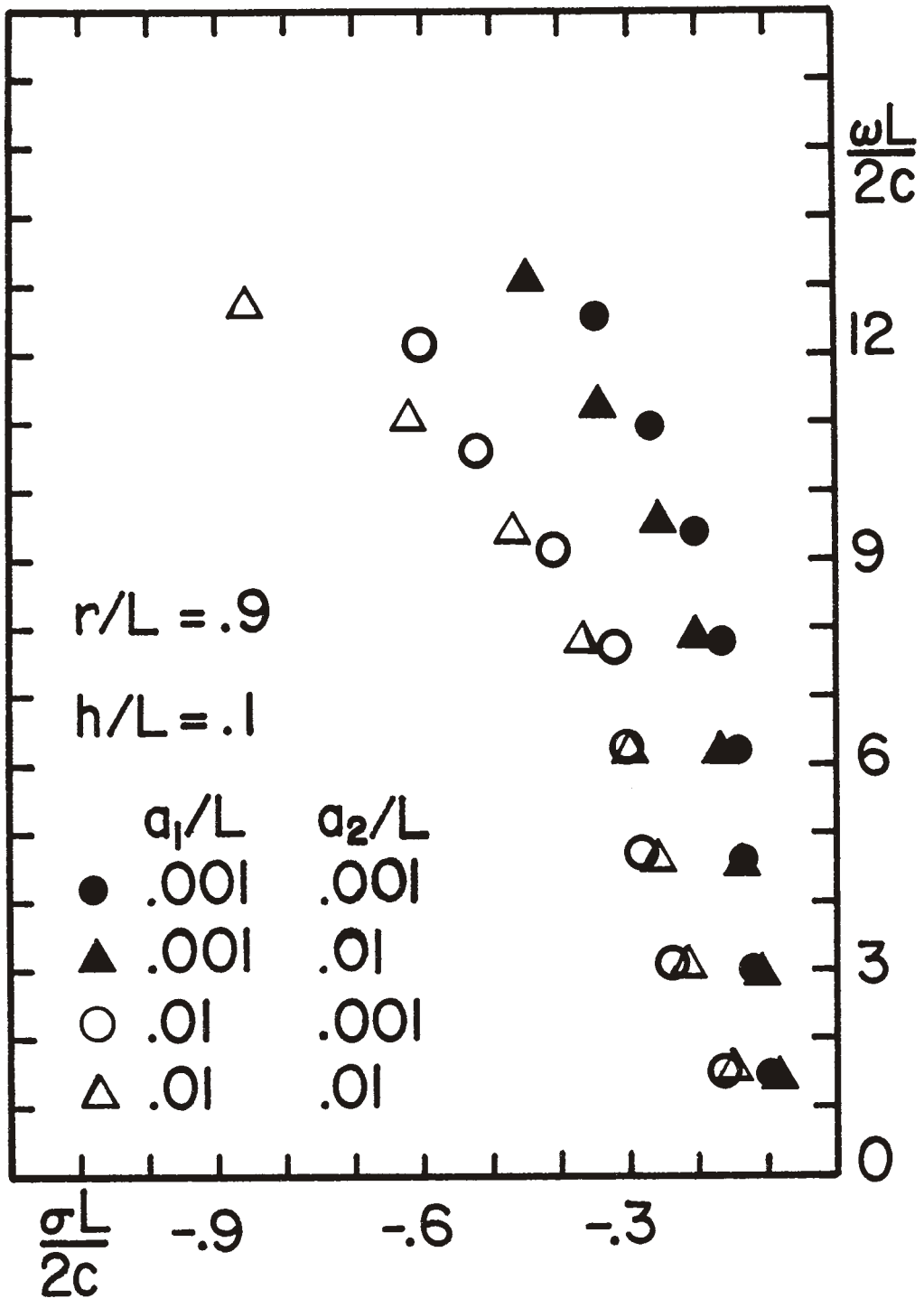

Figure 10. Natural frequencies of L-wire, r/L = 0.9.

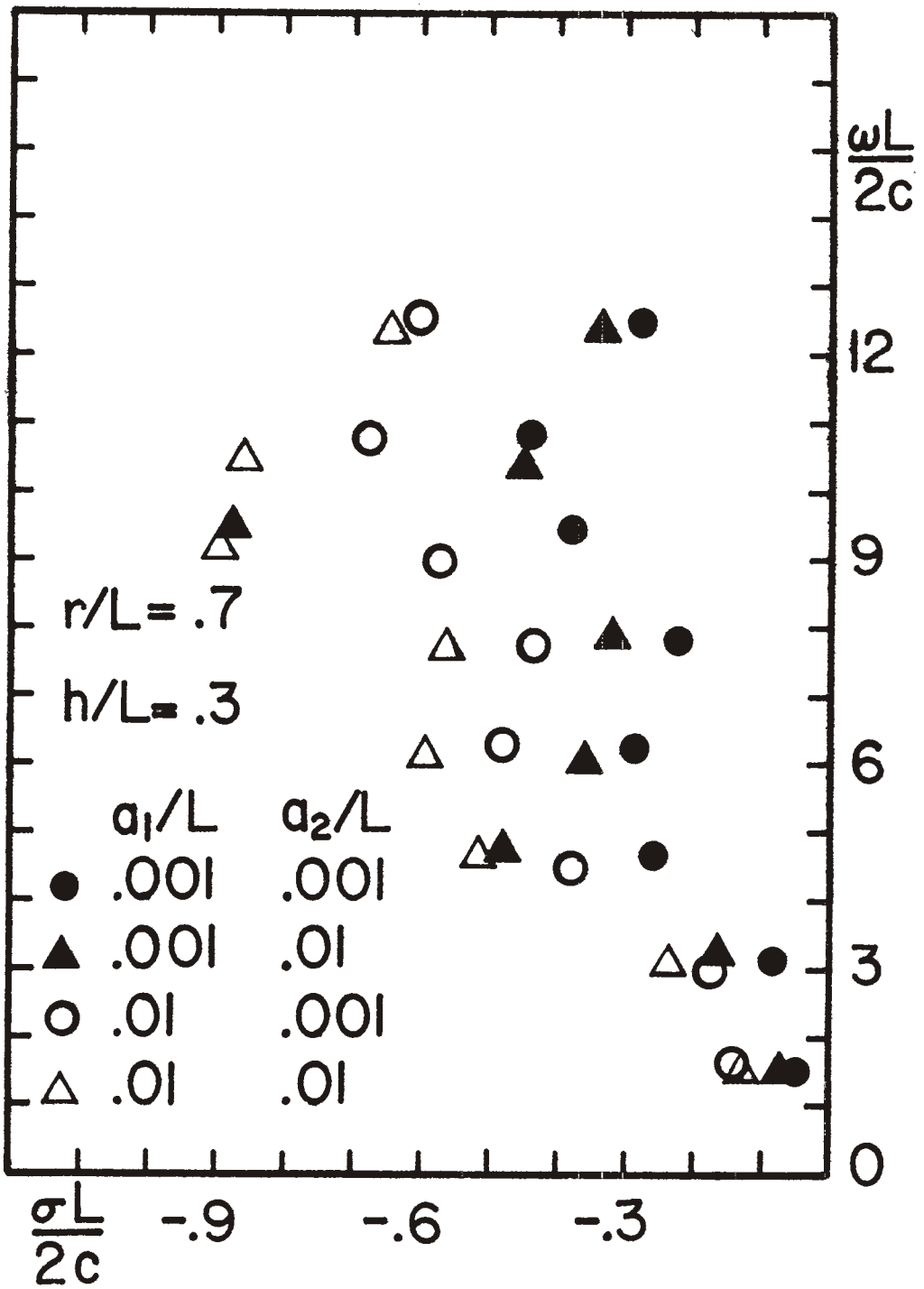

Figure 11. Natural frequencies of L-wire, r/L = 0.7.

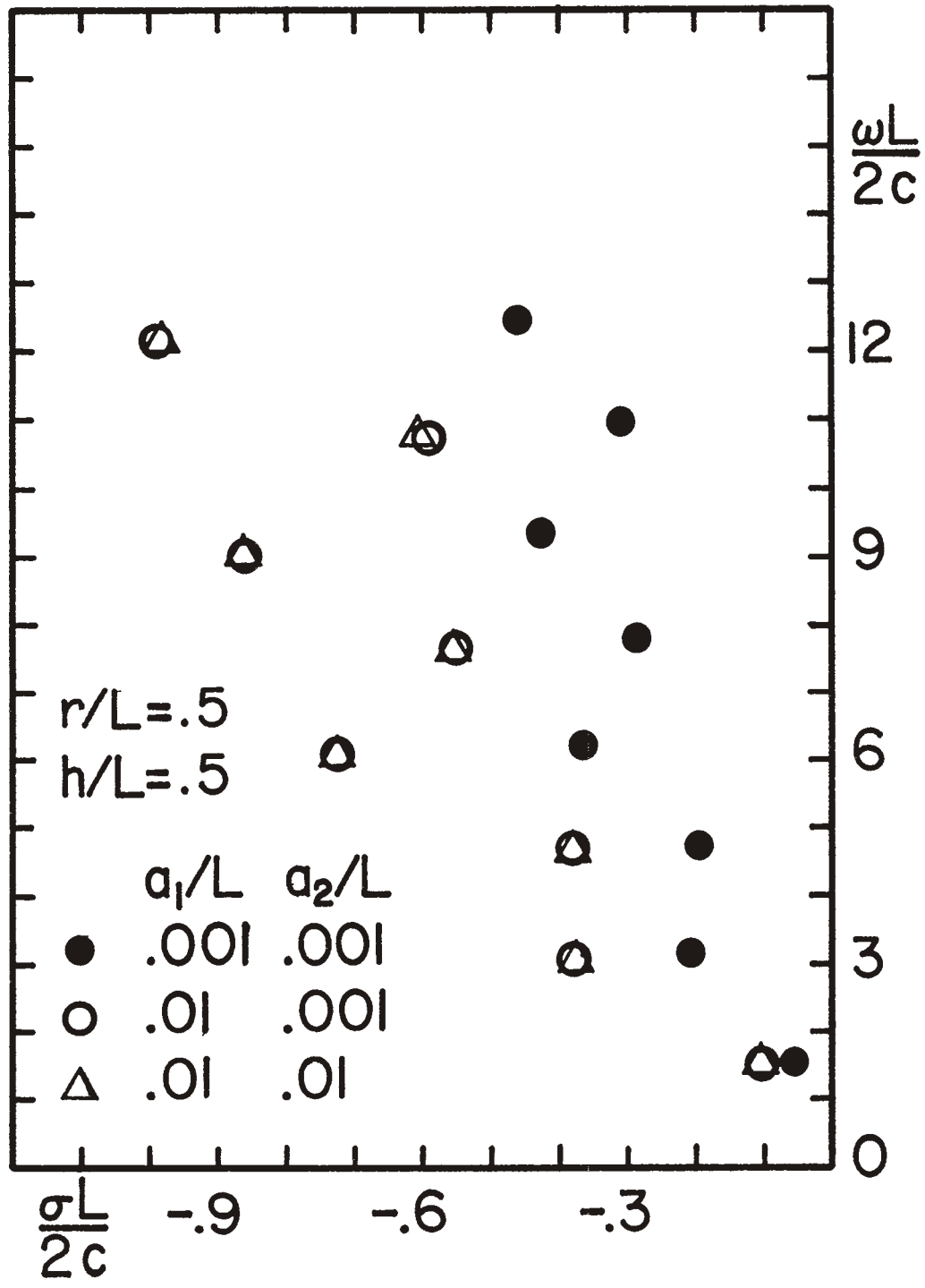

Figure 12. Natural frequencies of L-wire, r/L = 0.5.

poles in the same layer. This shift is attributed to the fact that (1) the coupling betweeen the two arms of the L-wire comes primarily from the region very near the bend and (2) the modal current is almost zero in the neighborhood of the bend for modes satisfying Eq. (5.1) and hence the two arms of the L-wire are relatively uncoupled. The uncoupling effectively results in two isolated wires both of which have larger radius-to-length ratios than does the whole structure and hence have resonant frequencies with larger damping constants. Conversely, poles s_{iq} where q satisfies

$$q = (m - \tfrac{1}{2})\left[\frac{L}{h}\right], \quad m = 1,2,\ldots, \tag{5.2}$$

correspond to the case where the bend is located approximately at an anti-node of the modal current, hence the arms of the L-wire are strongly coupled and the pole shifts to the right. If we follow the trajectory of a given pole as the bend position is continuously varied, the pole position should oscillate right and left as Eqs. (5.1) and (5.2) are alternately satisfied. This effect is shown in Fig. 13 for the first three poles in the $\ell = 1$ layer.

The effect of changes in wire radius on pole locations is illustrated in Figures 14 and 15, where the radii of both wires are the same and the radius is varied for three bend positions.

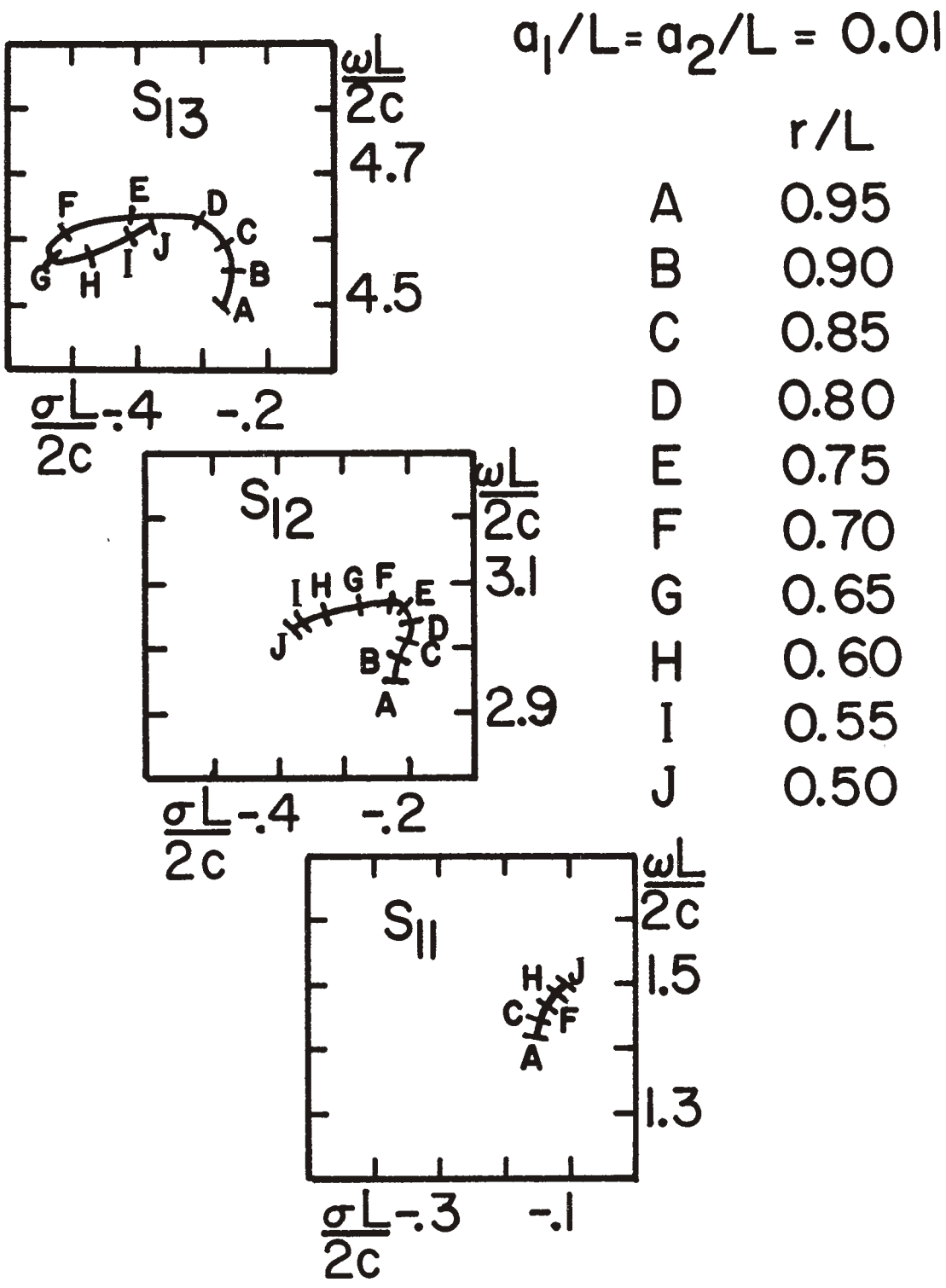

Figure 13. Trajectory of poles s_{11}, s_{12} and s_{13} as r/L is varied.

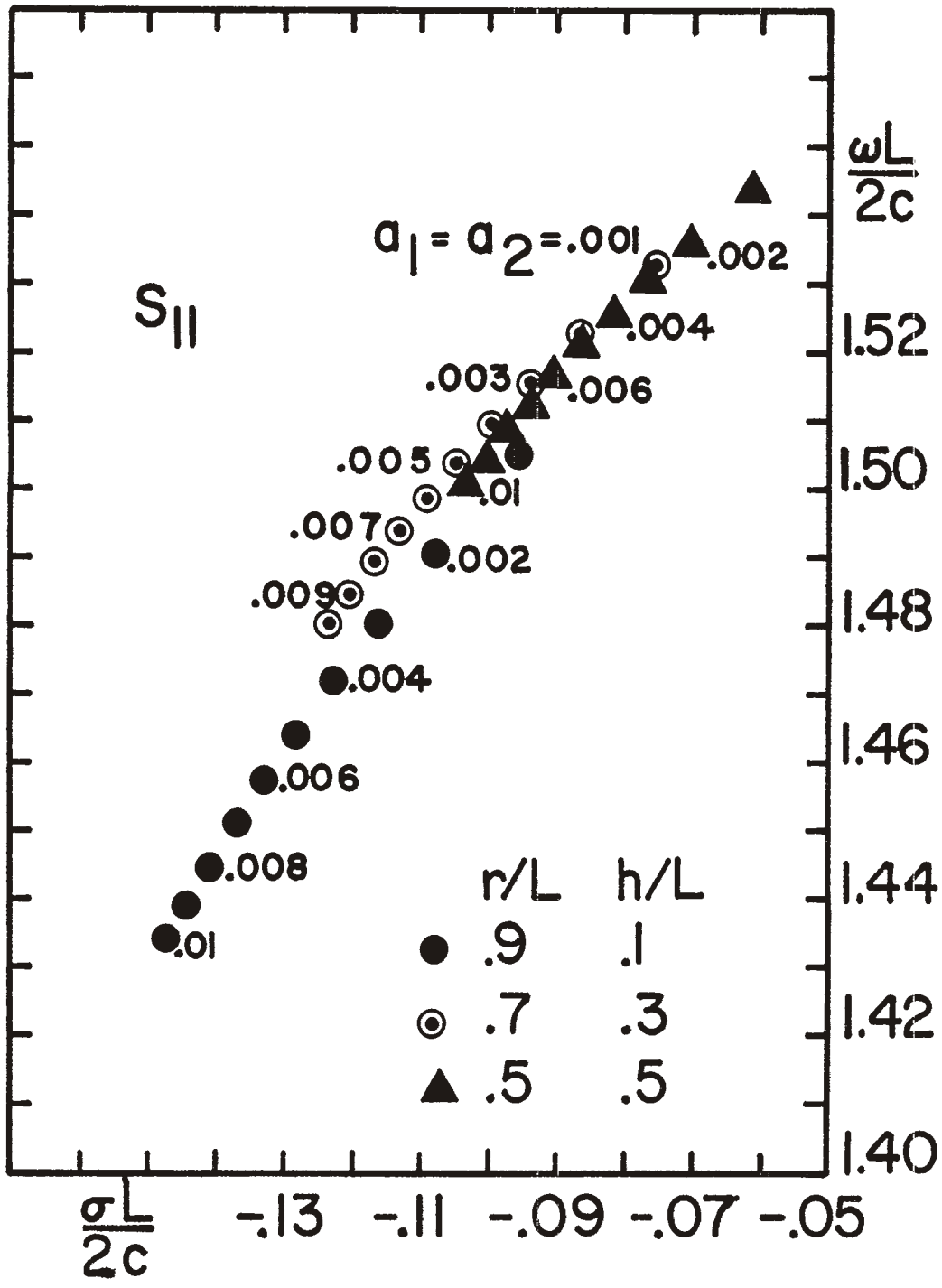

Figure 14. Trajectory of the pole s_{11} as a function of radius of L-wire.

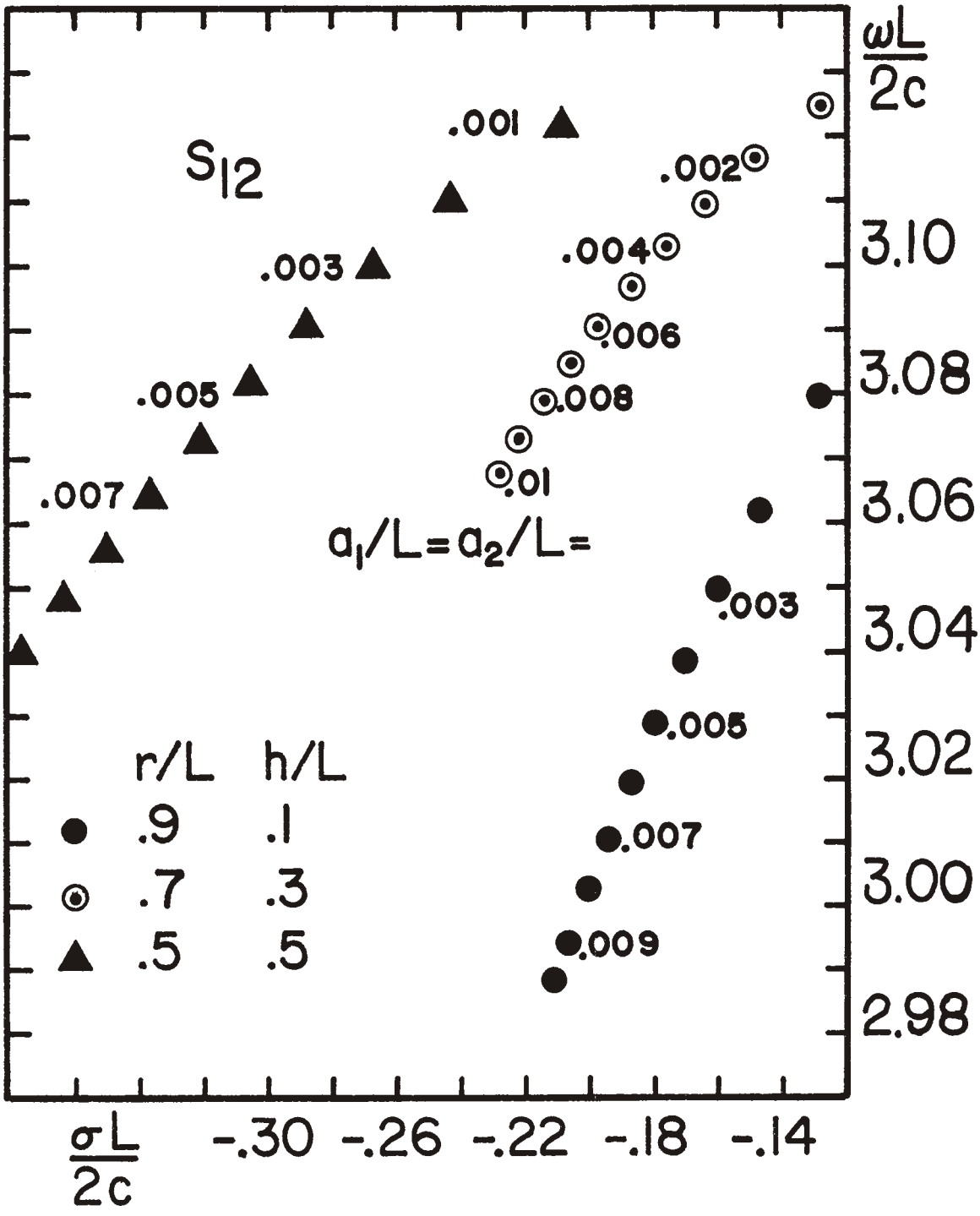

Figure 15. Trajectory of the pole s_{12} as a function of radius of L-wire.

Modal Currents and Charge Distributions, Coupling Coefficients

Figures 16-23 show the modal current and charge distributions as well as the coupling coefficients for a delta function plane wave excitation. The results given are for the first eight resonances in the $\ell = 1$ layer.

The curve designations relate to the various radii combinations according to the following key:

	$a_{1/L}$	$a_{2/L}$
Case A	0.001	0.001
Case B	0.001	0.01
Case C	0.01	0.001
Case D	0.01	0.01

When $r/L = 0.5$, cases B and C become identical if the wire arms are interchanged and hence only one of these cases is shown in the figures.

Current and charge distributions are shown as functions of the normalized position variable ζ/L measured from the wire end at $x = -r$ (Fig. 1). For convenience, the currents were found at only 29 points along the wire and linear interpolation was used to obtain the modal distributions shown. This was found to be a sufficient number of points to insure convergence of the pole locations as well as to approximately represent the modal currents at the highest

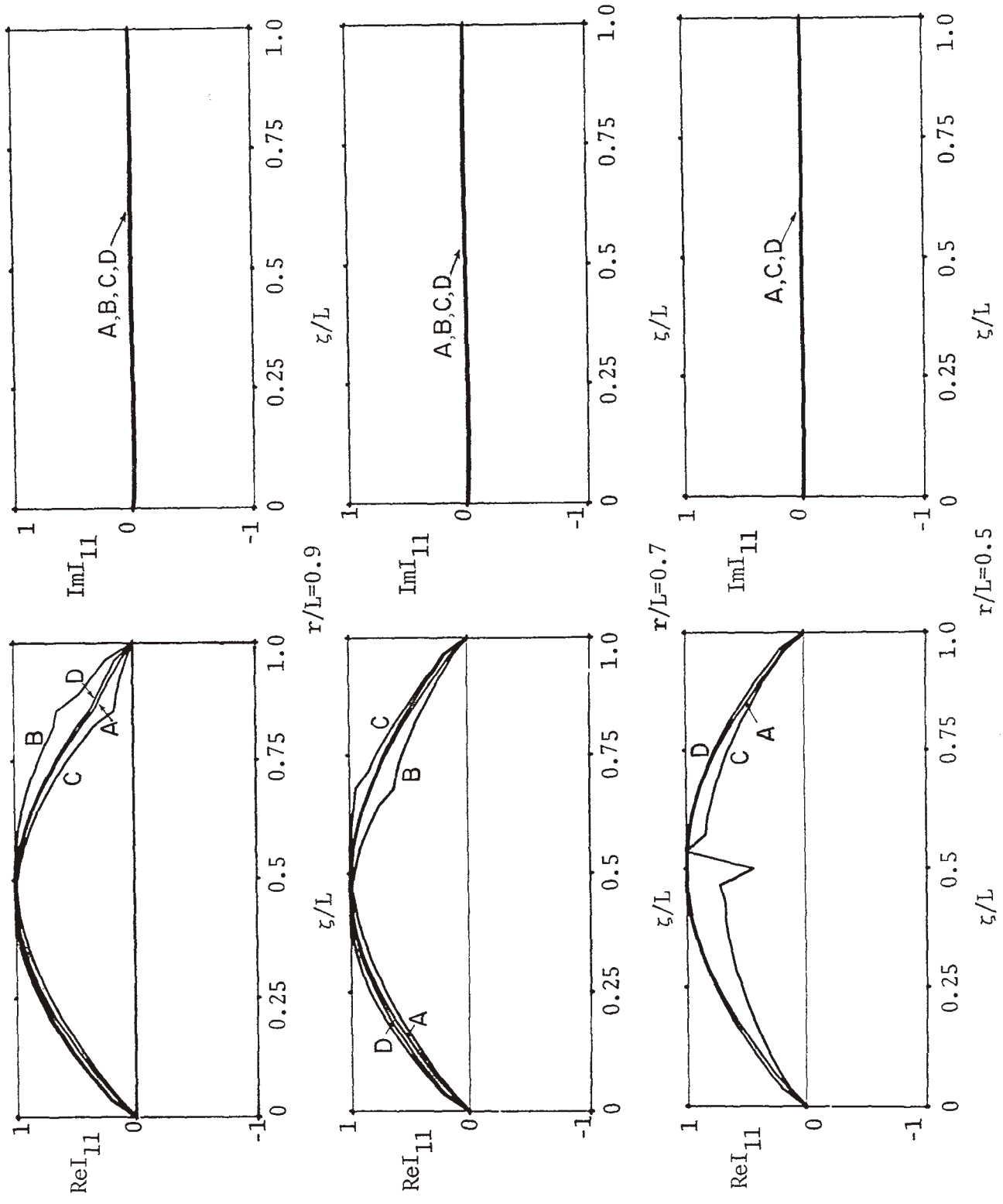

Figure 16a. Current distribution of natural modes of L-wire for resonant frequency s_{11}.

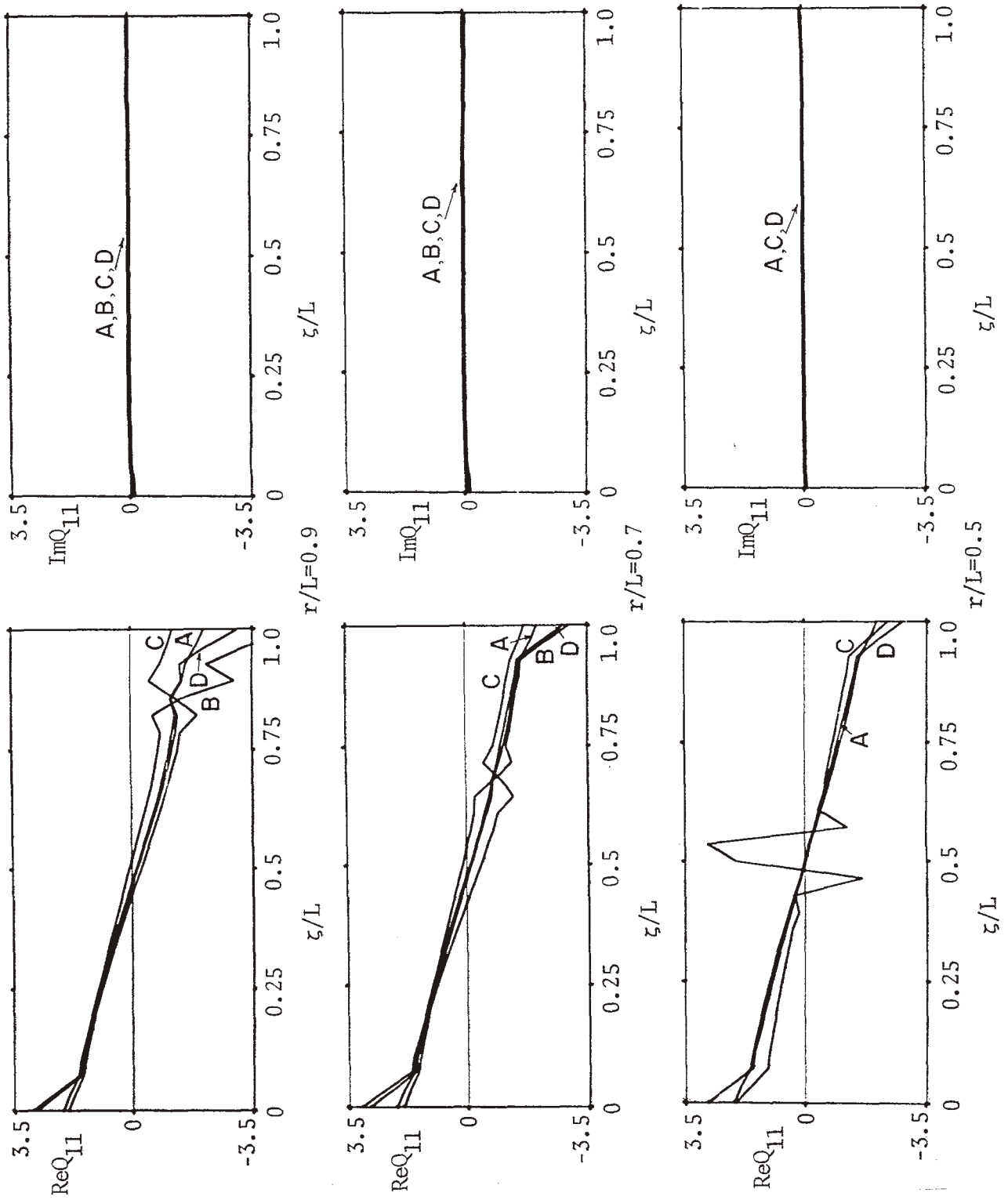

Figure 16b. Charge distribution of natural modes of L-wire for resonant frequency s_{11}.

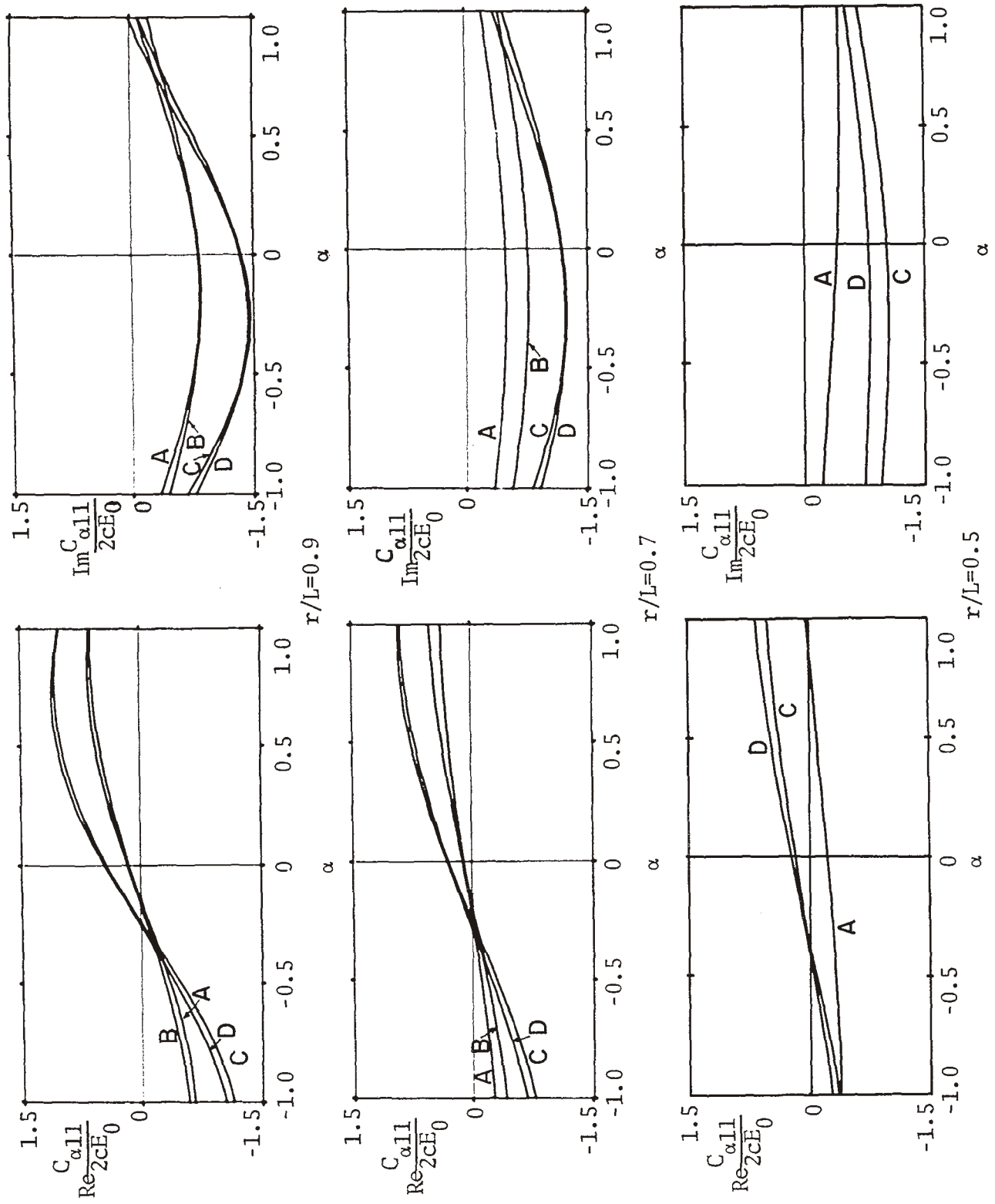

Figure 16c. Coupling coefficient C_α in milliampere of L-wire for resonant frequency s_{11} as a function of α.

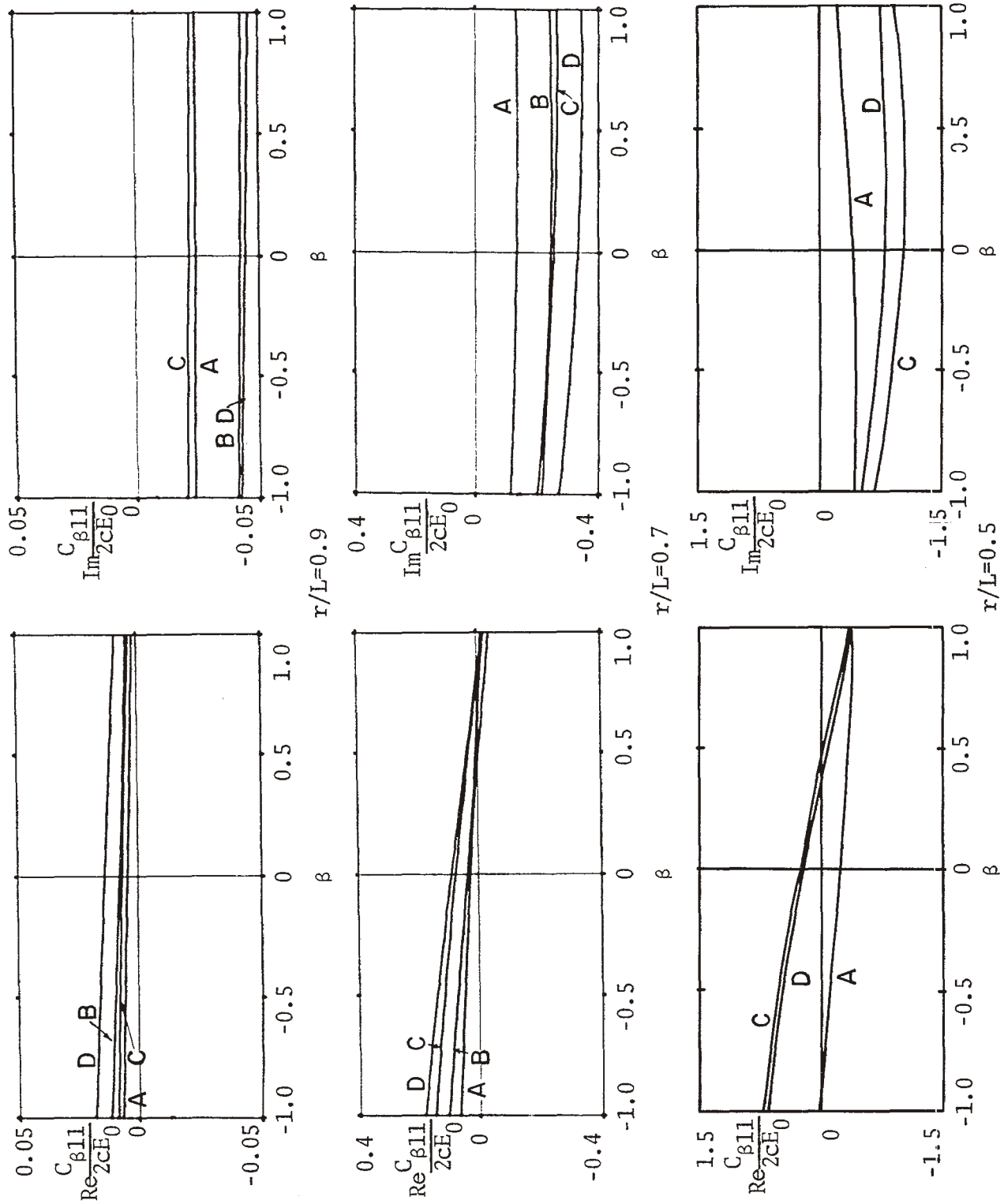

Figure 16d. Coupling coefficient C_β in milliampere of L-wire for resonant frequency s_{11} as a function of β.

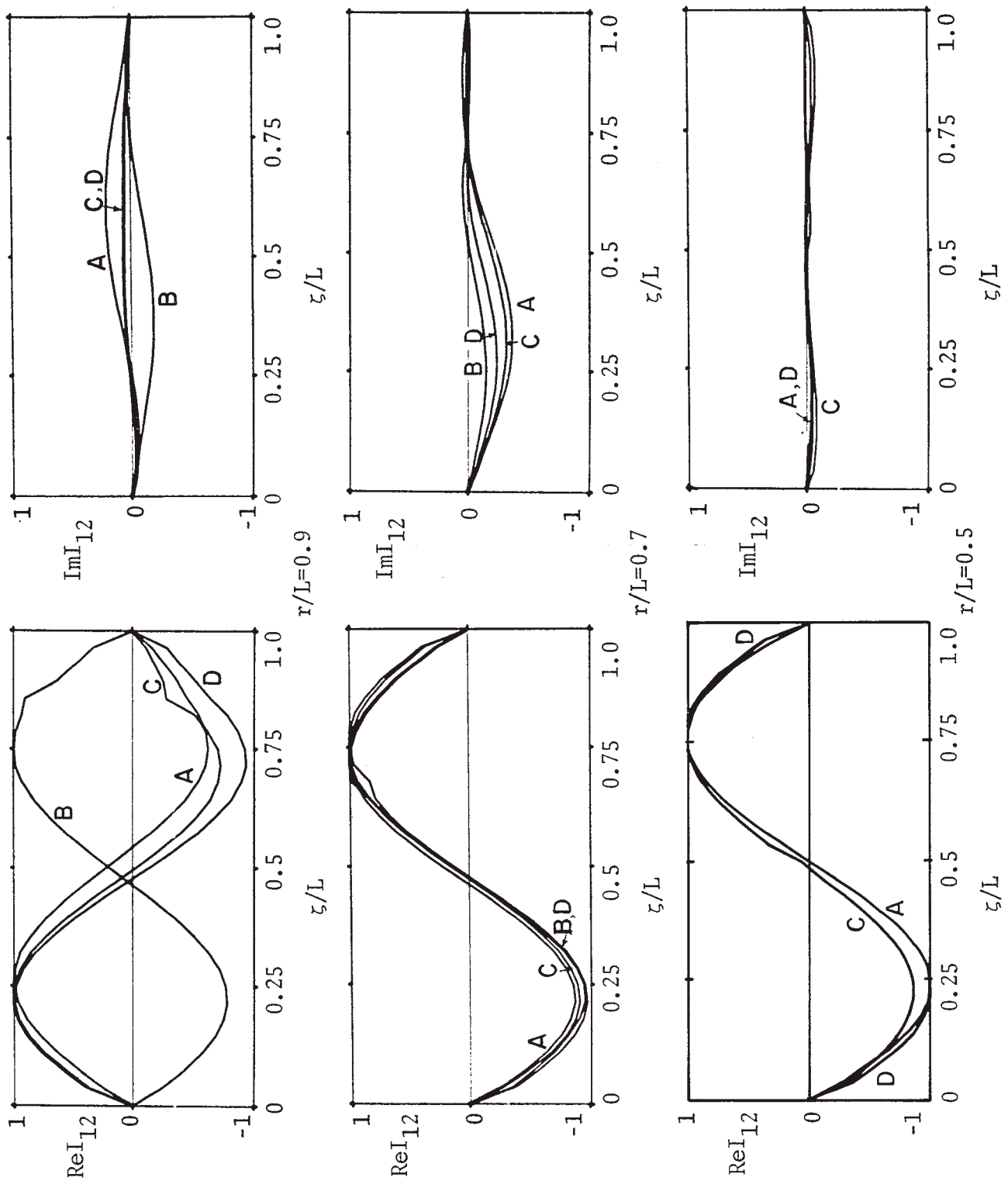

Figure 17a. Current distributions of natural modes of L-wire for resonant frequency s_{12}.

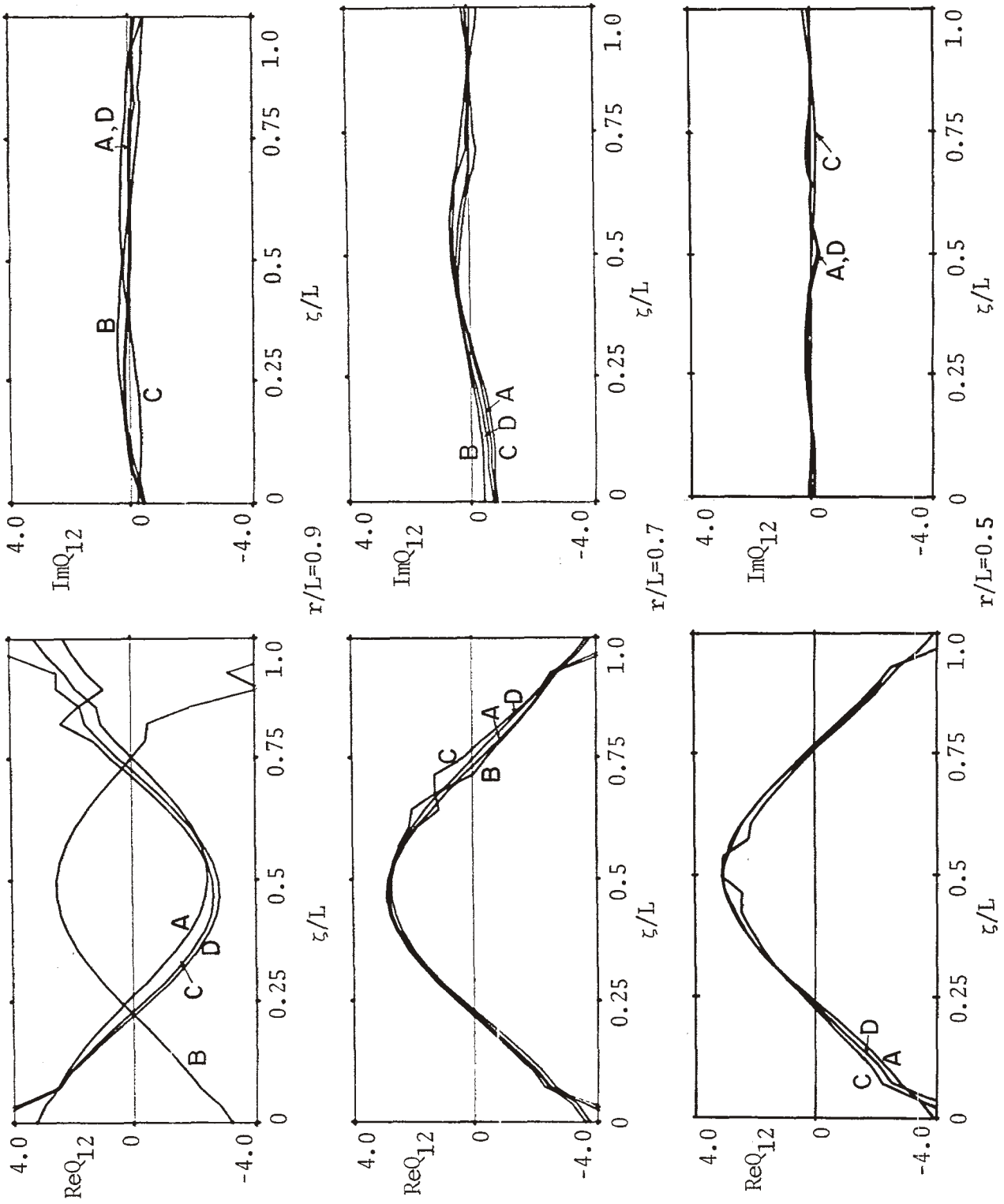

Figure 17b. Charge distribution of natural modes of L-wire for resonant frequency s_{12}.

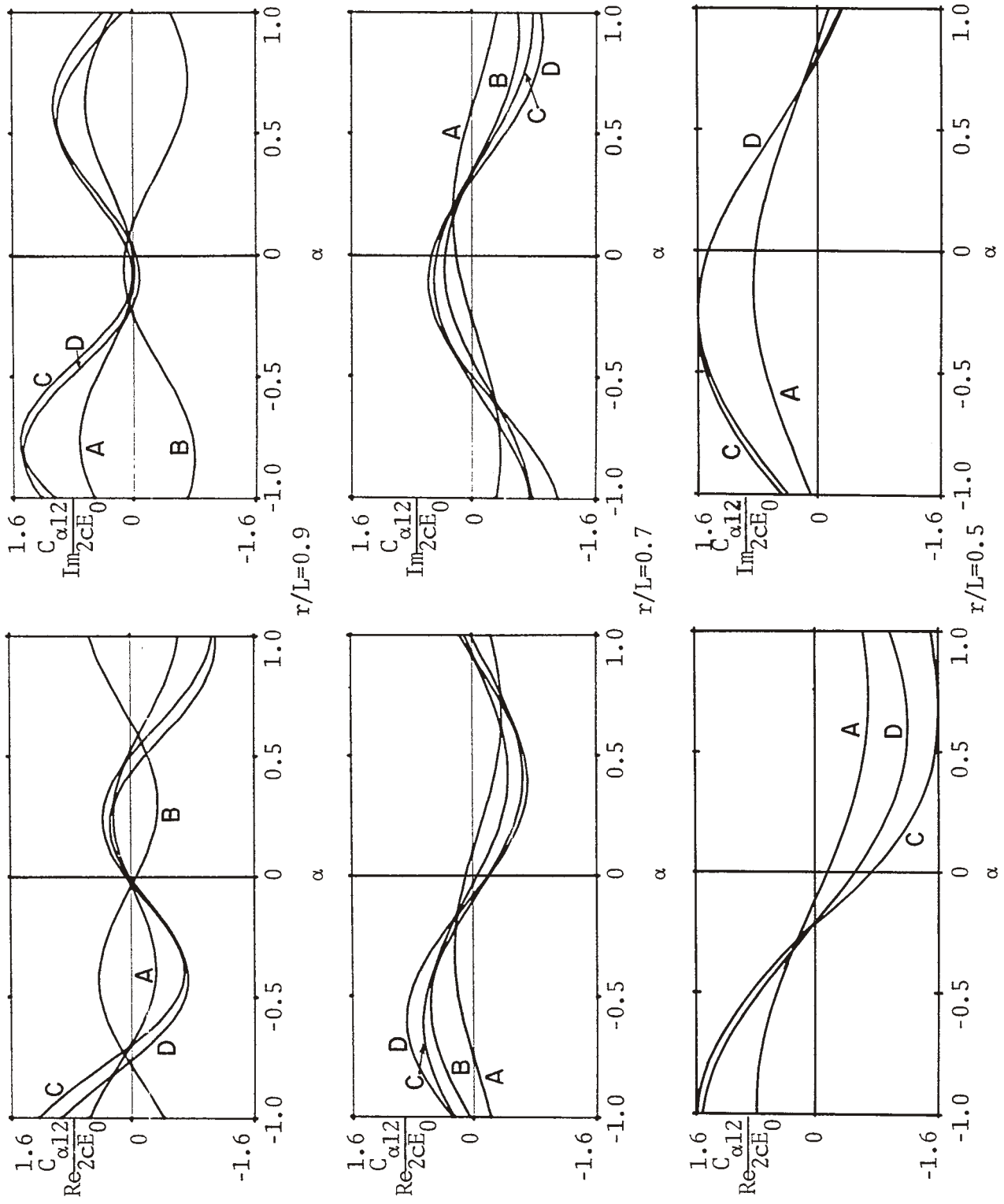

Figure 17c. Coupling coefficient C_α in milliampere of L-wire for resonant frequency s_{12} as a function of α.

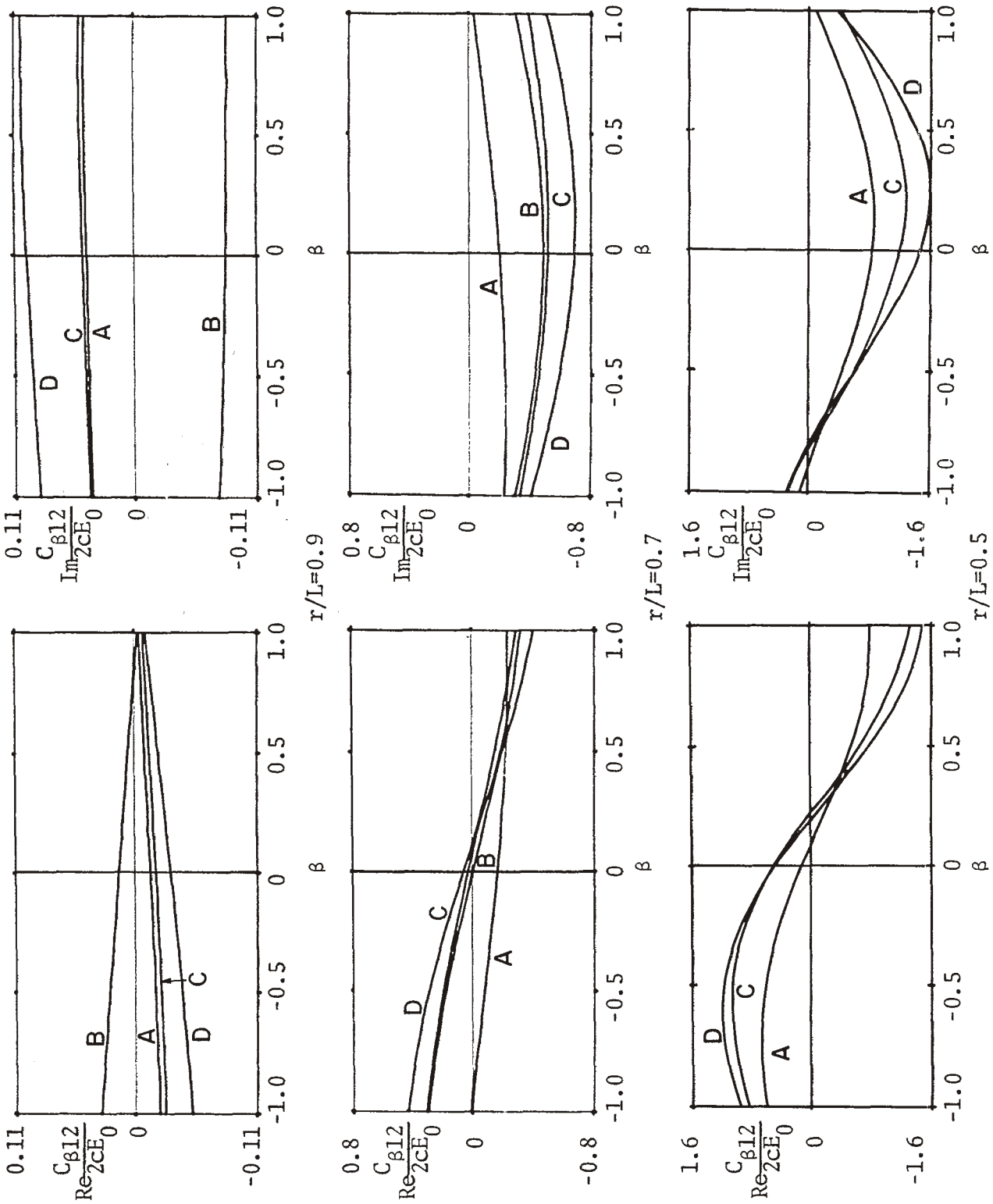

Figure 17d. Coupling coefficients C_β in milliampere of L-wire for resonant frequency s_{12} as a function of β.

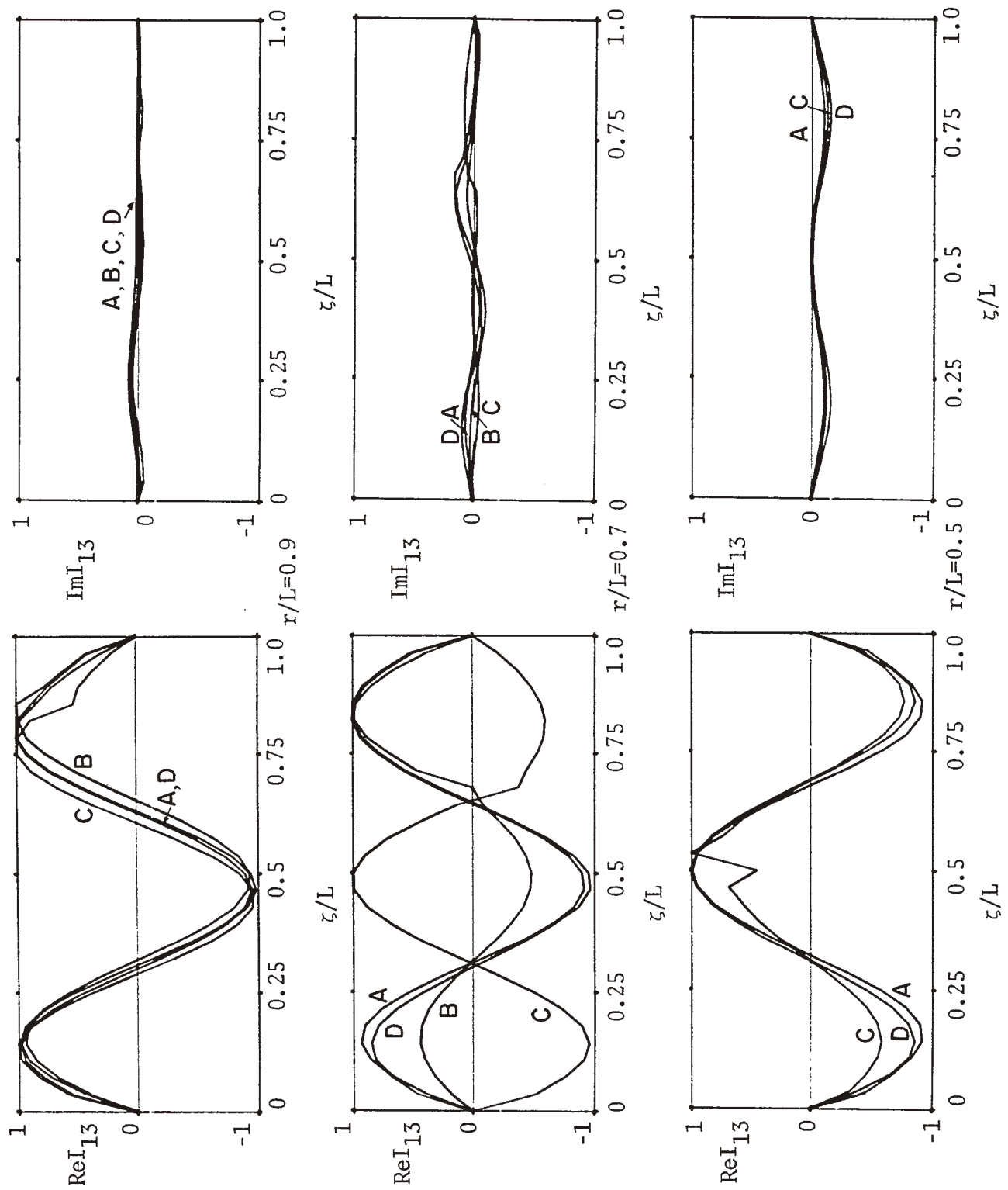

Figure 18a. Current distribution of natural modes of L-wire for resonant frequency s_{13}.

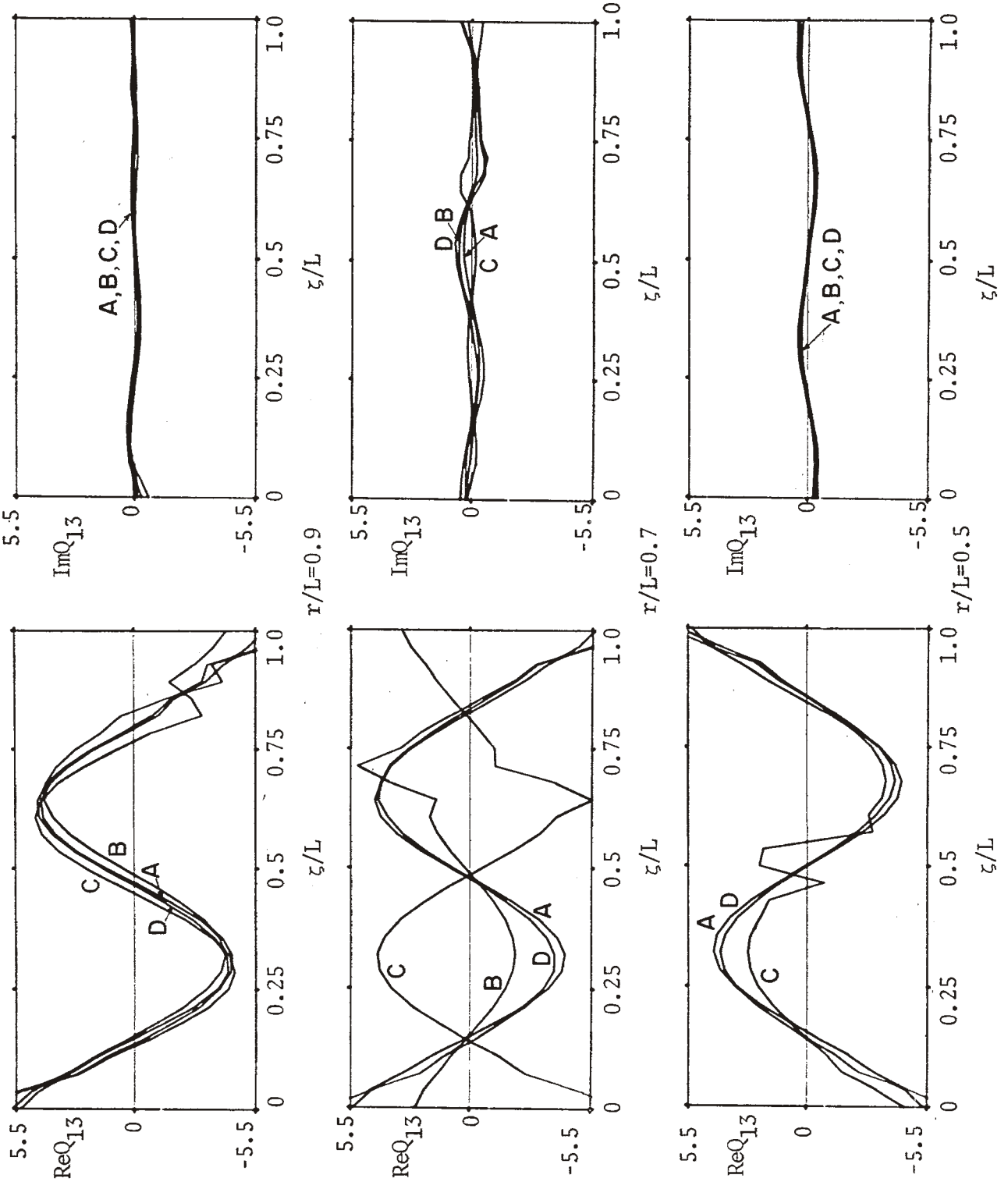

Figure 18b. Charge distribution of natural modes of L-wire for resonant frequency s_{13}.

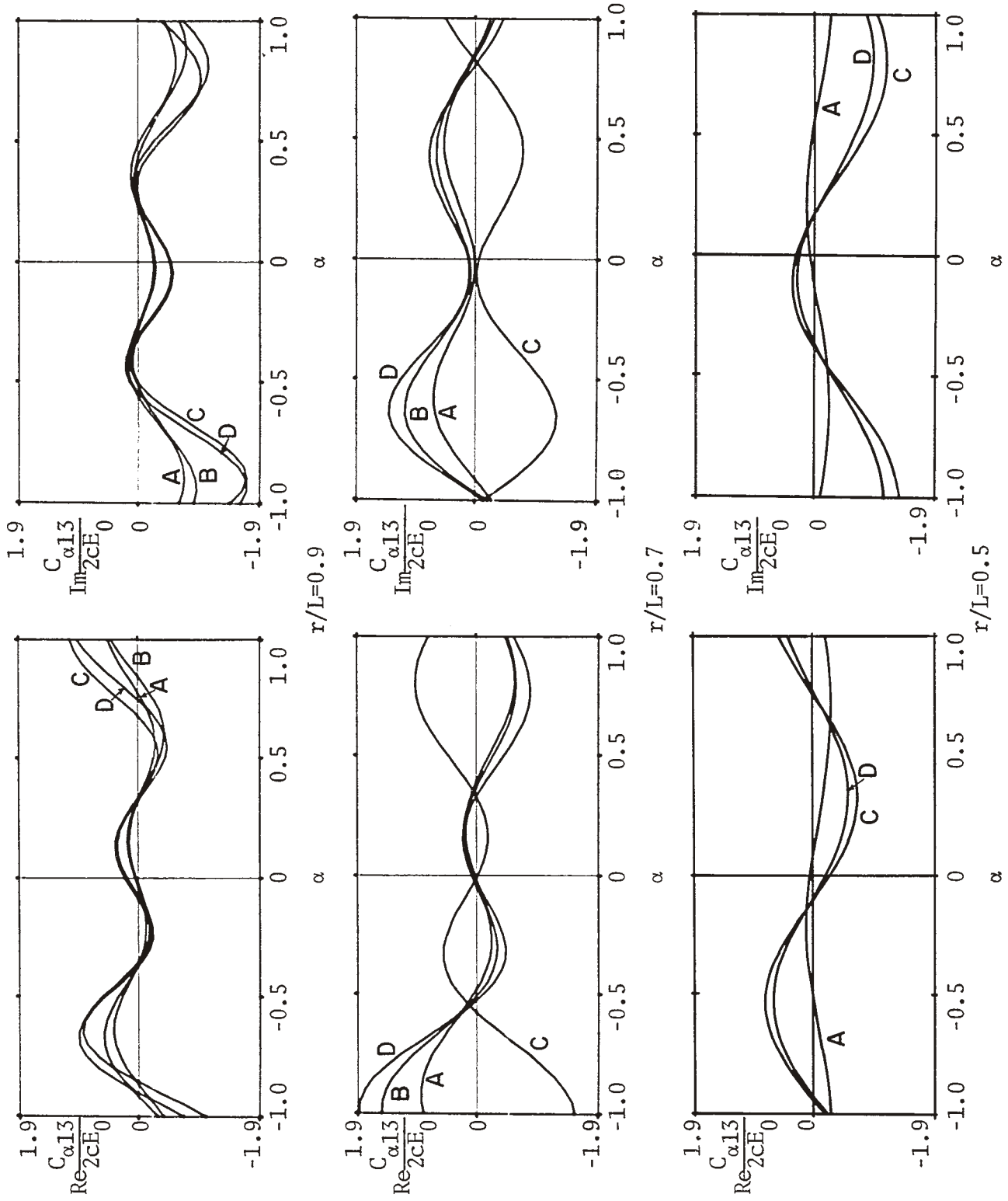

Figure 18c. Coupling coefficient C_α in milliampere of L-wire for resonant frequency s_{13} as a function of α.

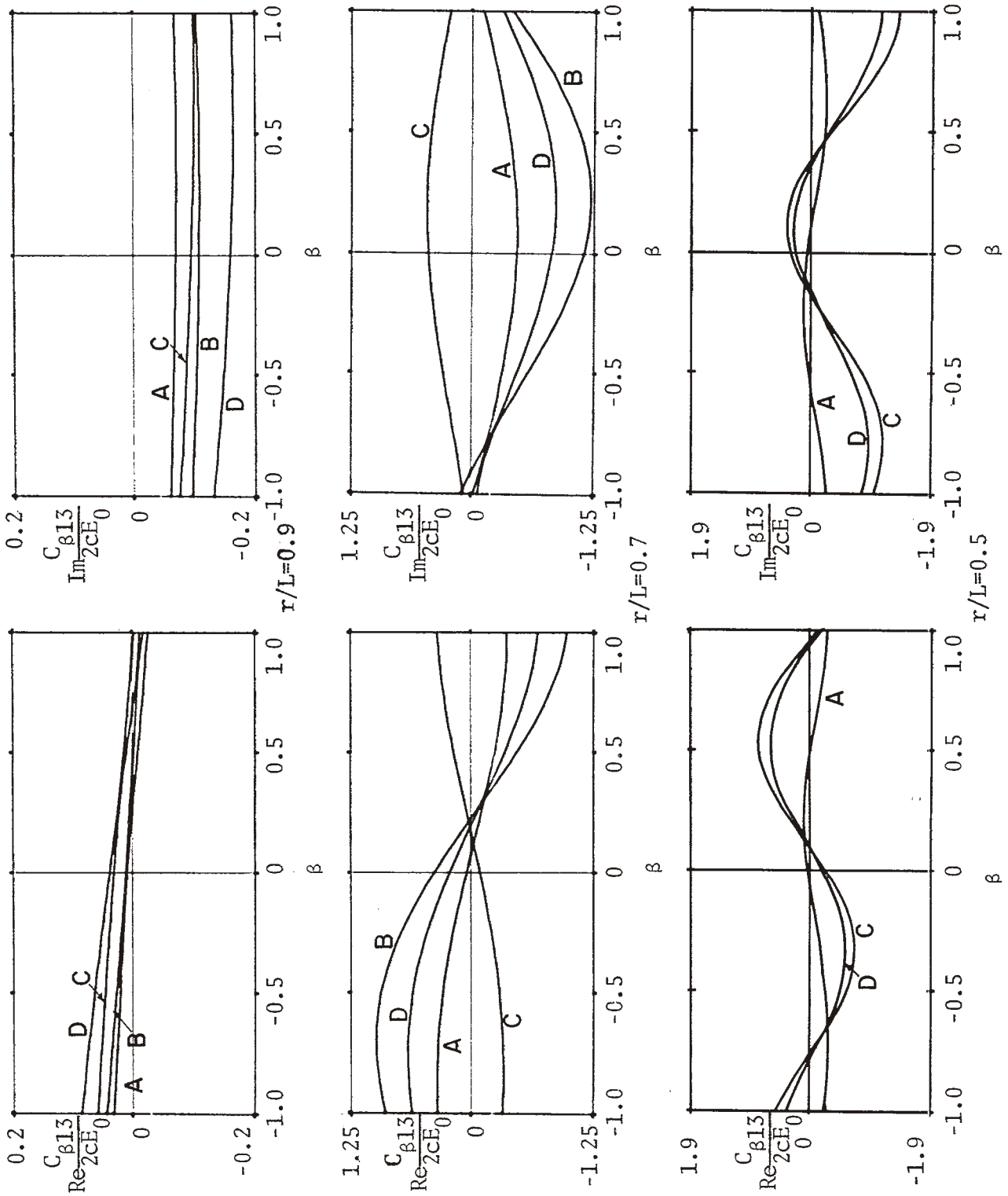

Figure 18d. Coupling coefficient C_{β} in milliampere of L-wire for resonant frequency s_{13} as a function of β.

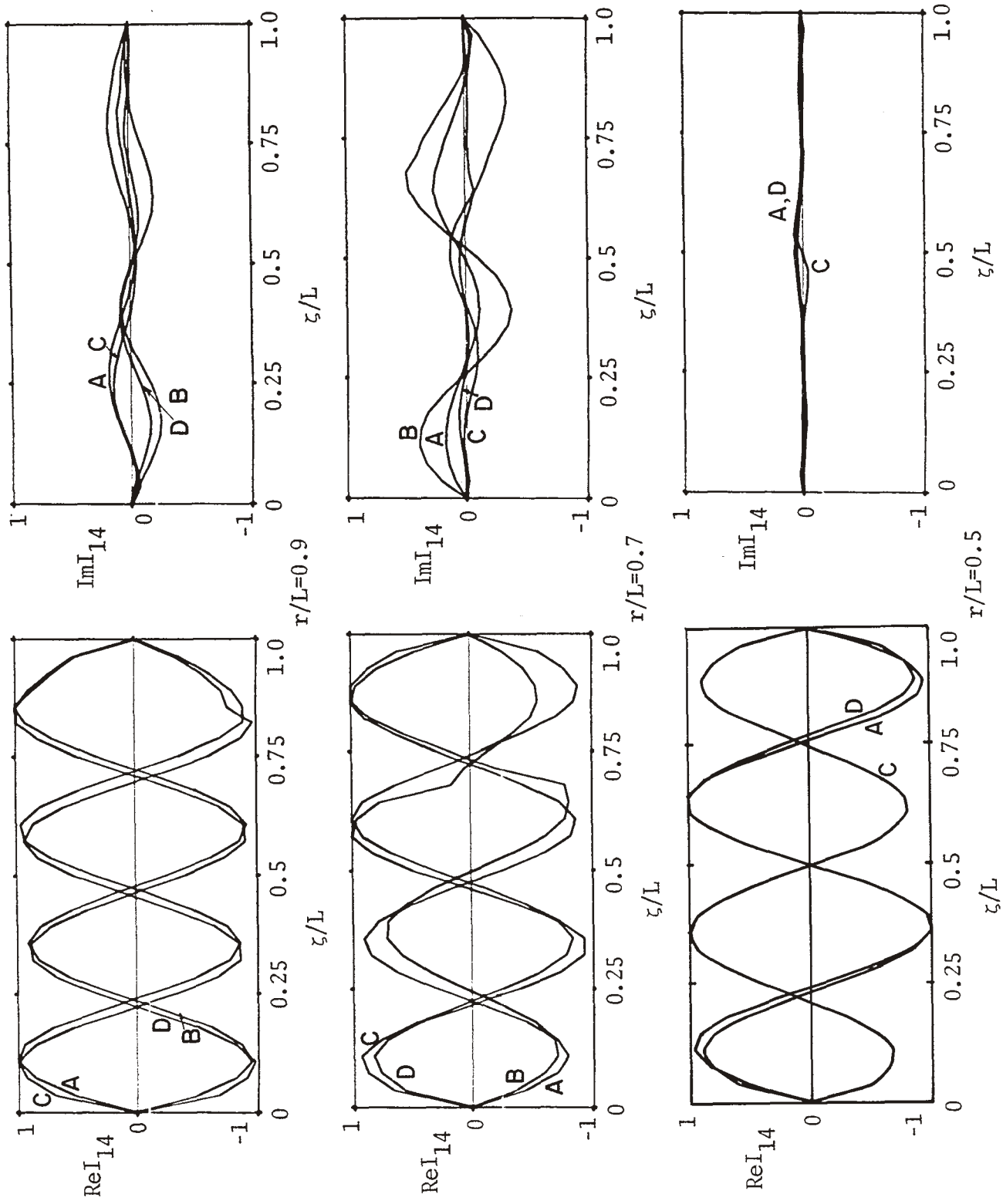

Figure 19a. Current distribution of natural modes of L-wire for resonant frequency s_{14}.

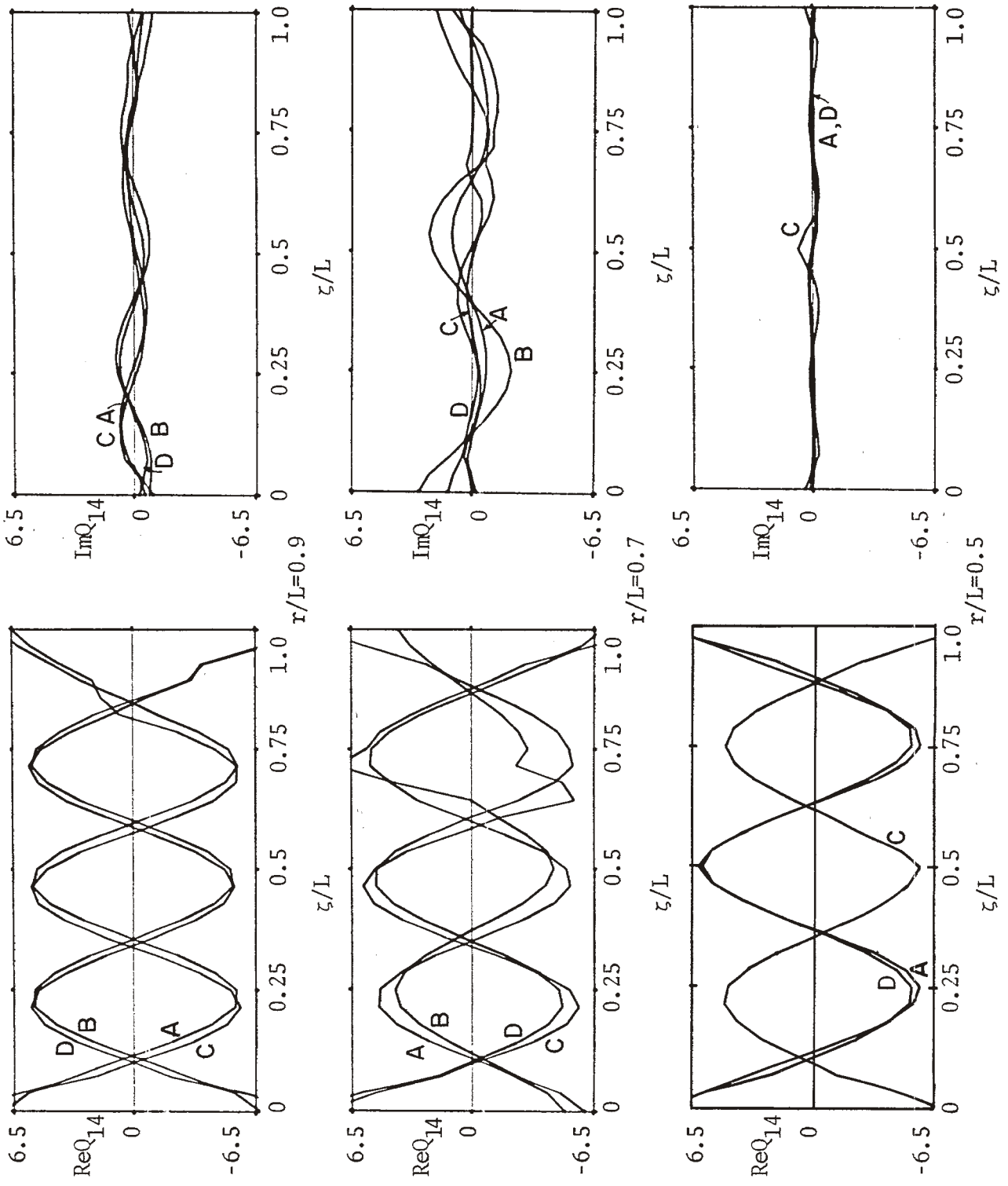

Figure 19b. Charge distribution of natural modes of L-wire for resonant frequency s_{14}.

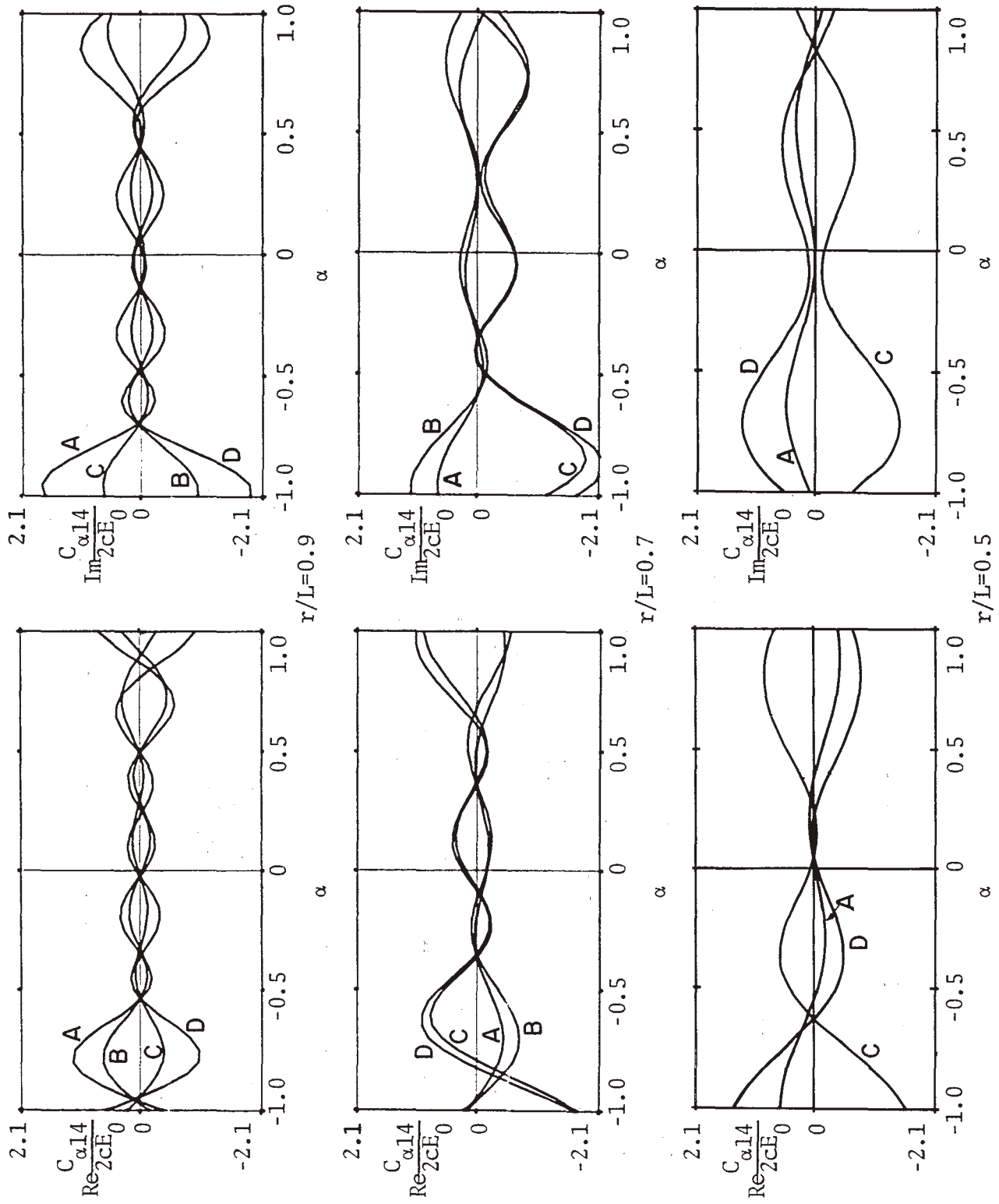

Figure 19c. Coupling coefficient C_α in milliampere of L-wire for resonant frequency s_{14} as a function of α.

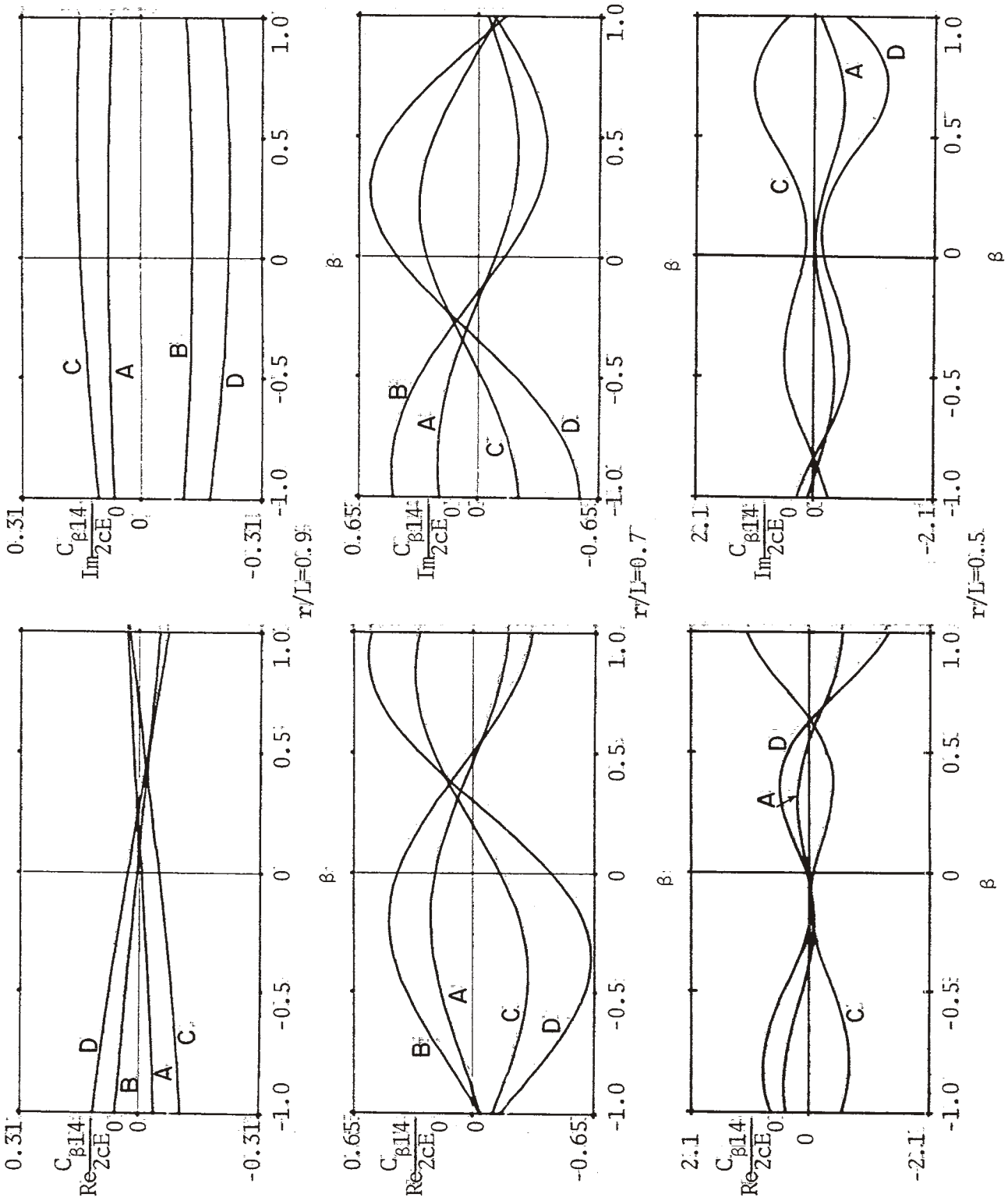

Figure 19d. Coupling coefficient C_{β} in milliampere of L-wire for resonant frequency s_{14} as a function of β.

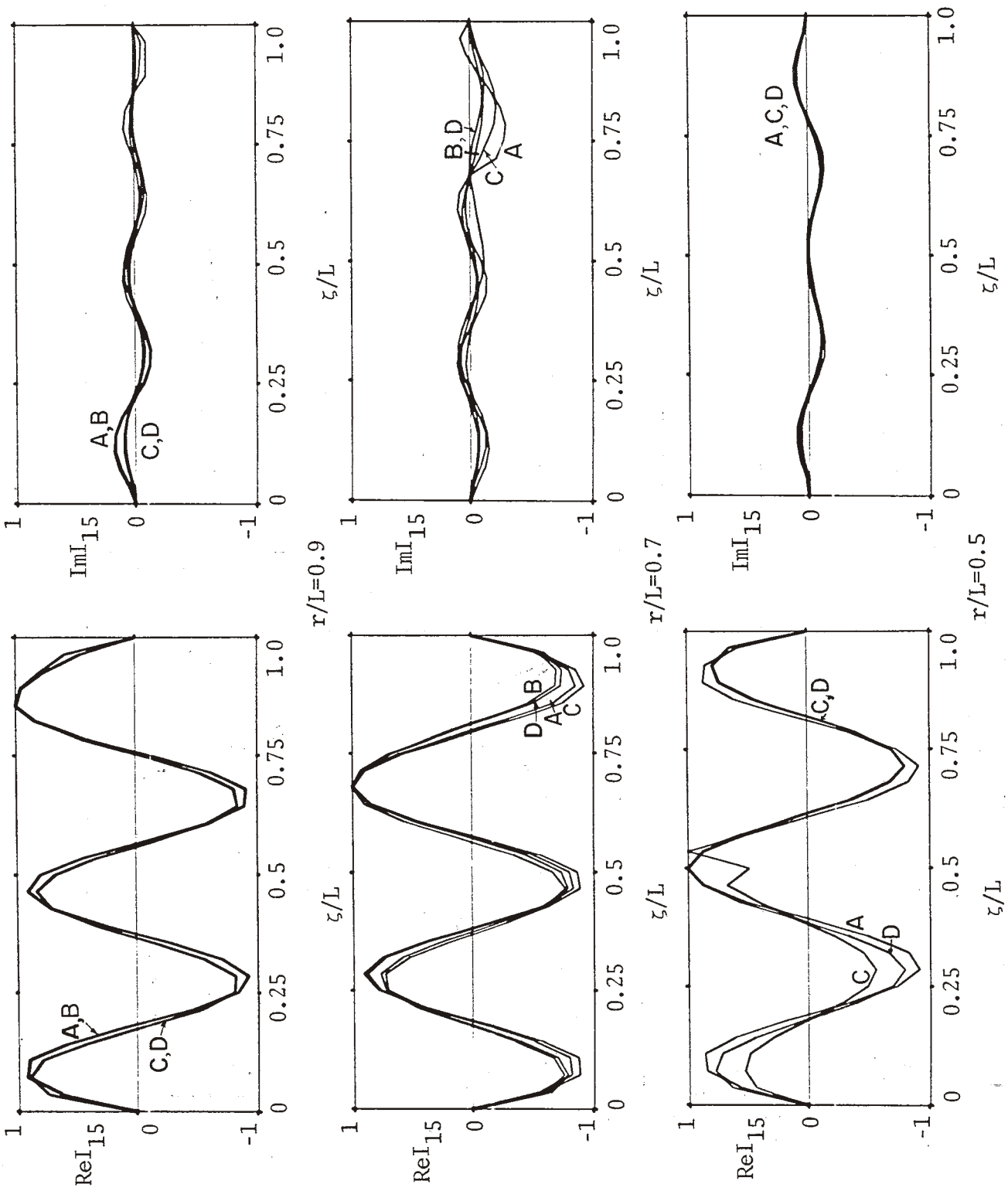

Figure 20a. Current distribution of natural modes of L-wire for resonant frequency s_{15}.

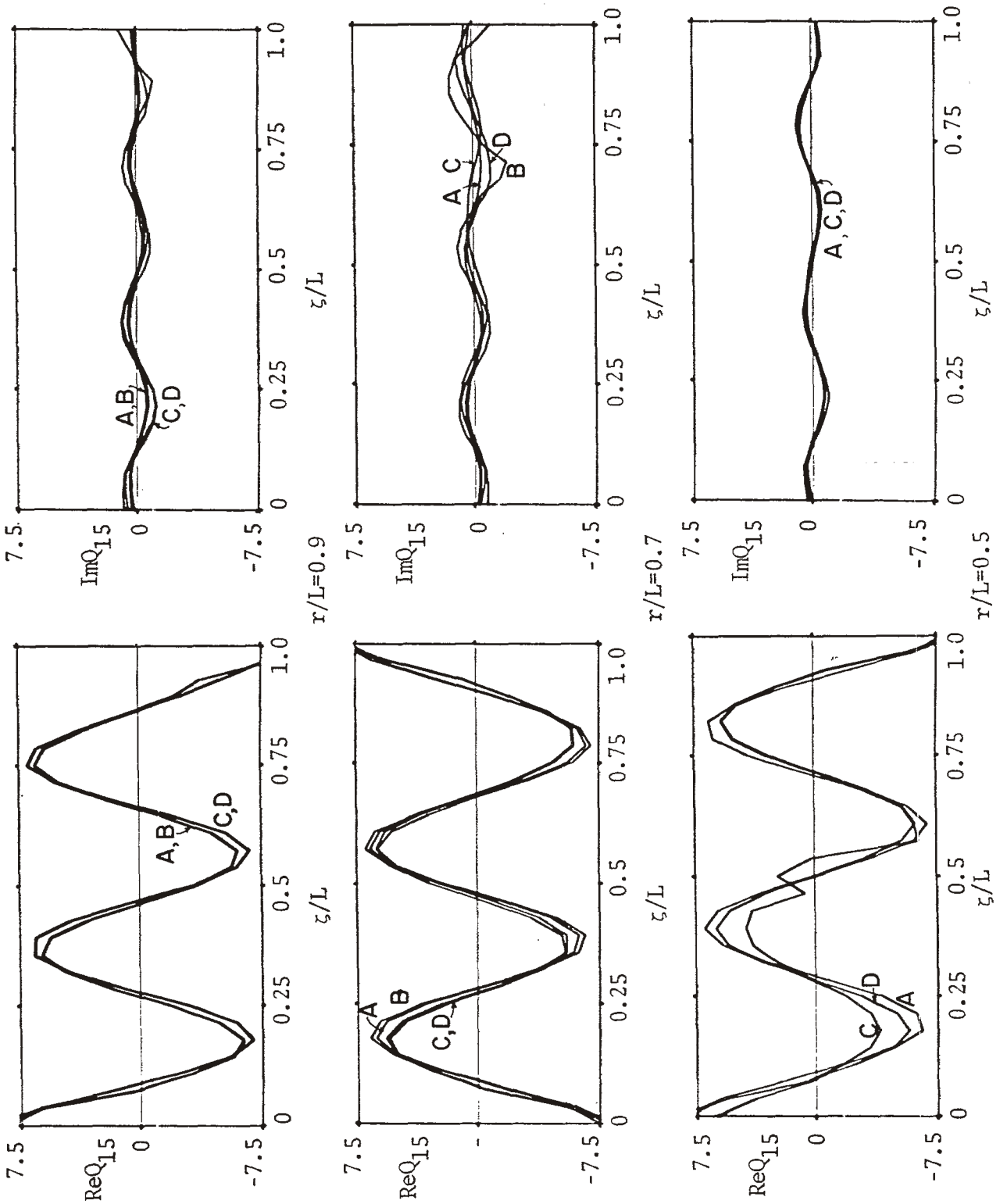

Figure 20b. Charge distribution of natural modes of L-wire for resonant frequency s_{15}.

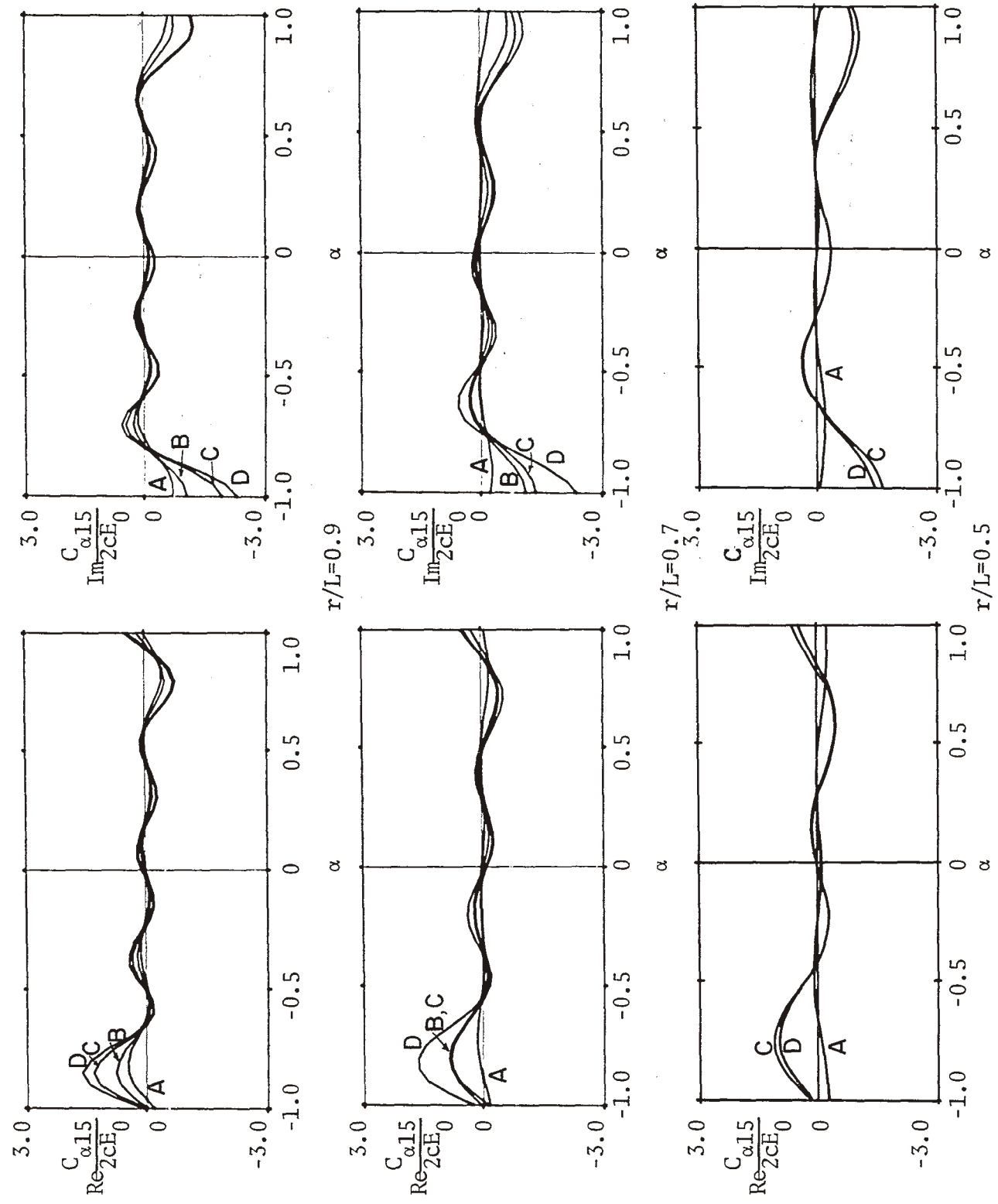

Figure 20c. Coupling coefficient C_α in milliamperer of L-wire for resonant frequency s_{15} as a function of α.

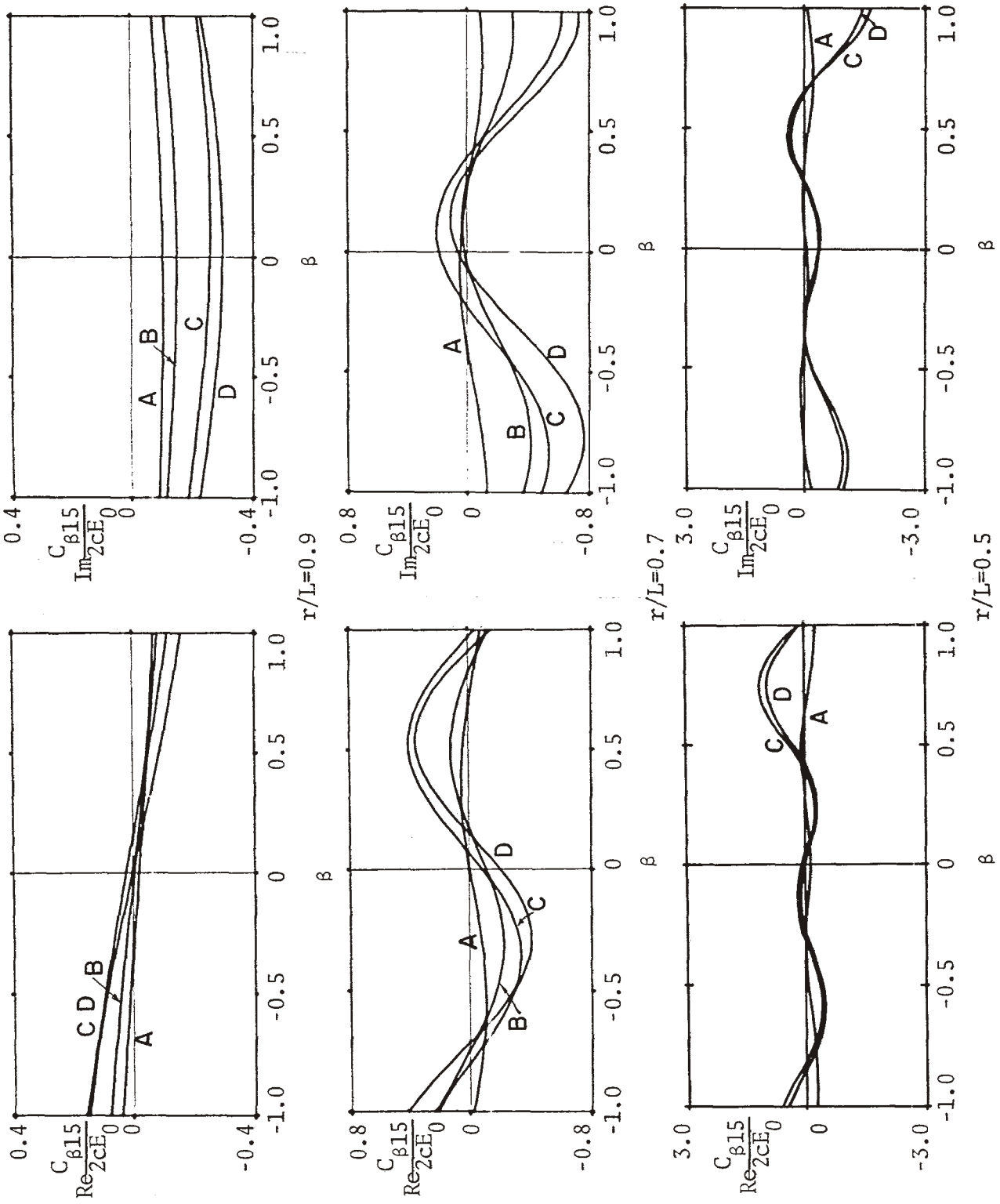

Figure 20d. Coupling coefficient C_β in milliampere of L-wire for resonant frequency s_{15} as a function of β.

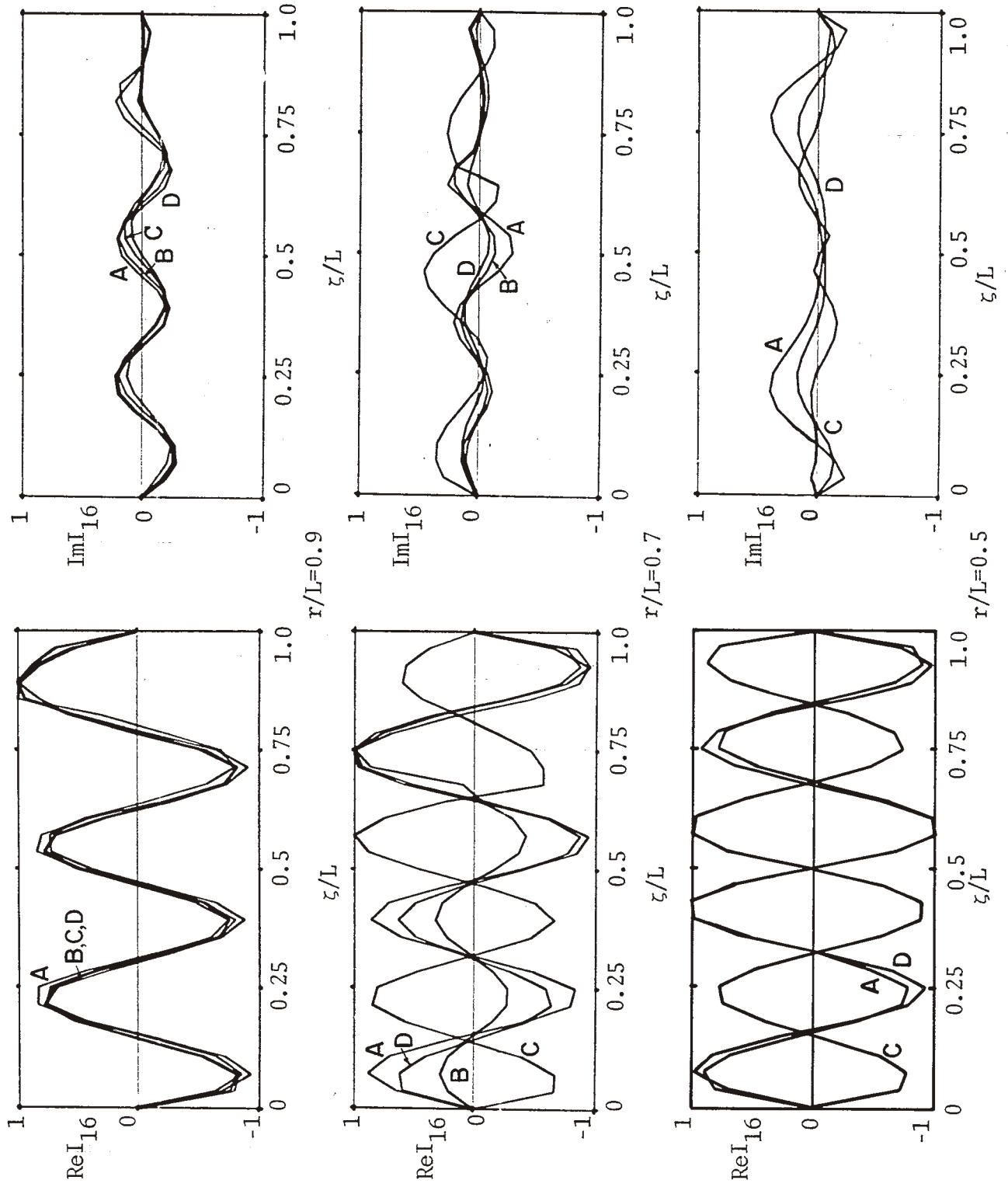

Figure 21a. Current distribution of natural modes of L-wire for resonant frequency s_{16}.

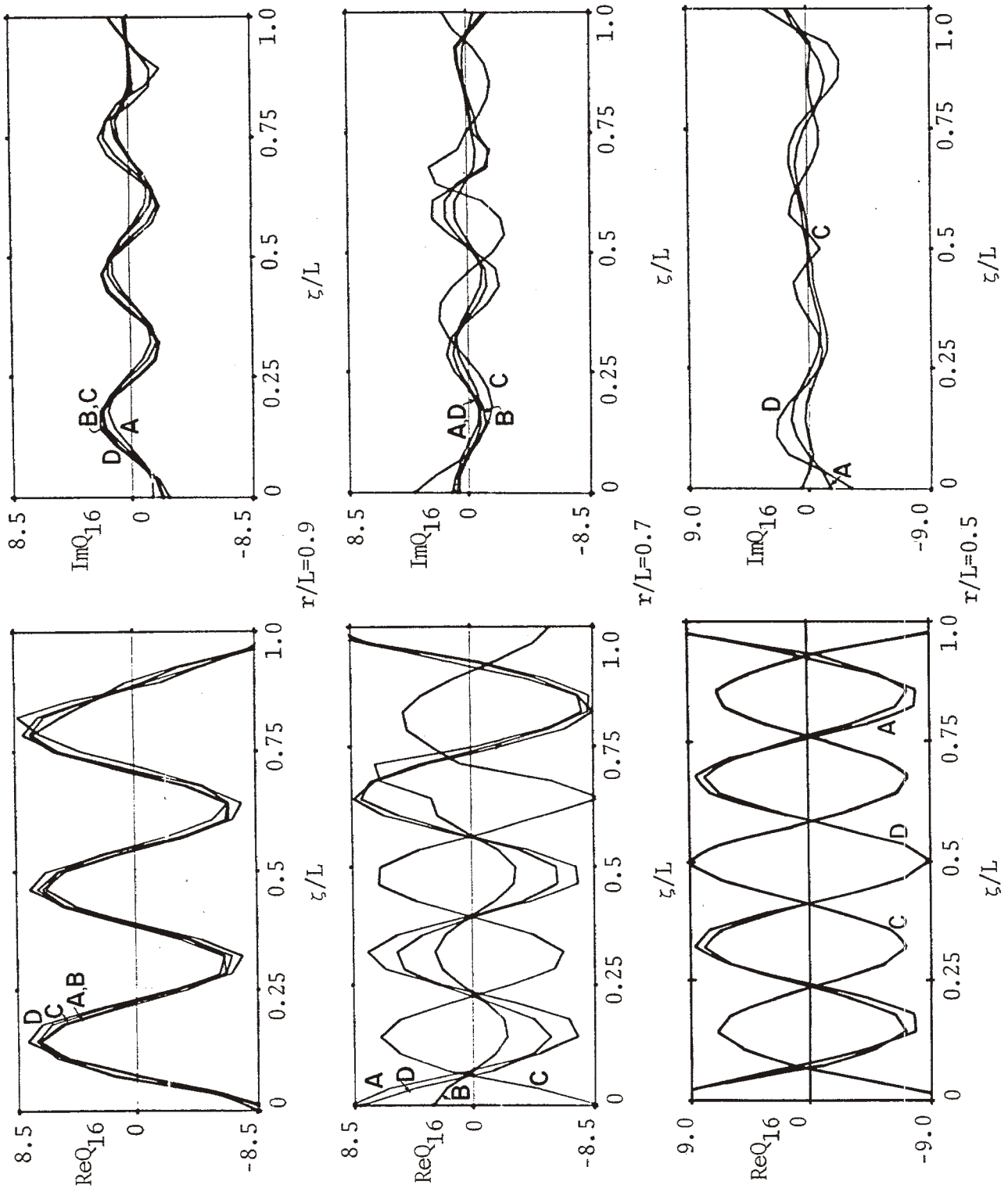

Figure 21b. Charge distribution of natural modes of L-wire for resonant frequency s_{16}.

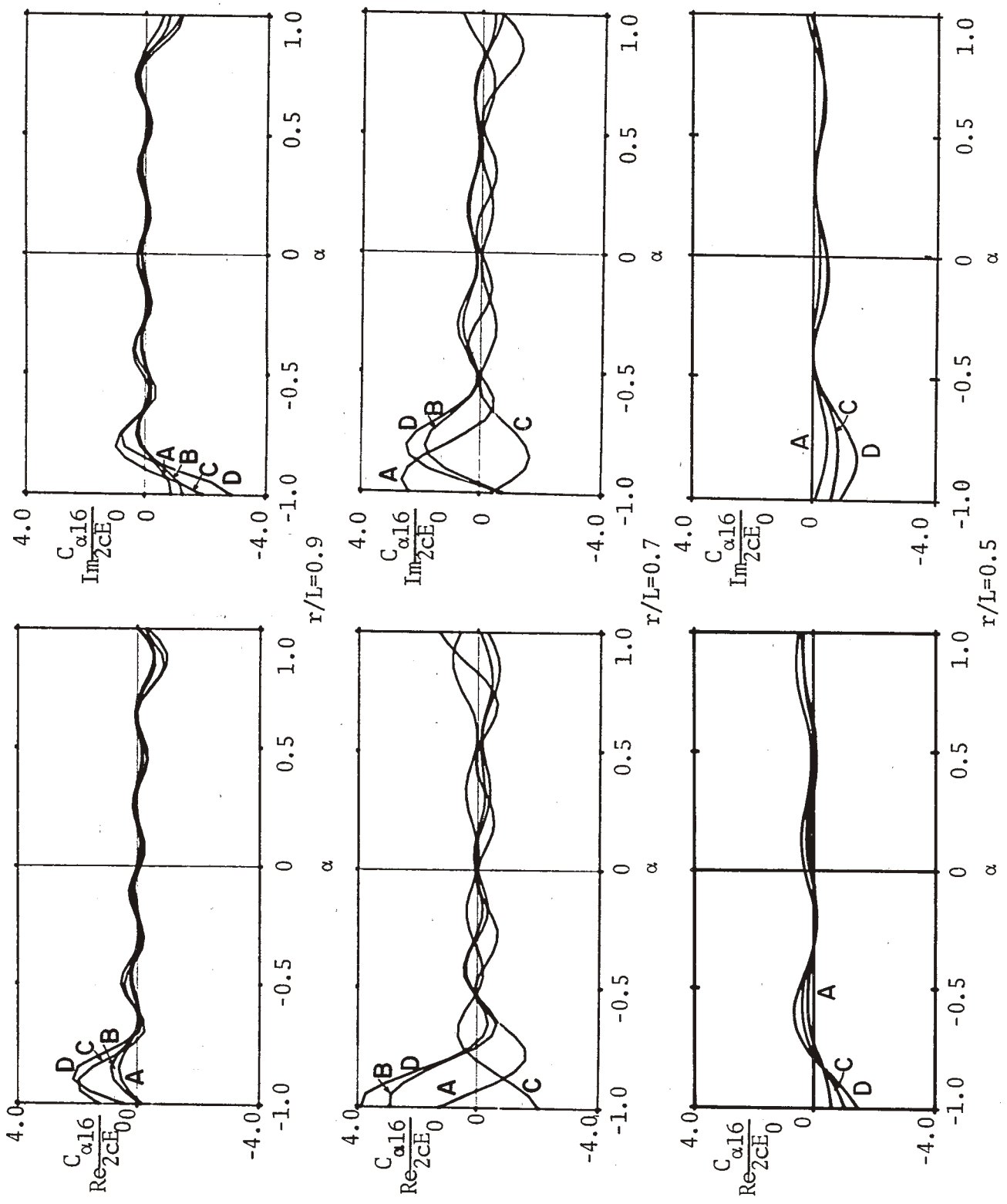

Figure 21c. Coupling coefficient C_{α} in milliampere of L-wire for resonant frequency s_{16} as a function of α.

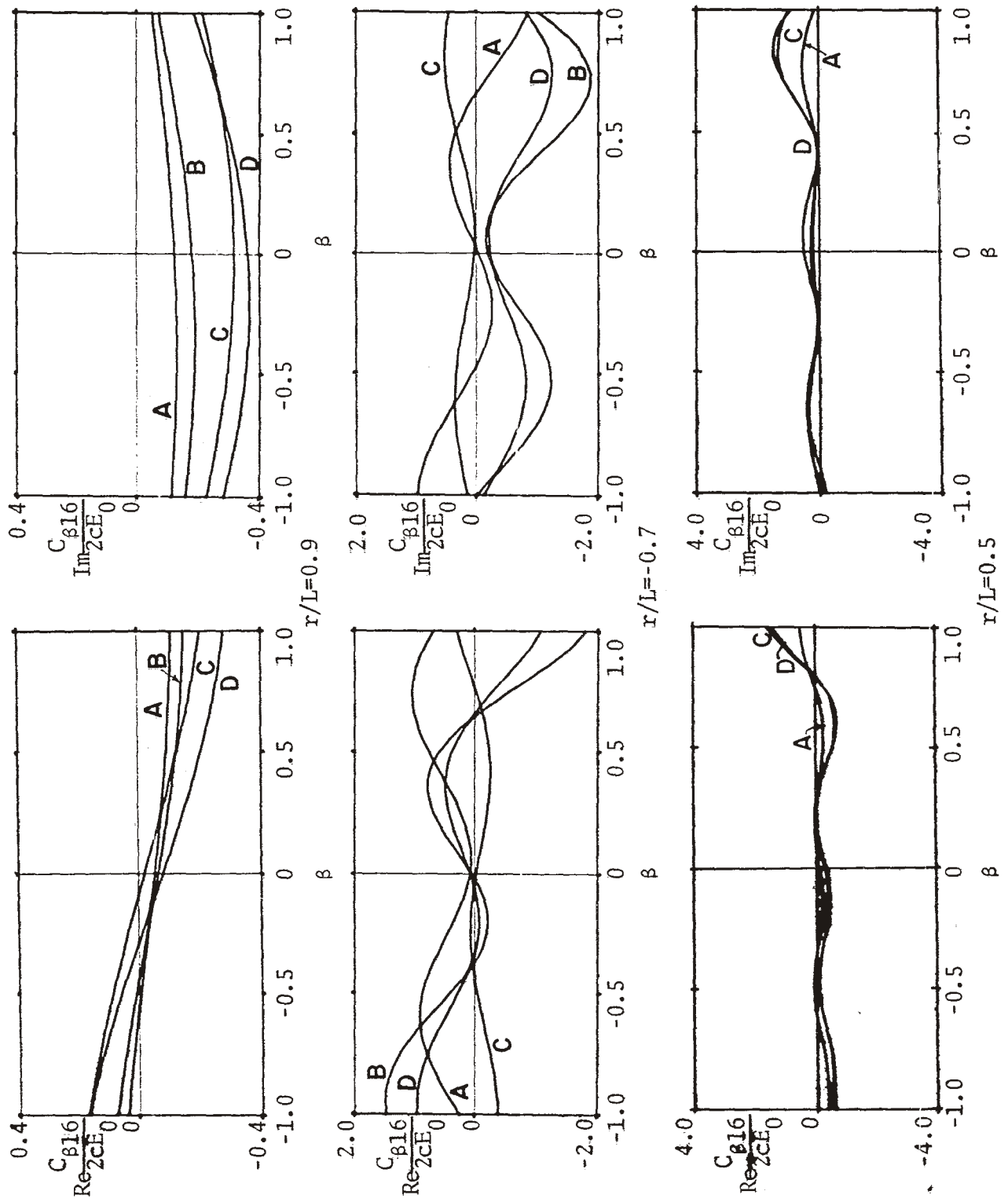

Figure 21d. Coupling coefficient C_β in milliampere of L-wire for resonant frequency s_{16} as a function of β.

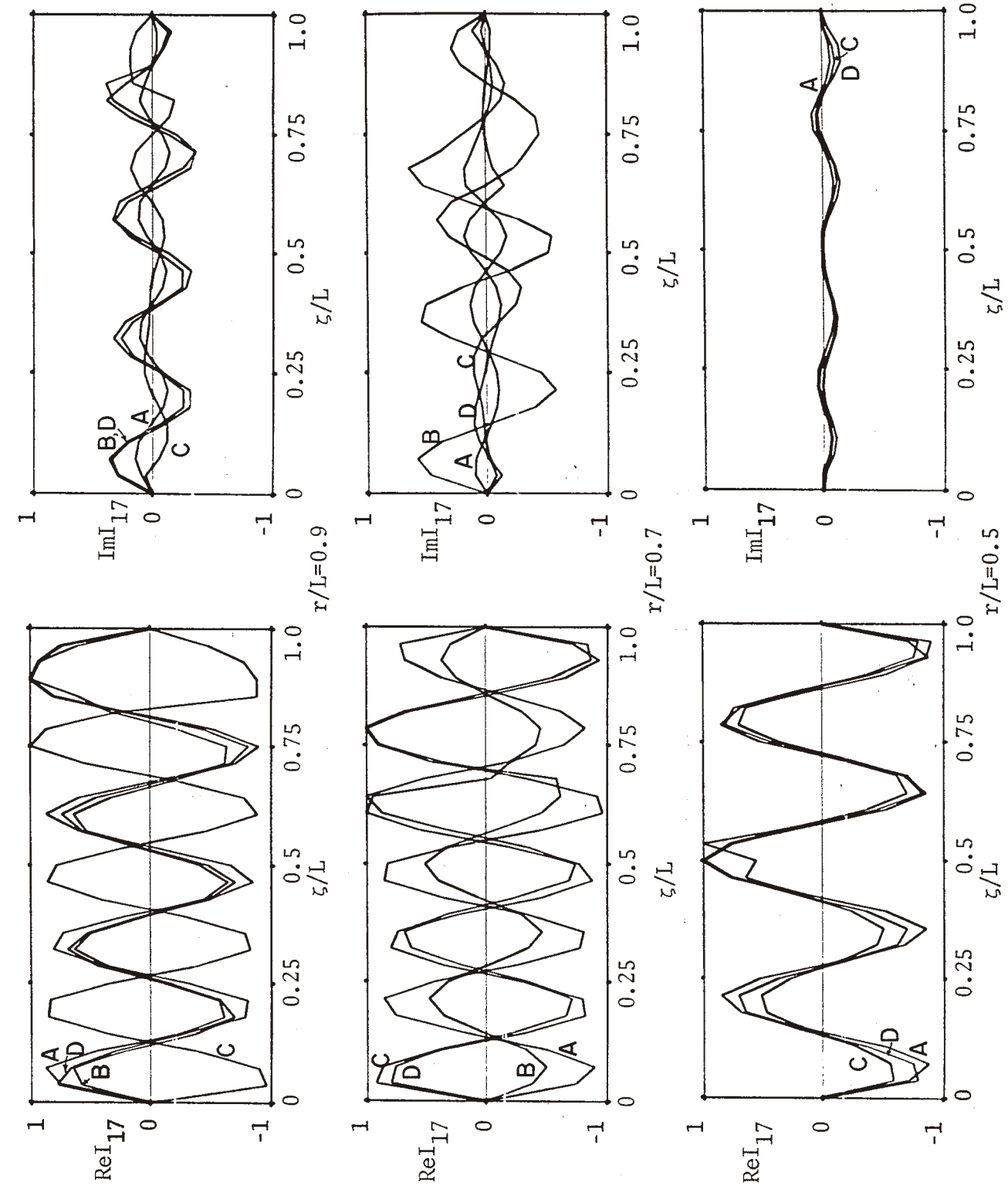

Figure 22a. Current distribution of natural modes of L-wire for resonant frequency s_{17}.

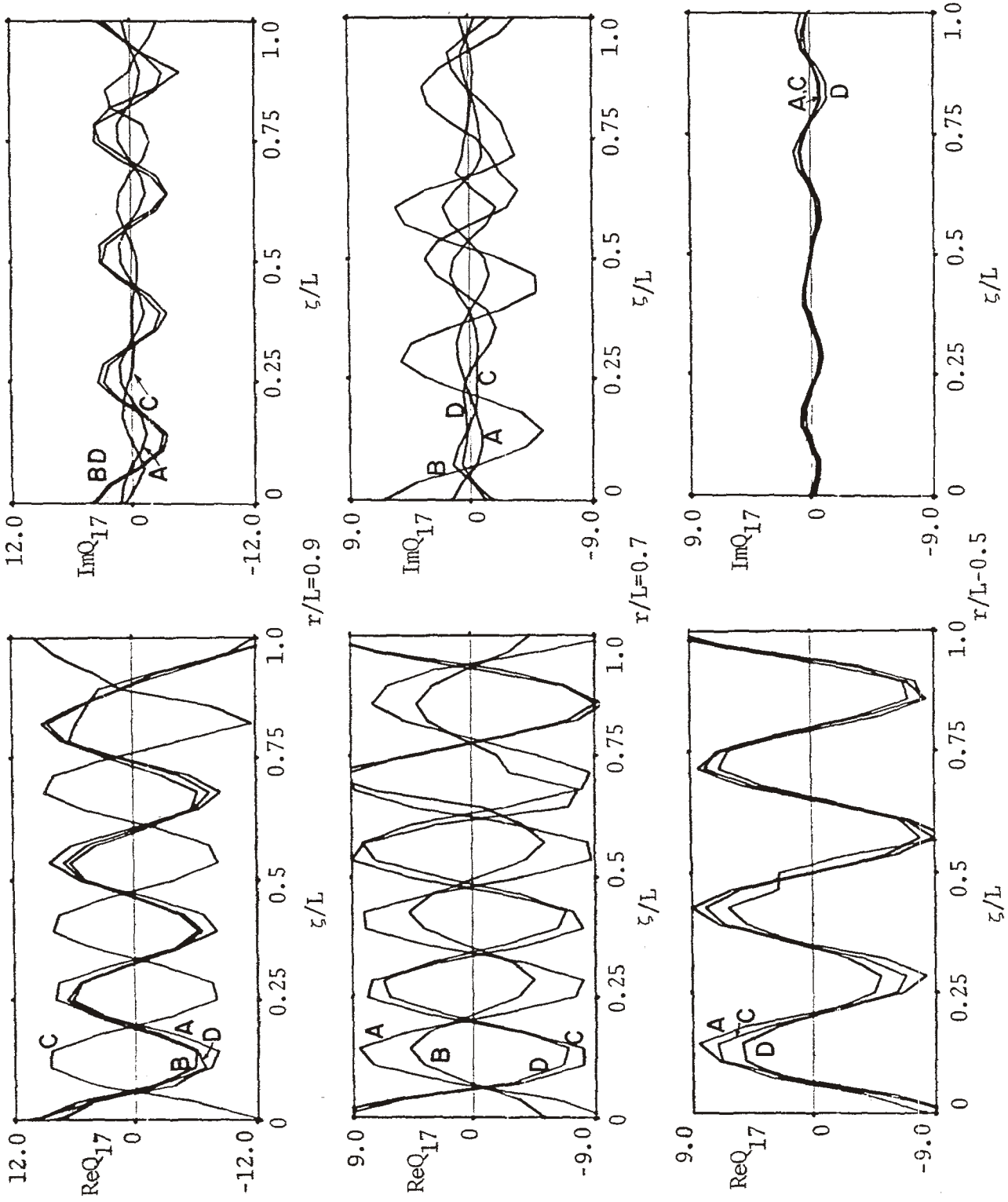

Figure 22b. Charge distribution of natural modes of L-wire for resonant frequency s_{17}.

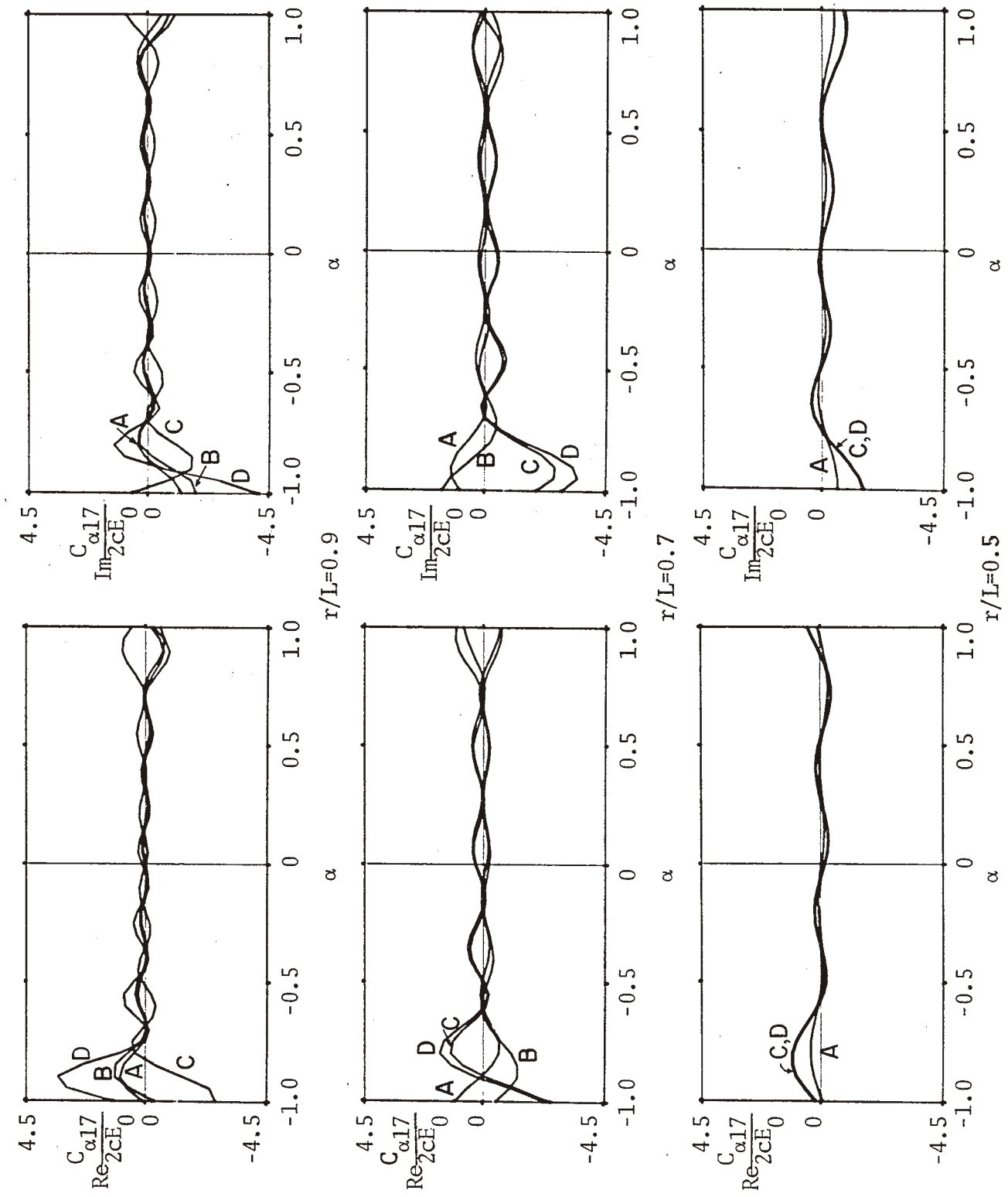

Figure 22c. Coupling coefficient C_{α} in milliampere of L-wire for resonant frequency s_{17} as a function of α.

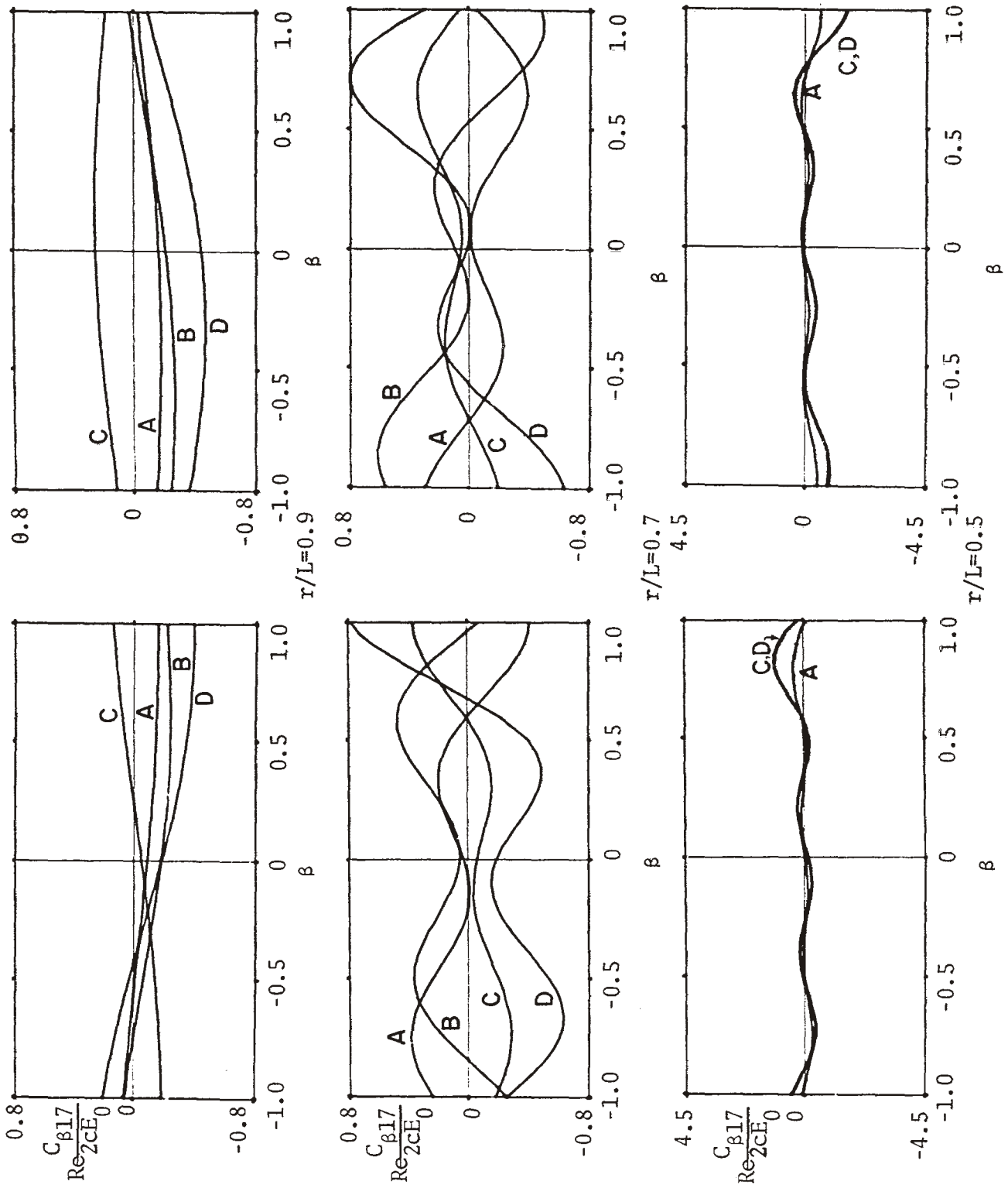

Figure 22d. Coupling coefficient C_β in milliampere of L-wire for resonant frequency s_{17} as a function of β.

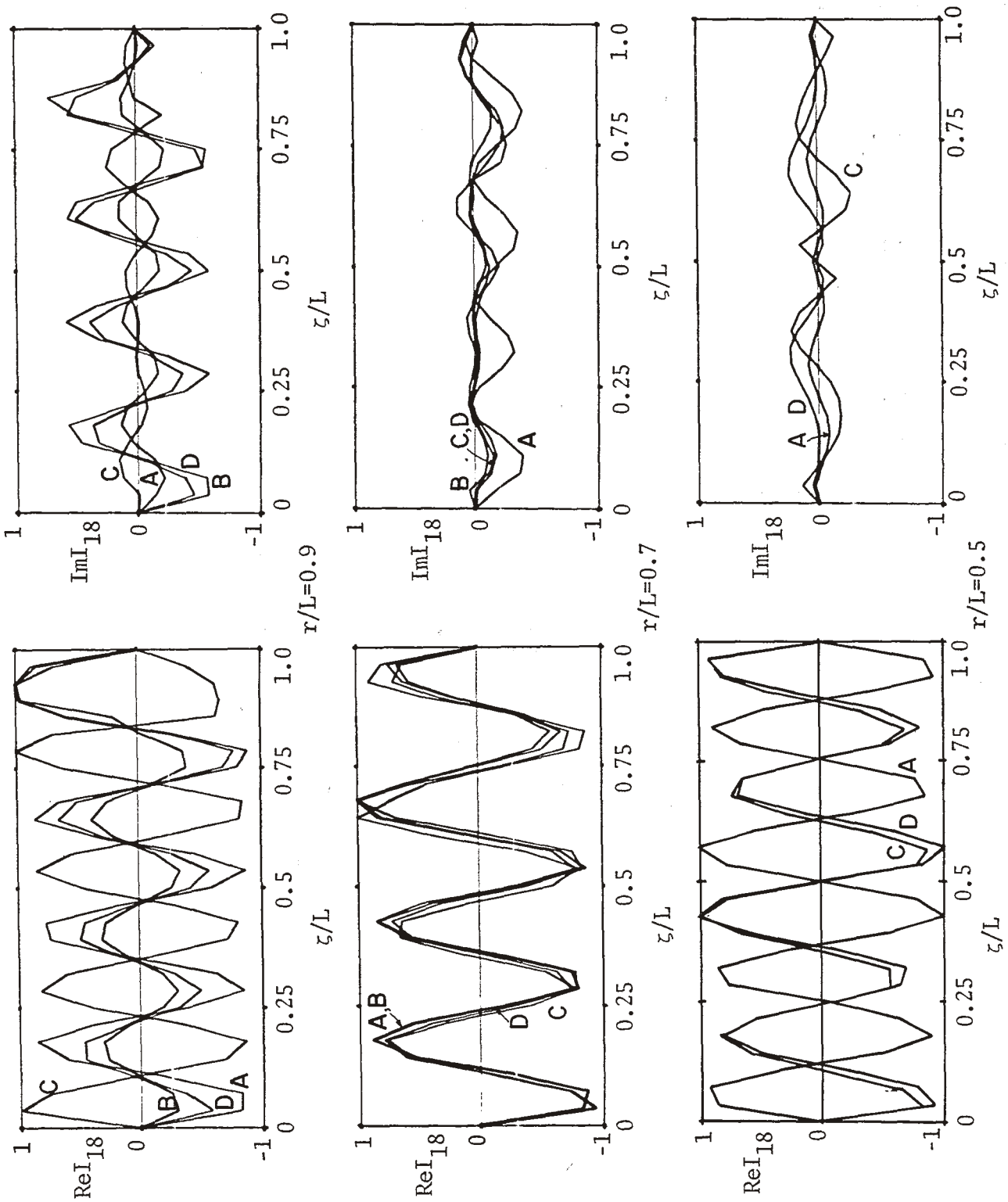

Figure 23a. Current distribution of natural modes of L-wire for resonant frequency s_{18}.

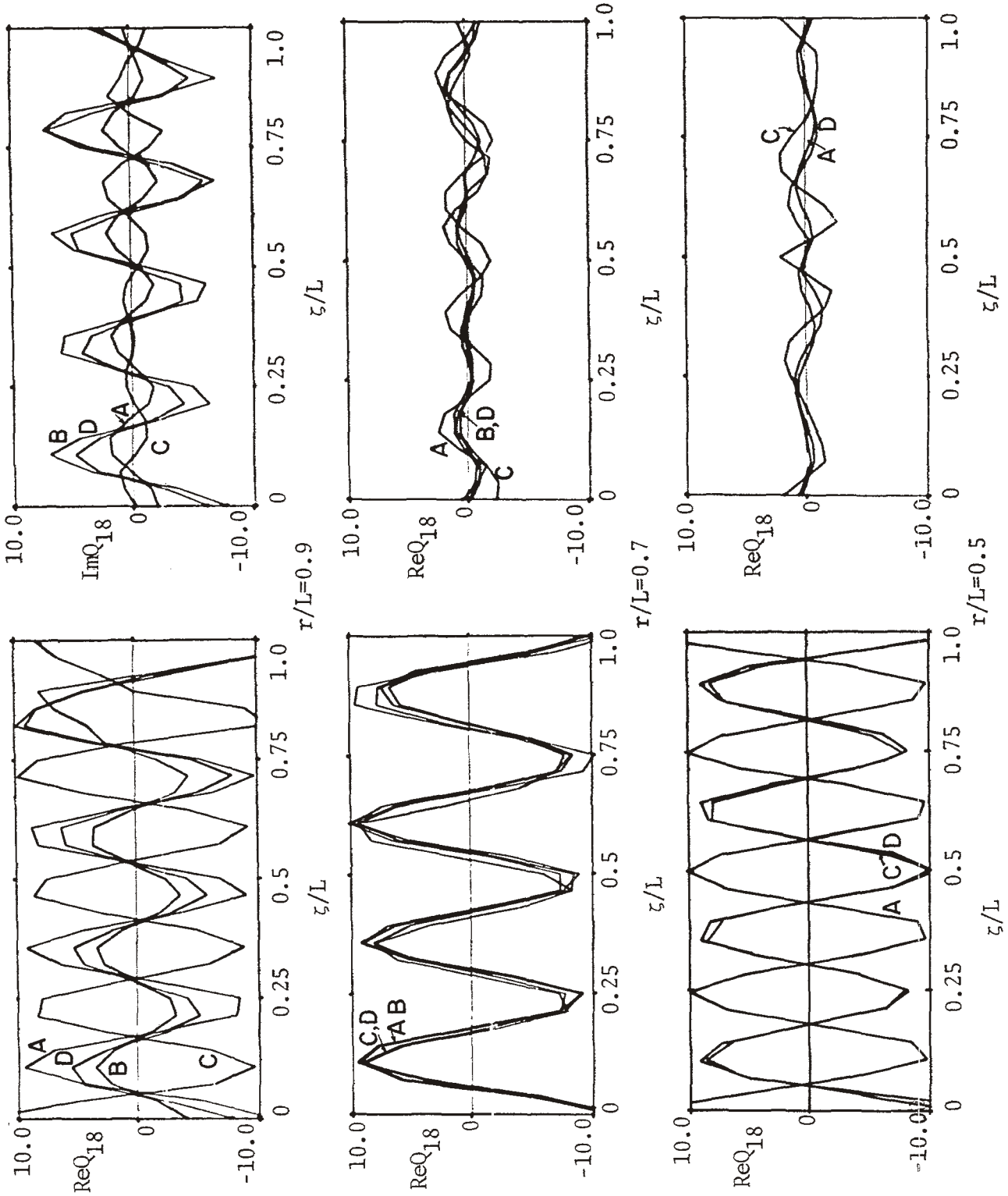

Figure 23b. Charge distribution of natural modes of L-wire for resonant frequency s_{18}.

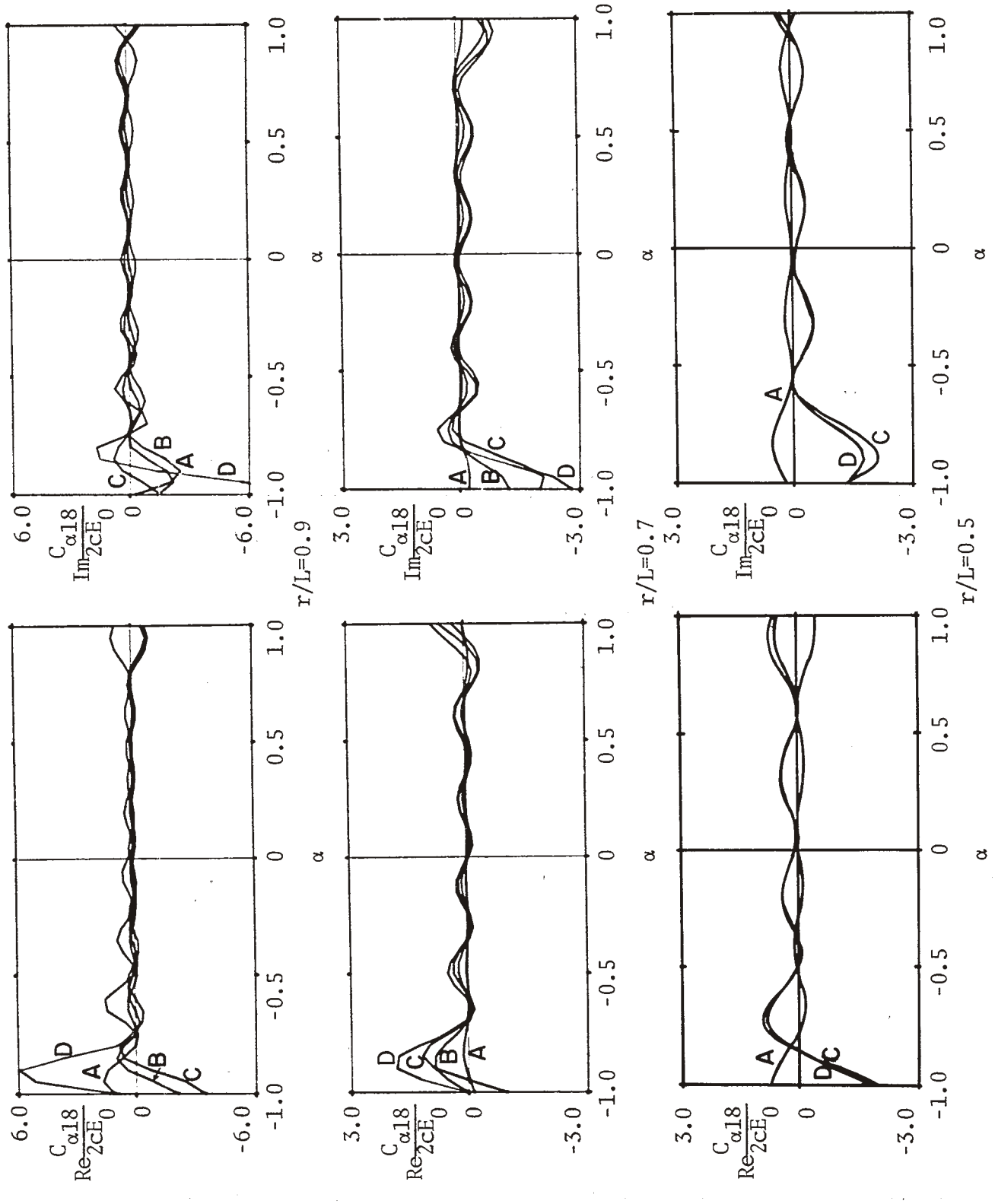

Figure 23c. Coupling coefficient C_α in milliampere of L-wire for resonant frequency s_{18} as a function of α.

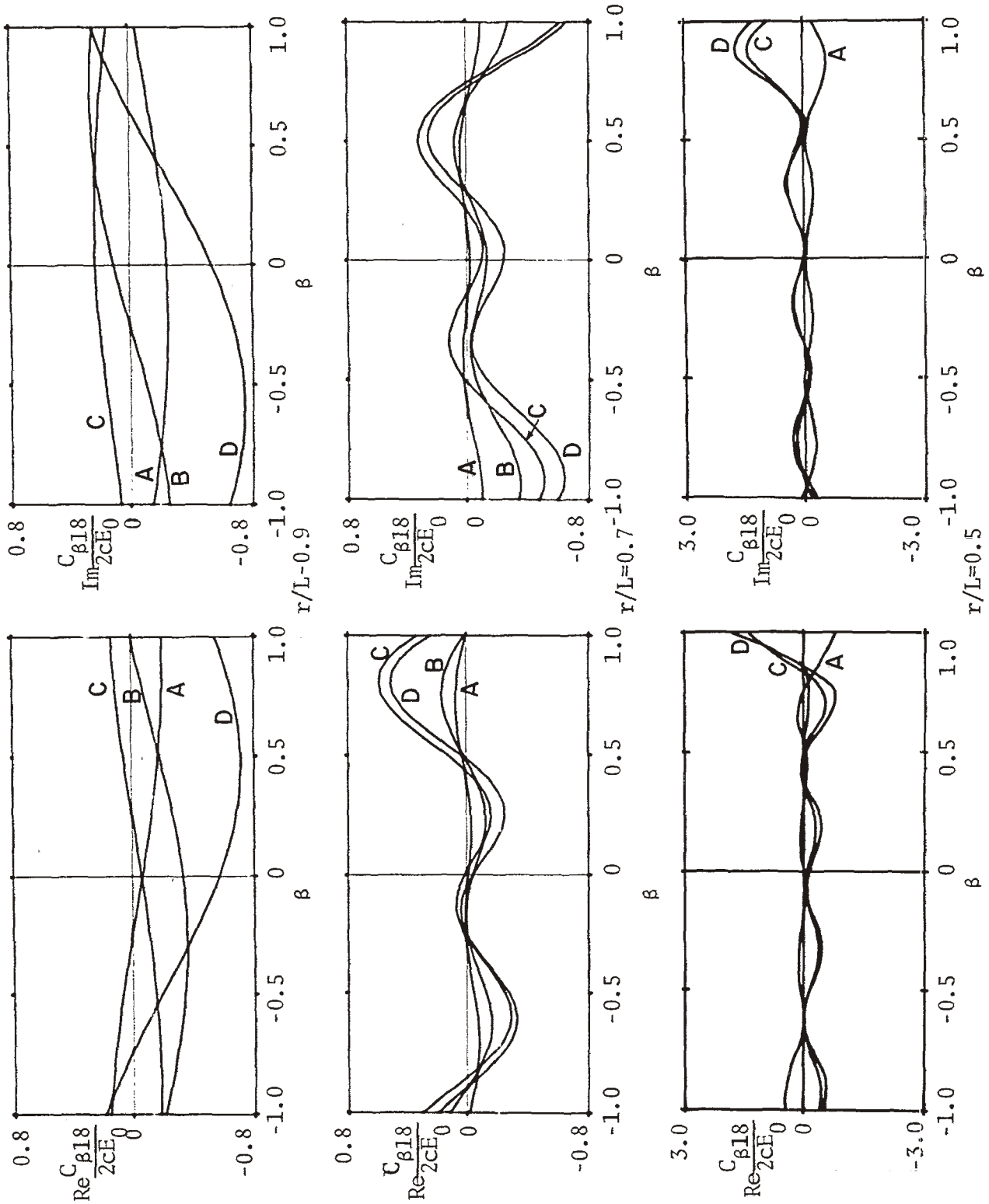

Figure 23d. Coupling coefficient C_β in milliampere of L-wire for resonant frequency s_{18} as a function of β.

frequencies considered.

One notes that the modal currents exhibit discontinuities for cases where there is a radius discontinuity at the bend. Such discontinuities commonly arise at wire junctions for large radius changes such as those considered here. Unfortunately, at present there is no adequate mathematical model available to treat such junctions. It is felt, however, that except in the neighborhood of the bend, the modal current distributions are substantially correct. Furthermore, it is also felt that all related quantities (resonant frequencies and coupling coefficients) corresponding to these currents are correct. The charge distributions in the figure are calculated using a finite difference approximation of the derivative of the current and hence exhibit the same discontinuities as the currents do.

The coupling coefficients in Figure 16-23 are calculated for a delta function excitation which excites the bend at t = 0. For a more general time dependent plane wave, the time dependence may be factored (in the Laplace domain) and the time dependence convolved with the delta function response. Alternatively, each coupling coefficient may be multiplied by the time dependence term evaluated at $s = s_i$ and extra terms included in the expansion to account for singularities in the s-domain arising from the excitation [1]. The forms of the excitation assumed are (cf. Eq. (4.5)]

$$E^i_{x\alpha}(s) = E_{0x}\, e^{-\frac{s}{c}\alpha x}$$

$$E^i_{z\alpha}(s) = 0, \qquad -1 < \alpha < 1 \qquad (5.3)$$

from which the coefficients C_α are determined, and

$$E^i_{x\beta} = 0$$

$$E^i_{z\beta} = E_{0z}\, e^{-\frac{s}{c}\beta z}, \qquad -1 < \beta < 1 \qquad (5.4)$$

from which the coefficients C_β are determined.

For a step function plane wave having components E_θ, E_ϕ and traveling in the direction θ,ϕ, the field components exciting the structure are

$$E^i_x = (E_\theta \cos\theta \cos\phi - E_\phi \sin\phi)\, e^{-\frac{sx}{c}\sin\theta\cos\phi}$$

$$E^i_z = -E_\theta \sin\theta\, e^{-\frac{sz}{c}\cos\theta} \qquad (5.5)$$

from which we find

$$\alpha = \sin\theta\cos\phi$$

$$\beta = \cos\theta$$

$$E_{0x} = E_\theta \cos\theta\cos\phi - E_\phi \sin\phi$$

$$E_{0z} = -E_\theta \sin\theta \qquad (5.6)$$

Using these relations, the coupling coefficients may be found from the graphs and one may construct the response by superposition of the response due to the individual coupling coefficients C_α and C_β using Eq. (4.27).

Frequency Domain Results

Steady state currents due to time-harmonic plane wave excitation

at three points on the structure are given in Figures 24 and 25 as a function of the excitation frequency for a fixed angle of incidence. Also shown is one case calculated directly from the integral equation in the frequency domain. The currents are calculated using Eq. (4.6) and it is seen that the resonance peaks are caused by the fact that the denominator in Eq. (4.6) is very small in the neighborhood of a pole. Furthermore, at positions on the structure corresponding to nodes in one of the modal currents, the corresponding resonance is suppressed.

Time Domain Results

Figures 26 - 28 illustrate the time domain currents and charge at selected points on an L-wire due to a θ-polarized incident step function plane wave traveling in the direction $\theta = \phi = 45°$. The time is referred to the instant the wave first strikes the end of the wire at $x = -r$. The various time delays as the wavefront passes along the structure are clearly evident in Figure 26 using only eight poles. The convergence of the solution as a function of the number of poles included in the time domain is indicated in Figure 27. Figure 28 shows the time domain charge at two points on the wire. It has also been verified that the total charge on the L-wire is indeed zero at $t = \infty$. Figures 29 - 31 show the corresponding results for the E_ϕ polarization. For comparison, Figures 26 and 29 also show one case computed by taking the Fourier inverse of frequency domain results obtained from solving the integral equation directly. The correspondence is seen to be quite good.

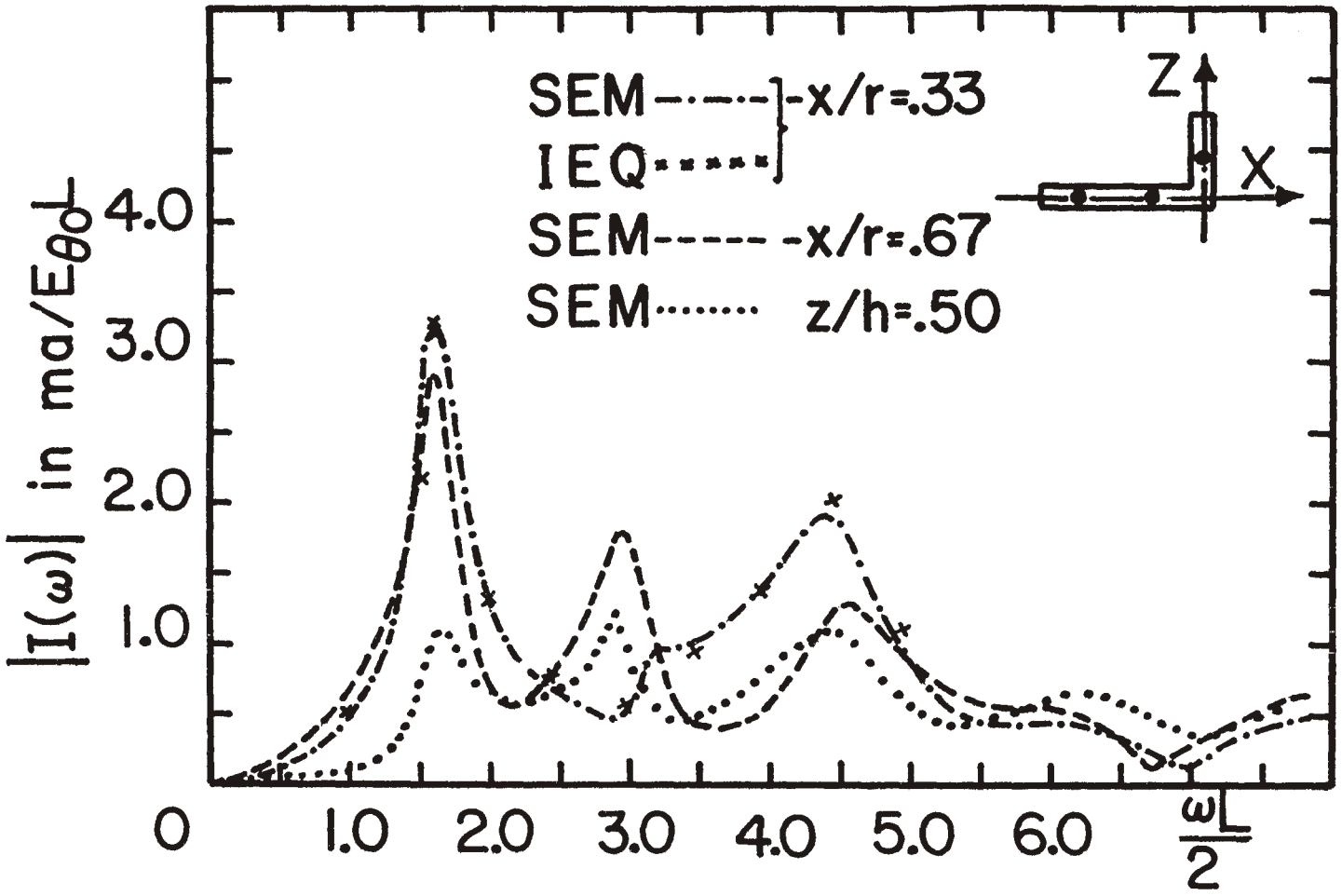

Figure 24. Variation of current on the L-wire as a function of frequency for a plane wave incident, $\theta = 45°$, $\phi = 45°$, E_θ - polarization.

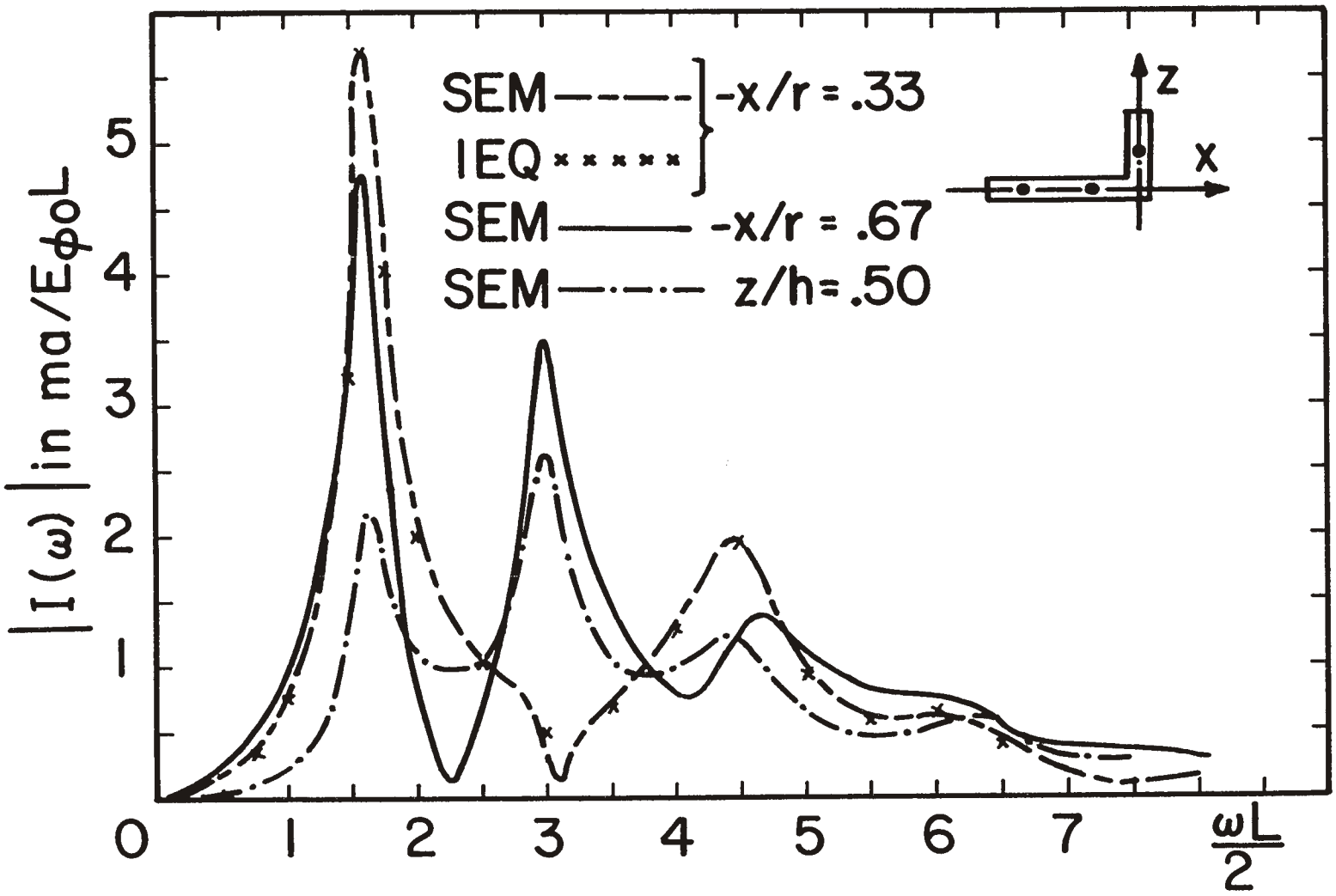

Figure 25. Variation of current on the L-wire as a function of frequency for a plane wave incident $\theta = 45°$, $\phi = 45°$, E_ϕ - polarization.

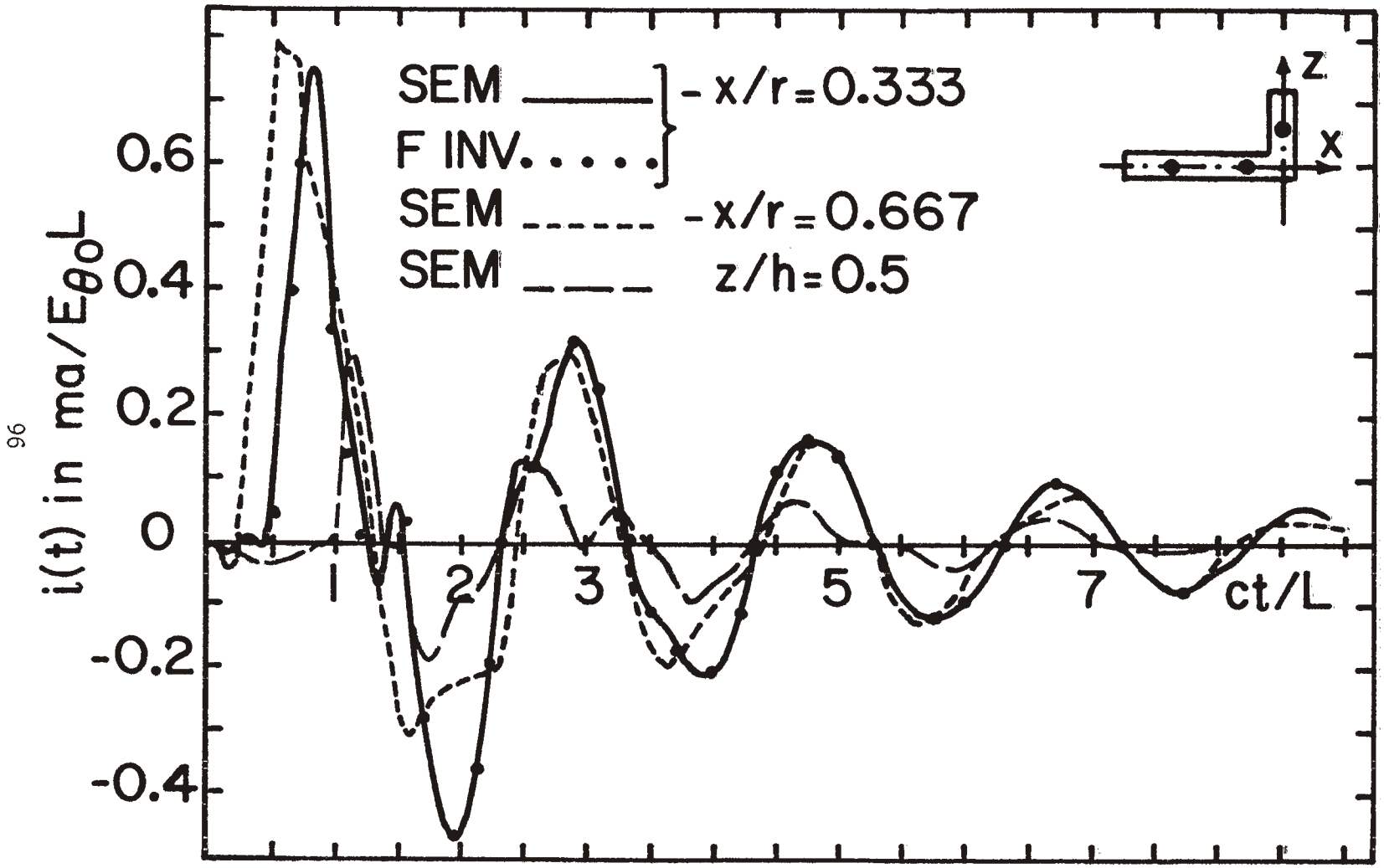

Figure 26. Time domain current, step function plane incident, $\theta = 45°$, $\phi = 45°$, E_θ - polarization, t = 0 at x = -r.

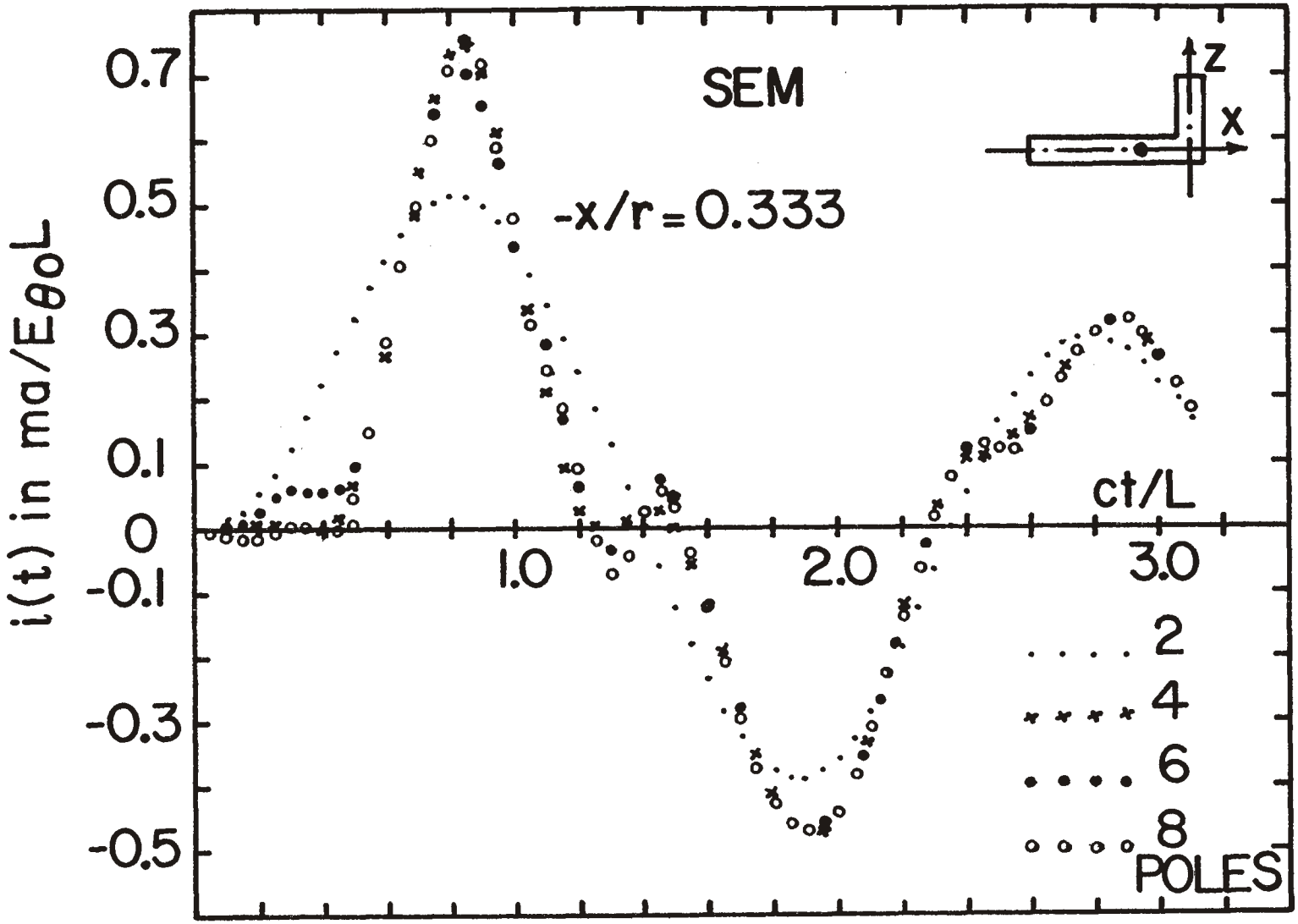

Figure 27. Convergence of time domain current, $\theta = 45°$, $\phi = 45°$, E_θ - polarization, step function plane wave incident.

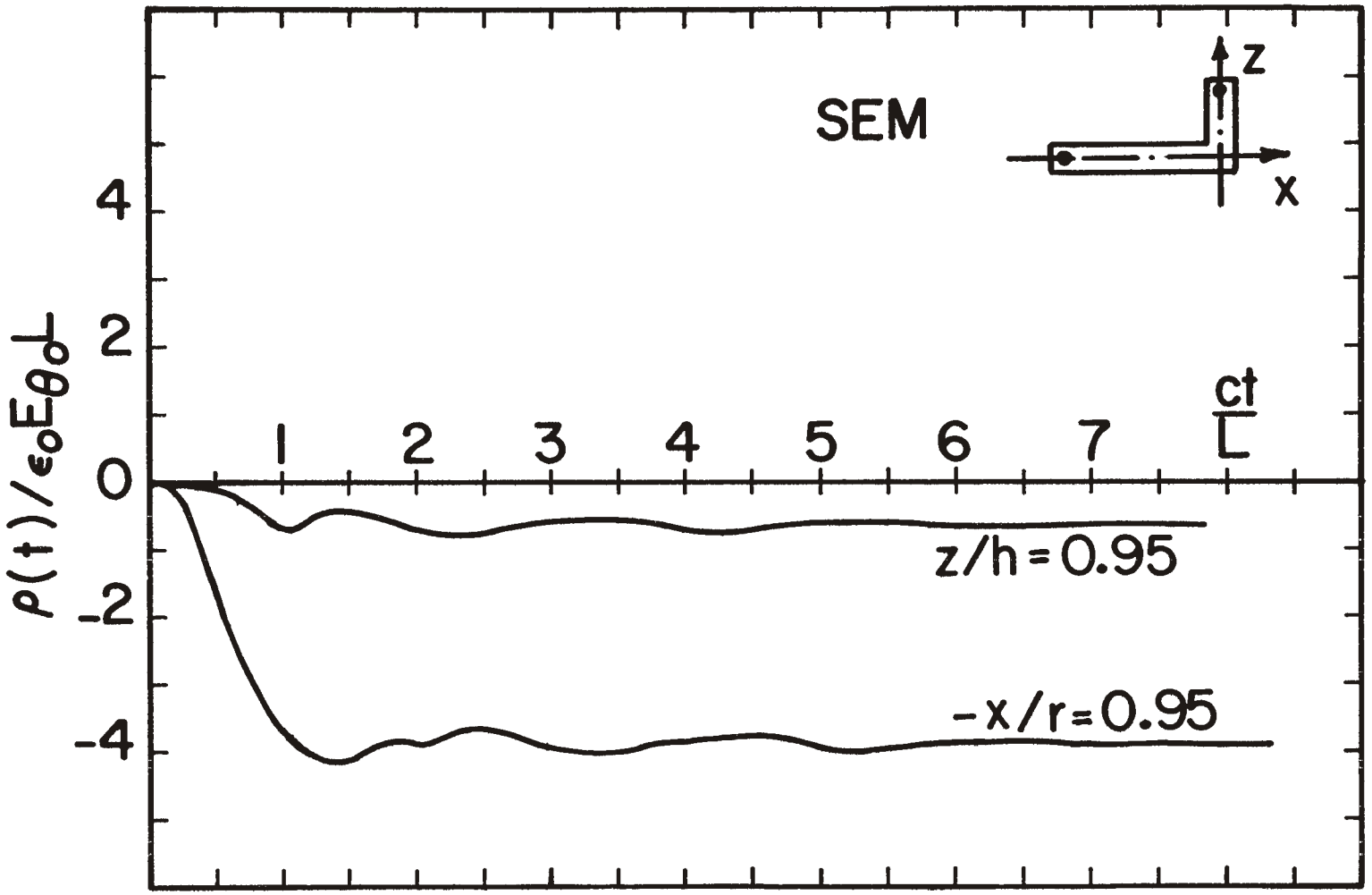

Figure 28. Time domain charge, step function plane wave incident, $\theta = 45°$, $\phi = 45°$, E_θ-polarization, $t = 0$ at $x = -r$.

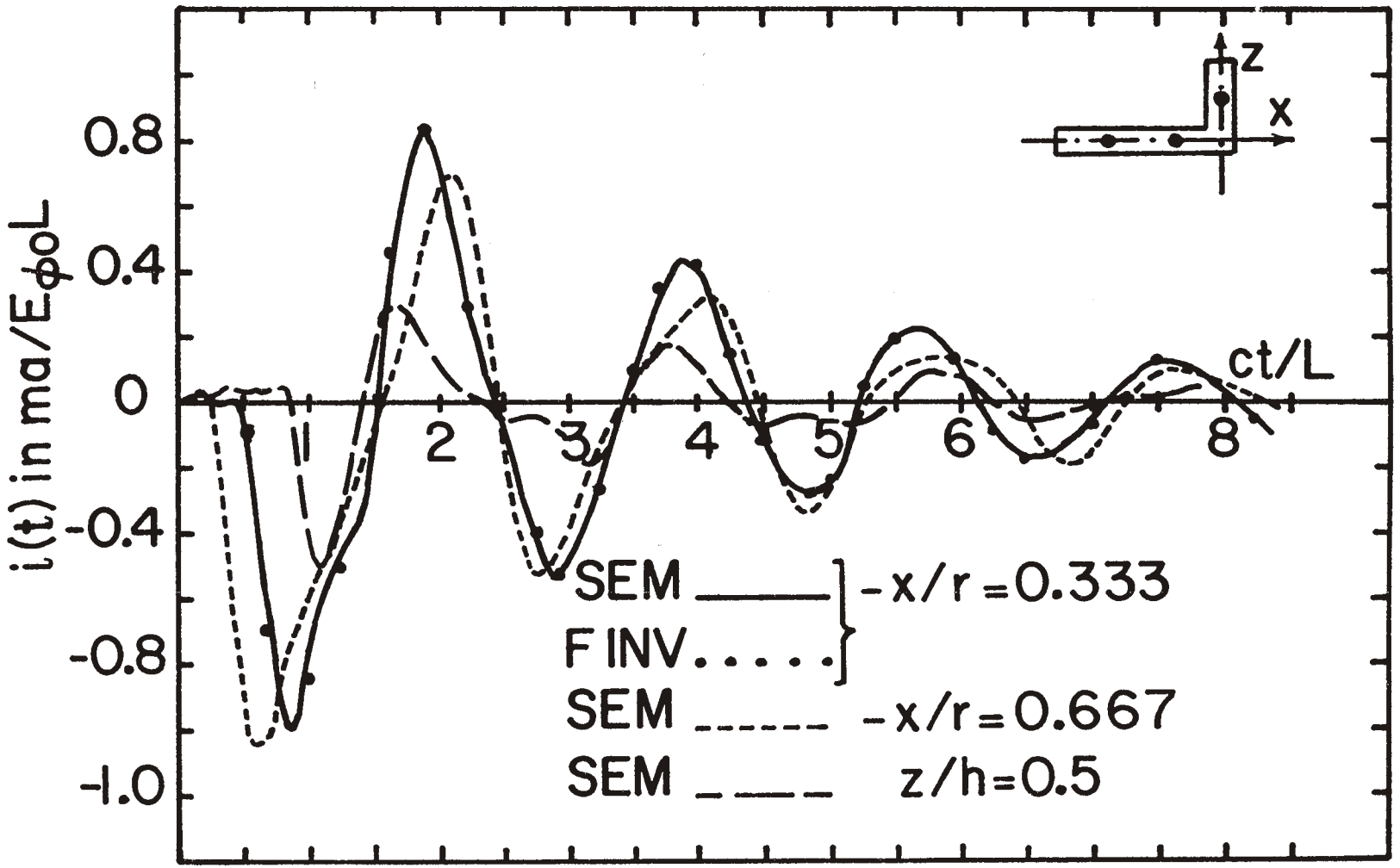

Figure 29. Time domain currents, step function plane wave incident, $\theta = 45°$, $\phi = 45°$, E_ϕ-polarization, $t = 0$ at $x = -r$.

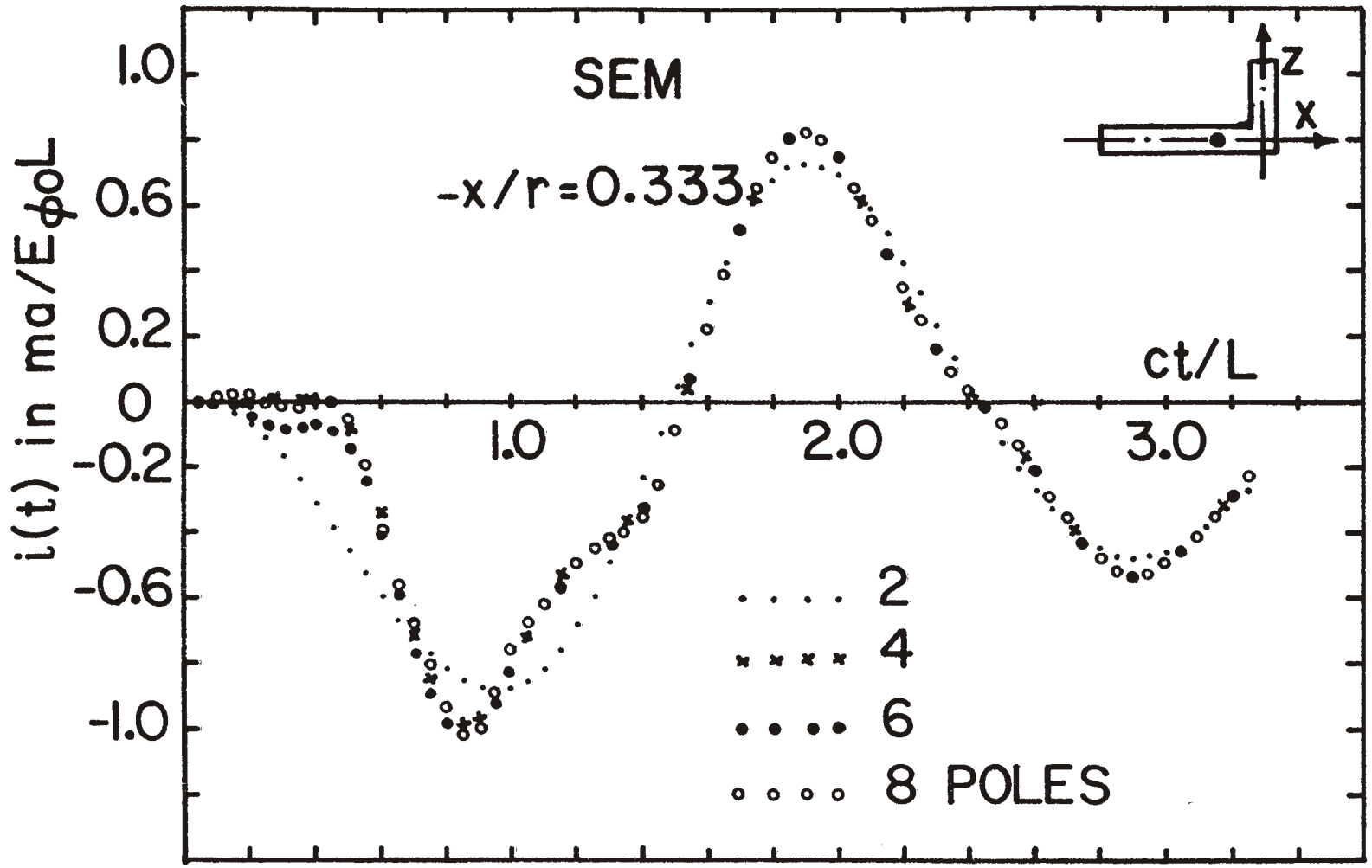

Figure 30. Convergence of time domain current, $\theta = 45°$, $\phi = 45°$, E_ϕ-polarization, step function plane wave incident.

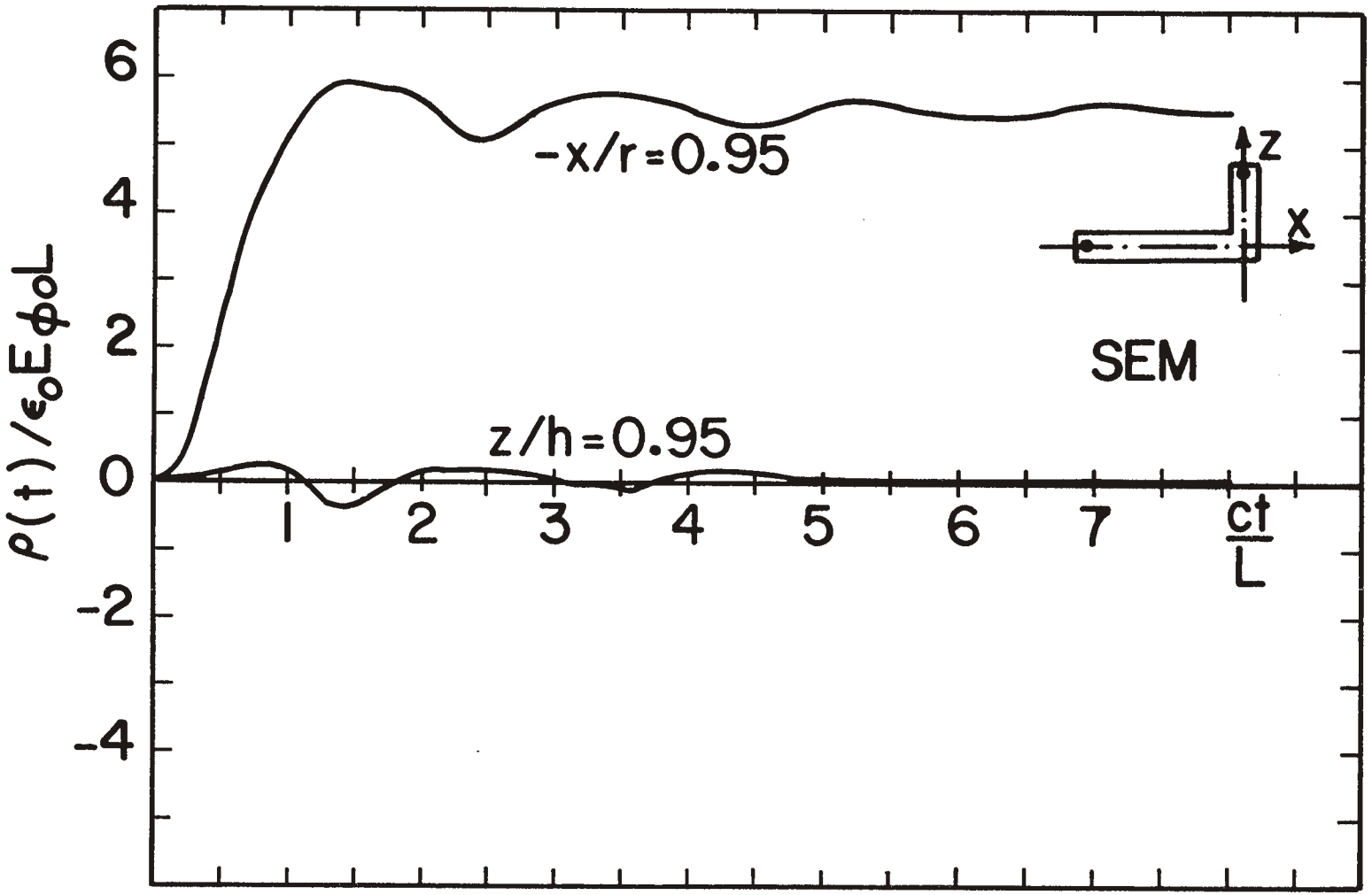

Figure 31. Time domain charge, step function plane wave incident, $\theta = 45°$, $\phi = 45°$, E_ϕ-polarization, $t = 0$ at $x = -r$.

APPENDIX A

REDUCTION OF A DOUBLE INTEGRAL TO A SINGLE INTEGRAL

In formulating the coupled integral equations (2.13), (2.14) for the L-wire structure, there resulted double integral terms due to mutual coupling of the type

$$\int_{x'=-r}^{0} i_x(x') \left\{ \int_{\zeta=0}^{z} \left[\frac{\partial}{\partial x} K_x'(0,x',a_2,\zeta) \right] \cos k(z-\zeta) d\zeta \right\} dx'$$

where

$$K_x'(0,x',a_2,\zeta) = \left. \frac{e^{-jkr_x}}{r_x} \right|_{x=0} \tag{1A}$$

$$r_x^2 = (x-x')^2 + a_2^2 + \zeta^2$$

The internal integral of the double integral (1A), can be analytically evaluated.

We have

$$\frac{\partial}{\partial x} K_x'(0,x',a_2,\zeta) = x' \left\{ j\frac{k}{r_{0x}^2} + \frac{1}{r_{0x}^3} \right\} e^{-jkr_{0x}} \tag{2A}$$

where

$$r_{0x} = x'^2 + a_2^2 + \zeta^2$$

Also

$$\frac{\partial}{\partial \zeta}\left[\frac{e^{-jk(r_{0x}-\zeta)}}{r(r_{0x}-\zeta)}\right] = \left[j\frac{k}{r_{0x}^2} + \frac{1}{r_{0x}^3}\right] e^{-jk(r_{0x}-\zeta)} \qquad (3A)$$

In view of (2A) and (3A), the double integral (1A) may be written as

$$\int_{x'=-r}^{0} i_x(x')\, G(x')dx'$$

where

$$G(x') = \int_{\zeta=0}^{z}\left[\frac{\partial}{\partial x} K'_x(0,x',a_2,\zeta)\right] \cos k(z-\zeta)d\zeta$$

$$= \int_{\zeta=0}^{z} x'\left[j\frac{k}{r_{0x}^2} + \frac{1}{r_{0x}^3}\right] e^{-jkr_{0x}}\left[\frac{e^{+jk(z-\zeta)} + e^{-jk(z-\zeta)}}{2}\right]d\zeta$$

$$= \left\{\frac{x'e^{-jkr_{0x}}}{(a_2^2+x'^2)r_{0x}}\left[\zeta \cos k(z-\zeta) - jr_{0x} \sin k(z-\zeta)\right]\right\}_{\zeta=0}^{z} \qquad (4A)$$

APPENDIX B

CALCULATION OF MODAL CURRENTS COUPLING VECTORS, AND COUPLING COEFFICIENTS

In applying the Singularity Expansion Method (SEM) to obtain numerical solutions for EMP problems, one typically encounters a matrix equation of the form

$$\overline{\overline{Z}}(s)\ \overline{I}(s) = \overline{V}(s) \tag{1B}$$

where the matrix $\overline{\overline{Z}}$ is an approximate representation of some integral operator, the vector $\overline{I}$ is a set of coefficients for expanding the induced current in terms of a suitable set of basis functions, and $\overline{V}$ is a vector whose elements are related to the fields illuminating the object [9]. At the so-called natural resonant frequencies, $s=s_i$, there exist non-trivial solutions $\overline{I}_i$ to the homogeneous problem

$$\overline{\overline{Z}}_i\ \overline{I}_i = 0$$

where $\overline{\overline{Z}}_i = \overline{\overline{Z}}(s_i)$. There also exist non-trivial solutions to the homogeneous adjoint problem

$$\overline{\overline{Z}}_i^{\,T}\ \overline{H}_i = 0 \tag{2B}$$

or

$$\overline{\overline{Z}}_i^{\,\dagger}\ \overline{H}_i^{*} = 0 \tag{3B}$$

where T denotes the transpose, the asterisk denotes complex conjugate, and the dagger denotes complex conjugate transpose or adjoint. In order for (2B) and (3B) to hold, the determinant

$$\Delta(s) = |\overline{\overline{Z}}(s)| \tag{4B}$$

must vanish at $s = s_i$. We will assume for convenience in the following that $\Delta(s)$ has only simple zeros and that there is only one set of solution vectors $\overline{\overline{I}}_i$ and $\overline{H}_i$ of equations (2B) and (3B) respectively. The extension to the more general case when $\Delta(s)$ has multiple zeros or when (2B) and (3B) have a degenerate set of solutions is relatively straightforward [1].

The first step in the SEM is the determination of the zeros of $\Delta(s)$ which in turn are poles of the induced current $I(s)$. These zeros are the complex resonant frequencies and are found by a numerical search procedure in the complex s-plane. One convenient algorithm for accomplishing this is Muller's method which is described in detail elsewhere [12]. Essentially, the method begins with three initial estimates of the location of the root and interpolates a quadratic surface through the three corresponding values of the function $\Delta(s)$. A root of the quadratic is then used as the next estimate of the zero of $\Delta(s)$. Using the three most up-to-date estimates, the algorithm continues iteratively to predict an improved value of the root until some convergence criterion is satisfied. In order to

prevent the algorithm from converging to previously found roots, the known roots are divided out of $\Delta(s)$. To illustrate, suppose that at one stage we have determined the roots $s_1, s_2, \ldots, s_n$ and are attempting to find the root s_{n+1}. We then apply Muller's method to the "deflated function"

$$\Delta^{(n)}(s) = \frac{\Delta(s)}{(s-s_1)(s-s_2)\ldots(s-s_n)} \tag{5B}$$

which does not have roots at $s_1, s_2, \ldots, s_n$ but otherwise has the same roots as $\Delta(s)$. Since in the SEM, it is known a priori that roots in the s-plane appear in complex conjugate pairs, the complex conjugate roots are also to be included in the deflation of $\Delta(s)$.

It is also convenient to use a "normalized" determinant obtained by dividing each element in rows of $\overline{\overline{Z}}(s)$ by the magnitude of the vector formed by the elements in the row [12]. This "normalization" of the determinant permits one to use a single criterion throughout large regions of the s-plane for determining values of the determinant which are acceptable as zero. Otherwise, one generally must gauge whether or not a zero has been obtained at a point by examining the determinant in adjacent regions.

We may write the solution of (1B) in several equivalent forms;

$$\bar{I}(s) = \bar{\bar{Z}}(s)^{-1}\,\bar{V}(s) = \bar{\bar{Y}}(s)\bar{V}(s) = \sum_i \frac{\bar{\bar{Y}}_i^r}{s-s_i}\,\bar{V}(s) \tag{6B}$$

The last expression is obtained by expanding the matrix $\bar{\bar{Y}}(s)$ in a partial fraction expansion in terms of its poles at s_i and their corresponding residue matrices

$$\bar{\bar{Y}}_i^r = \lim_{s\to s_i} (s-s_i)\bar{\bar{Y}}(s) \tag{7B}$$

Since we assumed that $\Delta(s)$ has only simple zeros, $\bar{\bar{Y}}(s)$ has only simple poles. The elements of $\bar{\bar{Y}}(s)$ are all meromorphic functions of the complex frequency variable and the numerical method discussed in Appendix C may be used to evaluate the residue matrix $\bar{\bar{Y}}_i^r$.

If it were necessary to use the form of the singularity expansion of $\bar{I}(s)$ given in (6B), SEM would be somewhat impractical for numerical computation because the residue matrix $\bar{\bar{Y}}_i^r$ would have to be stored for each resonant frequency. For most practical problems, this requirement could quickly use up all available machine storage. Fortunately, it can be shown that $\bar{\bar{Y}}_i^r$ is a dyadic; that is, its elements can be calculated as the product of elements taken from two column vectors. One of these column vectors is just the modal current $\bar{I}_i$ of equation (2B). To show this we note that

$$\overline{\overline{Z}}(s)\ \overline{\overline{Y}}(s) = \overline{\overline{Y}}(s)\ \overline{\overline{Z}}(s) = \overline{\overline{U}}$$

$$= \sum_i \frac{\overline{\overline{Z}}(s)\ \overline{\overline{Y}}_i^r}{s-s_i} = \sum_i \frac{\overline{\overline{Y}}_i^r\ \overline{\overline{Z}}(s)}{s-s_i}$$

where $\overline{\overline{U}}$ is the identity matrix. Hence

$$\lim_{s\to s_i} (s-s_i)\ \overline{\overline{Z}}(s)\ \overline{\overline{Y}}(s) = \lim_{s\to s_i} (s-s_i)\ \overline{\overline{Y}}(s)\ \overline{\overline{Z}}(s)$$

$$= \lim_{s\to s_i} (s-s_i)\ \overline{\overline{U}}$$

$$= \overline{\overline{Z}}_i\ \overline{\overline{Y}}_i^r = \overline{\overline{Y}}_i^r\ \overline{\overline{Z}}_i = 0$$

or equivalently,

$$\overline{\overline{Z}}_i\ \overline{\overline{Y}}_i^r = 0$$

and

$$\overline{\overline{Z}}_i^\dagger\ \overline{\overline{Y}}_i^{r\dagger} = 0 \qquad (8B)$$

Comparison of (8B) with (2B) and (3B) shows that the columns of $\overline{\overline{Y}}_i^r$ must be proportional to $\overline{I}_i$ and the rows must be proportional to $\overline{H}_i^\dagger$. Hence $\overline{\overline{Y}}_i^r$ can be written in the form

$$\overline{\overline{Y}}_i^r = \beta_i \overline{I}_i \overline{H}_i^\dagger \qquad (9B)$$

where β_i is a constant to be determined. Using (9B), $\bar{\bar{Y}}(s)$ may be expressed as

$$\bar{\bar{Y}}(s) = \sum_i \beta_i \frac{\bar{I}_i \bar{H}_i^\dagger}{s-s_i} \tag{10B}$$

To determine β_i, we note that

$$\bar{H}_j^\dagger \bar{\bar{Z}}(s) \bar{\bar{Y}}(s) \bar{H}_j = \bar{H}_j^\dagger \bar{\bar{U}} \bar{H}_j = ||\bar{H}_j||^2 \tag{11B}$$

where $||\bar{A}||$ denotes the norm of a vector $\bar{A}$,

$$||\bar{A}|| = \sqrt{\bar{A}^\dagger \bar{A}}$$

With (10B) and (11B), we have

$$\sum_i \beta_i \frac{\bar{H}_j^\dagger \bar{\bar{Z}}(s) \bar{I}_i \bar{H}_i^\dagger \bar{H}_j}{s-s_i} = ||H_j||^2$$

If we note that

$$\bar{H}_j^\dagger \bar{\bar{Z}}_j \bar{I}_i = \bar{H}_j^\dagger \bar{\bar{Z}}_j^{\dagger\dagger} \bar{I}_i$$

$$= (\bar{\bar{Z}}_j^\dagger \bar{H}_j)^\dagger \bar{I}_i = 0$$

then we can write

$$\sum_i \beta_i \frac{\bar{H}_j^\dagger (\bar{\bar{Z}}(s) - \bar{\bar{Z}}_j) \bar{I}_i \bar{H}_i^\dagger \bar{H}_j}{s-s_i} = ||\bar{H}_j||^2$$

We now take the limit on the left hand side as s approaches s_j and note that

$$\lim_{s \to s_j} \frac{\bar{\bar{Z}}(s) - \bar{\bar{Z}}_j}{s-s_i} = \bar{\bar{Z}}_j' \delta_{ij}$$

where $\bar{\bar{Z}}_j'$ is the derivative

$$\left.\frac{d\bar{\bar{Z}}}{ds}\right|_{s=s_j} = \bar{\bar{Z}}_j'$$

and δ_{ij} is the Kronecker delta. The result is

$$\beta_j \bar{H}_j^\dagger \bar{\bar{Z}}_j' \bar{I}_j ||H_j||^2 = ||H_j||^2$$

from which we conclude

$$\beta_i = \frac{1}{\bar{H}_i^\dagger \bar{\bar{Z}}_i' \bar{I}_i} \qquad (12B)$$

Hence $\overline{\overline{Y}}(s)$ is given by

$$\overline{\overline{Y}}(s) = \sum_i \frac{\overline{I}_i \overline{H}_i^{\dagger}}{(s-s_i)\overline{H}_i^{\dagger}\overline{\overline{Z}}_i\overline{I}_i} \tag{13B}$$

Note that since $\overline{I}_i$ and $\overline{H}_i$ are solutions to the homogeneous equations (2B) and (3B), they may be defined only to within an arbitrary constant. That this constant is arbitrary can be seen from the fact that these vectors appear in (13B) in such a way that each term in the expression is independent of the choice of normalization.

There are several alternative approaches to the calculation of the quantities $\overline{I}_i$ and $\overline{H}_i$. For the work in this report, these quantities are found directly from $\overline{\overline{Y}}_i^r$ which is determined by the method of Appendix C. Since the columns of $\overline{\overline{Y}}_i^r$ are proportional to $\overline{I}_i$, the vector formed by summing all elements of the rows of $\overline{\overline{Y}}_i^r$ is also proportional to $\overline{I}_i$ and may be normalized arbitrarily by choosing the peak magnitude of $\overline{I}_i$ equal to unity. Summing the elements of the rows yields a weighted average of the vectors $\overline{I}_i$ formed by the columns of $\overline{\overline{Y}}_i^r$ and presumably reduces the deviation of the error in $\overline{I}_i$ found in the individual columns of $\overline{\overline{Y}}_i^r$. Similarly, the rows of $\overline{\overline{Y}}_i^r$ are proportional to $\overline{H}_i^{\dagger}$ and summing the elements of columns of $\overline{\overline{Y}}_i^r$ yields a row vector which when normalized is $\overline{H}_i^{\dagger}$. However, one must first determine the interelement phases along a row (column) before adding the elements in

the row (column) and then shift the phase of the elements in the row (column) before adding so they will add essentially in phase. Otherwise, for odd functions $\overline{H}_i$ or $\overline{I}_i$, the resulting sum may be zero.

An array of values for β_i can be easily obtained at this stage by dividing the elements of the matrix $\overline{I}_i\overline{H}_i^{\dagger}$ into the corresponding elements of $\overline{\overline{Y}}_i^r$. Again, an averaging procedure can be used with these values to reduce the deviation of the error in the individual values. This method has the advantage that $\overline{I}_i$, $\overline{H}_i$, and β_i can all be determined once $\overline{\overline{Y}}_i^r$ has been calculated. In the following methods, separate considerations are required for calculating each of the quantities $\overline{I}_i$, $\overline{H}_i$, and β_i.

β_i may also be calculated according to equation (12B) once $\overline{I}_i$, $\overline{H}_i$, and $\overline{\overline{Z}}_i'$ have been obtained. The latter matrix may be calculated by the method described in Appendix C. The vectors $\overline{I}_i$ and $\overline{H}_i$ can also be found by solving (2B) and (3B) directly. Probably the simplest and most direct procedure for doing this is simply a modification of the usual Gaussian elimination procedure for solving an inhomogeneous linear system. If pivoting on the maximum element in the array is used, the last pivot element will be zero, (or more likely, extremely small) since the determinant is simply the product of all the pivots in the elimination process and must vanish at the pole. Hence in the diagonalized matrix, the element in the unknown column vector whose coefficient is the last pivot element cannot be determined, but can be chosen arbitrarily. With a convenient choice for this element, all

the other unknowns may be determined by back substitution as is usually done in linear equation solving. The elements of the solution vector will be proportional to the arbitrarily chosen element. The resulting vector may then be renormalized appropriately.

Another method of solving for $\overline{I}_i$ and $\overline{H}_i$ stems from the observation that equations (2B) and (3B) are eigenvalue problems with an eigenvalue which is zero. That is, the eigenvalue problems

$$\begin{aligned} \overline{\overline{Z}}_i \overline{I}_{in} &= \lambda_{in} \overline{I}_{in} \\ \overline{\overline{Z}}_i^{\dagger} \overline{H}_{in} &= \mu_{in} \overline{H}_{in} \end{aligned} \tag{14B}$$

must have an eigenvalue $\lambda_{in} = \mu_{in} = 0$ according to (2B) and (3B). The corresponding eigenvectors are then just the desired vectors $\overline{I}_i$ and $\overline{H}_i$. Any of the standard matrix eigenvalue methods, such as the Jacobi method, may be used to determine the $\overline{I}_i$ and $\overline{H}_i$ by choosing the eigenvectors whose corresponding eigenvalues are smallest in magnitude. An advantage of this method is that the magnitude of the smallest eigenvalue may provide some idea of the extent to which the solution vectors are accurate solutions of equations (2B) and (3B) since the right hand side of equation (14B) is just the residual error. Furthermore, this method can easily be modified to handle the case wherein there are degenerate solutions to (2B) and (3B). However, most of the

eigenvalue methods are iterative rather than direct methods and are hence more time consuming.

Another direct method for solving (2B) and (3B) permits one to use standard linear equation solving routines with no modification for SEM. Applying the method to an arbitrary homogeneous system of N × N equations,

$$\bar{\bar{A}}\bar{X} = 0 \tag{15B}$$

which might represent either (2B) or (3B), we first isolate an element of $\bar{X}$ which is known to be non-zero. Designating this element by X_j, we partition the equation into the form

$$[\bar{\bar{A}}' \,|\, \bar{A}_j \,|\, \bar{\bar{A}}'] \begin{bmatrix} \bar{X}' \\ \hline X_j \\ \hline \bar{X}'' \end{bmatrix} = 0 \tag{16B}$$

The vector $\bar{A}_j$ is just the column of coefficients of X_j. Since the vector $\bar{X}$ is arbitrary to within a constant, we may choose, for example, $X_j = 1$. With this choice, we may now rewrite (16B) in the form

$$[\bar{\bar{A}}' \,|\, \bar{\bar{A}}'] \begin{bmatrix} \bar{X}' \\ \hline \bar{X}'' \end{bmatrix} = -\bar{A}_j \tag{17B}$$

which is a system of N equations in N-1 unknowns. For over-determined systems of the form (17B), one often finds a solution which minimizes the squared error,

$$\varepsilon^2 = \left|\left|[\bar{\bar{A}}' \,|\, \bar{\bar{A}}'] \begin{bmatrix} \bar{X}' \\ \hline \bar{\bar{X}}' \end{bmatrix} + \bar{A}_j \right|\right|^2 \qquad (18B)$$

But (17B) is not really over-determined; it is instead a set of dependent equations since the determinant of the original matrix $\bar{\bar{A}}$ vanishes. Hence, in theory, the error in (18B) is reducible to zero and the error minimizing solution is then the solution of (15B). The solution is given by finding the "generalized inverse" or "pseudo-inverse" of (17B) given by

$$\begin{bmatrix} \bar{X}' \\ \hline \bar{\bar{X}}' \end{bmatrix} = - \left[[\bar{\bar{A}}' \,|\, \bar{\bar{A}}']^{\dagger} [\bar{\bar{A}}' \,|\, \bar{\bar{A}}'] \right]^{-1} [\bar{\bar{A}}' \,|\, \bar{\bar{A}}']^{\dagger} \bar{A}_j \qquad (19B)$$

that is, both sides of (17B) are multiplied by the transpose conjugate of the matrix defined there and the resulting coefficient matrix, which is a square matrix, is inverted to find the unknowns (or the resulting system is solved by the usual linear equation solving methods). This method is relatively simply to use; however, it is somewhat inefficient in that it requires a matrix multiplication on both sides of the equation before solving.

The method preferred by the authors is to calculate $\bar{\bar{Y}}_i^r$ since $\bar{I}_i$, $\bar{H}_i$, and β_i can all be calculated from this matrix. Furthermore, since all the columns are proportional to $\bar{I}_i$ and all the rows proportional to $\bar{H}_i$, the redundancy permits checking the results and averaging to improve accuracy.

APPENDIX C

CALCULATION OF $\overline{\overline{Y}}_i^r$ AND $\overline{\overline{Z}}_i'$

In this section we consider a method for calculating the residue matrix $\overline{\overline{Y}}_i^r$ and the derivative matrix $\overline{\overline{Z}}_i'$. The matrices are defined as follows:

$$\overline{\overline{Y}}_i^r = \lim_{s \to s_i} (s-s_i)\, \overline{\overline{Y}}(s) = \lim_{s \to s_i} (s-s_i)[\overline{\overline{Z}}(s)]^{-1} \tag{1C}$$

and

$$\overline{\overline{Z}}_i' = \frac{d\, \overline{\overline{Z}}(s)}{ds}\bigg|_{s=s_i} = \lim_{s \to s_i} \frac{\overline{\overline{Z}}(s) - \overline{\overline{Z}}_i}{s-s_i} \tag{2C}$$

The limit definitions (1C) and (2C) certainly suggest that the desired quantities can be found by numerical approximation to the limit. The danger in (1C), however, is that as s approaches s_i, the matrix $\overline{\overline{Z}}(s)$ becomes singular (by definition) and one could expect to encounter serious numerical instabilities. In (2C), numerical difficulties arise due to the subtraction of nearly equal quantities. Hence, in approximating the limit in both cases, one has to carefully choose an s which is "close but not too close" to s_i. In the following, we consider a method for calculating the desired quantities using values of s which do not have to be extremely close to s_i and yet can provide very accurate results. The penalty that one pays for this

feature is that several evaluations of a matrix and, in the case of (1C), its inverse are required.

In order to unify the discussion concerning the calculation of $\overline{\overline{Y}}_i^r$ and $\overline{\overline{Z}}_i'$, we introduce a matrix-valued auxiliary function $\overline{\overline{A}}(s)$ which we associate with either $\overline{\overline{Y}}(s)$ or $\overline{\overline{Z}}(s)$ depending on whether $\overline{\overline{Y}}_i^r$ or $\overline{\overline{Z}}_i'$ is the quantity of interest. In either case, $\overline{\overline{A}}(s)$ has similar properties; namely, that it is analytic at $s = s_i$ and can hence be written in a Taylor series about s_i in the form

$$\overline{\overline{A}}(s) = \overline{\overline{A}}_0 + \overline{\overline{A}}_1(s-s_i) + \overline{\overline{A}}_2\frac{(s-s_i)^2}{2!} + \frac{\overline{\overline{A}}_3(s-s_i)^2}{3!} + \ldots \tag{3C}$$

where

$$\overline{\overline{A}}_n = \frac{d^n}{ds^n}\overline{\overline{A}}(s)\bigg|_{s=s_i} \tag{4C}$$

The relation between $\overline{\overline{A}}(s)$ and $\overline{\overline{Y}}(s)$ is

$$\overline{\overline{Y}}(s) = \frac{\overline{\overline{A}}(s)}{s-s_i} \tag{5C}$$

so that using (1C), we have

$$\overline{\overline{Y}}_i^r = \overline{\overline{A}}_0 \tag{6C}$$

We relate $\overline{\overline{A}}(s)$ to $\overline{\overline{Z}}(s)$ through the equation

$$\overline{\overline{Z}}(s) = \overline{\overline{Z}}_i + (s-s_i)\,\overline{\overline{A}}(s) \tag{7C}$$

where

$$\overline{\overline{Z}}_i = \overline{\overline{Z}}(s_i) \tag{8C}$$

Note that according to (2C),

$$\overline{\overline{Z}}_i' = \overline{\overline{A}}_0 \tag{9C}$$

We emphasize here that the matrix-valued function $\overline{\overline{A}}(s)$, when associated with $\overline{\overline{Y}}(s)$, is not equal to that associated with $\overline{\overline{Z}}(s)$. It simply has similar properties; viz., that it is analytic at $s = s_i$ and that the desired quantity, according to (6C) and (9C), is $\overline{\overline{A}}_0$. This convention merely enables us to consider properties of the function $\overline{\overline{A}}(s)$ in the following without regard to whether $\overline{\overline{Y}}_i^r$ or $\overline{\overline{Z}}_i'$ is the desired quantity.

The method used here depends on the fact that $\overline{\overline{Y}}_i^r$ and $\overline{\overline{Z}}_i'$ may be calculated alternatively from the following contour integrals, where C_i denotes a contour enclosing only the pole at $s = s_i$ and directed as shown in Fig. 1C:

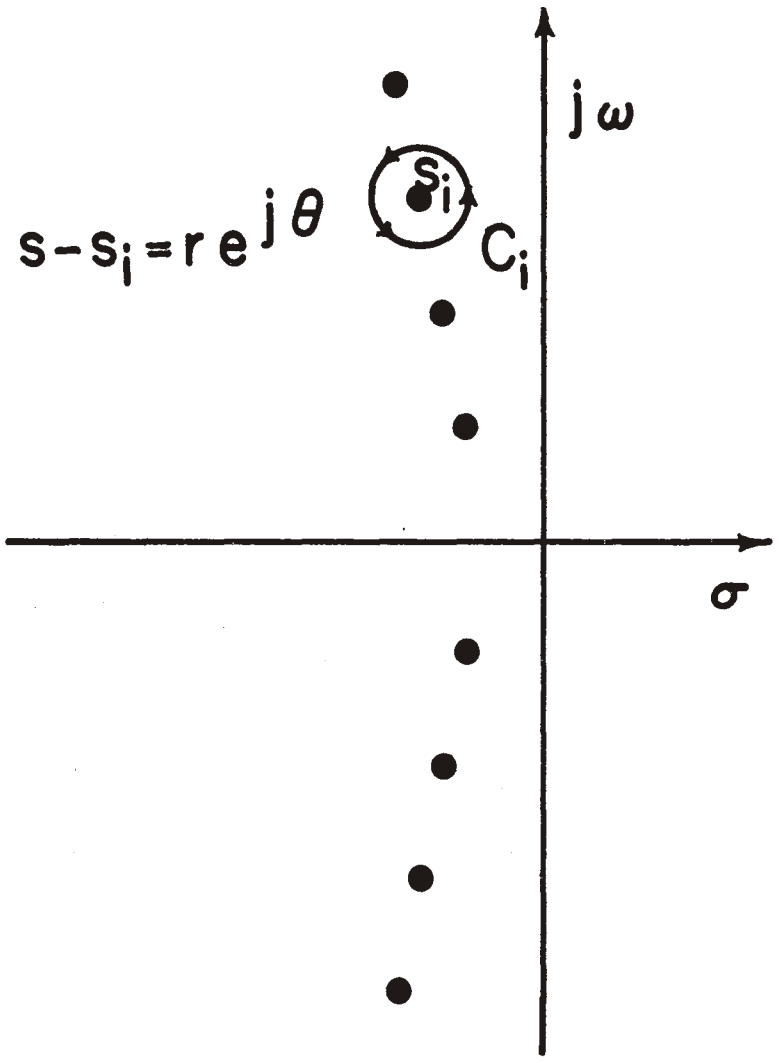

Figure 1C. Integration contour C_i about pole at s_i.

$$\overline{\overline{Y}}_i^r = \frac{1}{2\pi j}\int_{C_i} \overline{\overline{Y}}(s)\, ds = \frac{1}{2\pi j}\int_{C_i} \frac{\overline{\overline{A}}(s)}{s-s_i}\, ds = \overline{\overline{A}}_0 \qquad (10C)$$

$$\overline{\overline{Z}}_i' = \frac{1}{2\pi j}\int_{C_i} \frac{\overline{\overline{Z}}(s)}{(s-s_i)^2}\, ds$$

$$= \frac{1}{2\pi j}\int_{C_i} \frac{\overline{\overline{Z}}_i}{(s-s_i)^2}\, ds + \frac{1}{2\pi j}\int_{C_i} \frac{\overline{\overline{A}}(s)}{(s-s_i)}\, ds$$

$$= \overline{\overline{A}}_0 \qquad (11C)$$

The use of (10C) and (11C) allows us to determine quantities defined at the point of interest $s = s_i$ in terms of quantities evaluated at some distance away from the point where the various matrix functions are better behaved.

We approximate the integrals above by choosing the contour C_i to be circular, of radius r, and centered at $s = s_i$. We then make a change of variables to polar coordinates (r,θ) with origin at $s = s_i$;

$$(s-s_i) = re^{j\theta}$$

The integrals become

$$\overline{\overline{Y}}_i^r = \frac{r}{2\pi}\int_0^{2\pi} \left[\overline{\overline{Y}}(s)\Big|_{s=s_i+re^{j\theta}}\right] e^{j\theta} d\theta \qquad (12C)$$

$$= \frac{1}{2\pi} \int_0^{2\pi} \left[\overline{\overline{A}}(s) \Big|_{s=s_i+re^{j\theta}} \right] d\theta$$

$$\overline{\overline{Z}}_i' = \frac{1}{2\pi r} \int_0^{2\pi} \left[\overline{\overline{Z}}(s) \Big|_{s=s_i+re^{j\theta}} \right] e^{-j\theta} d\theta$$

$$= \frac{1}{2\pi r} \int_0^{2\pi} \overline{\overline{Z}}_i e^{-j\theta} d\theta + \frac{1}{2\pi} \int_0^{2\pi} \left[\overline{\overline{A}}(s) \Big|_{s=s_i+re^{j\theta}} \right] d\theta \qquad (13C)$$

We note that the term involving $\overline{\overline{Z}}_i$ in (11C) and (13C) should be identically zero but we keep it to show its effect on error in the numerical procedure. For computational purposes, we may approximate the integrations in (12C) and (13C) by dividing the interval of integration into N equally spaced segments and use the "rectangular rule," that is, we assume that the integrand is constant over a segment and evaluate it at the midpoint of a segment. The mid-points are defined by

$$\theta_\ell = \frac{(\ell-1)2\pi}{N} , \quad \ell = 1,2,3,\ldots,N$$

for a segment length

$$\Delta\theta_\ell = \theta_{\ell+1} - \theta_\ell = \frac{2\pi}{N}$$

Hence we approximate (12C) and (13C) by

$$\bar{\bar{Y}}_i^r \simeq \frac{r}{N}\sum_{\ell=1}^{N}\left[\bar{\bar{Y}}(s)\Big|_{s=s_i+re^{j\theta_\ell}}\right]e^{j\theta_\ell}$$

$$= \frac{1}{N}\sum_{\ell=1}^{N}\bar{\bar{A}}(s)\Big|_{s=s_i+re^{j\theta_\ell}} \qquad (14C)$$

$$\bar{\bar{Z}}_i' \simeq \frac{1}{rN}\sum_{\ell=1}^{N}\left[\bar{\bar{Z}}(s)\Big|_{s=s_i+re^{j\theta_\ell}}\right]e^{-j\theta_\ell}$$

$$= \frac{1}{rN}\sum_{\ell=1}^{N}\bar{\bar{Z}}_i e^{-j\theta_\ell} + \frac{1}{N}\sum_{\ell=1}^{N}\bar{\bar{A}}(s)\Big|_{s=s_i+re^{j\theta_\ell}} \qquad (15C)$$

Let us examine the terms involving $\bar{\bar{A}}(s)$ by employing the Taylor series representation for $\bar{\bar{A}}(s)$, Equation (3C);

$$\frac{1}{N}\sum_{\ell=1}^{N}\bar{\bar{A}}(s)\Big|_{s=s_i+re^{j\theta_\ell}} = \frac{1}{N}\sum_{\ell=1}^{N}\left[\sum_{n=0}^{\infty}\bar{\bar{A}}_n\frac{(s-s_i)^n}{n!}\right]_{s=s_i+re^{j\theta_\ell}}$$

$$= \frac{1}{N}\sum_{\ell=1}^{N}\left[\sum_{n=0}^{\infty}\bar{\bar{A}}_n\frac{r^n}{n!}e^{jn\theta_\ell}\right]$$

$$= \sum_{n=0}^{\infty}\bar{\bar{A}}_n\frac{r^n}{n!}\left[\frac{1}{N}\sum_{\ell=1}^{N}e^{jn\theta_\ell}\right] \qquad (16C)$$

We take note of the identity

$$\frac{1}{N}\sum_{\ell=1}^{N} e^{jn\theta_\ell} = \frac{1}{N}\sum_{\ell=1}^{N} e^{jn(\ell-1)2\pi/N}$$

$$= e^{jn\pi(1-1/N)}\,\frac{\sin n\pi}{N\sin\frac{n\pi}{N}} \qquad (17C)$$

Thus, the series (17C) sums to zero except when n is equal to an integer multiple of N, i.e.,

$$n = mN,\ m = 0, \pm1, \pm2, \ldots$$

In this case, the series sums to unity. Hence (16C) becomes

$$\frac{1}{N}\sum_{\ell=1}^{N} \bar{\bar{A}}(s)\Big|_{s=s_i+re^{j\theta_\ell}} = \sum_{m=0}^{\infty} A_{mN}\,\frac{r^{mN}}{(mN)!}$$

$$= \bar{\bar{A}}_0 + \sum_{m=1}^{\infty} \bar{\bar{A}}_{mN}\,\frac{r^{mN}}{(mN)!} \qquad (18C)$$

The remaining term in (15C) may also be evaluated using (17C) with n = -1;

$$\frac{1}{rN}\sum_{\ell=1}^{N}\overline{\overline{Z}}_i e^{-j\theta_\ell} = \frac{\overline{\overline{Z}}_i}{r}\left[\frac{1}{N}\sum_{\ell}^{N} e^{-j\theta_\ell}\right] = \frac{\overline{\overline{Z}}_i}{r}\,\delta_{1,N} \tag{19C}$$

where

$$\delta_{1,N} = \begin{cases} 0, & N \neq 1 \\ 1, & N = 1 \end{cases}$$

With (18C) and (19C), we may write the error in using (14C) and (15C) as

$$\text{error } (\overline{\overline{Y}}_i^{r}) = \sum_{m=1}^{\infty} A_{mN}\,\frac{r^{mN}}{(mN)!} \tag{20C}$$

$$\text{error } (\overline{\overline{Z}}_i') = \frac{\overline{\overline{Z}}_i}{r}\,\delta_{1,N} + \sum_{m=1}^{\infty} A_{mN}\,\frac{r^{mN}}{(mN)!} \tag{21C}$$

It is seen by (20C) and (21C) that for a moderate choice of N, one would generally expect a drastic reduction in error for r small. We note also that for N = 1 in (14C) and N = 2 in (15C), we have just the simplest approximation to the limits (1C) and (2C) respectively. Equations (14C) and (15C) are just averages of this simple one term finite difference approximation to the limit taken from different directions about $s = s_i$.

The considerations above have neglected any error due to a lack

of precise knowledge of the location of the natural resonant frequency $s = s_i$. If N is such that the terms in (20C) and (21C) are extremely small, the pole location error may be the most significant error. In the case of $\overline{\overline{Y}}^r_i$, however, we note that the pole is contained in the function $\overline{\overline{Y}}(s)$ and it is not extremely important to know its location accurately to get an accurate matrix of residues (compare (10C) and (11C)). Since the approximation (14C) converges to (10C) as N tends to infinity, the procedure described should still reduce the error as compared to using (1C) even when the pole location is not accurately known.

ACKNOWLEDGMENT

The authors would like to thank Dr. C.M. Butler for his helpful comments and discussions during the course of this work. Special thanks are also due Lt. M.G. Harrison of AFWL for his help in the initial programing and Mr. T. Brown of the Dikewood Corporation for his assistance in the data plotting. Typing of the manuscript by Mrs. L. Thibault is also gratefully acknowledged.

REFERENCES

1. Baum, C.E., "On the Singularity Expansion Method for the Solution of Electromagnetic Interaction Problems," EMP Interaction Note 88, December 1971.

2. Marin, L., and Latham, R.W., "Analytical Properties of the Field Scattered by a Pefectly Conducting, Finite Body," EMP Interaction Note 92, January 1972.

3. Tesche, F.M., "On the Singularity Expansion Method as Applied to Electromagnetic Scattering from Thin-Wires," EMP Interaction Note 102, April 1972.

4. J.P. Martinez, Z.L. Pine and F.M. Tesche, "Numerical Results of the Singularity Expansion Method as Applied to a Plane Wave Incident on a Perfectly Conducting Sphere," EMP Interaction Note 112, May 1972.

5. Lee, S.W., and Leung, B., "The Natural Resonance Frequency of a Thin Cylinder and its application to EMP Studies," EMP Interaction Note 96, February 1972.

6. Marin, L., "Application of the Singularity Expansion Method to Scattering from Imperfectly Conducting Bodies and Perfectly Conducting Bodies within a Parallel Plate Region," EMP Interaction Note 116, June 1972.

7. Marin, L., "Natural-Mode Representation of Transient Scattering from Rotationally Symmetric, Perfectly Conducting Bodies and Numerical Results for a Prolate Spheroid," EMP Interaction Note 119, September 1972.

8. Wilton, D.R., and Umashankar, K.R., "The Singularity Expansion Method and its Applications," Proceedings of 1973 IEEE Southeast Region 3 Conference, April-May 1973.

9. Harrington, R.F., Field Computation by Moment Methods, MacMillan, New York, 1968.

10. Butler, C.M., "Currents Induced on a Pair of Skew Crossed Wires," IEEE Trans. Antennas and Propagation, Vol. AP-20, pp. 731-736, November 1972.

11. King, R.W.P., Theory of Linear Antennas, Harvard Press, Cambridge, Mass., 1956.

12. Conte, S.D., Elementary Numerical Analysis, McGraw-Hill, N.Y., 1965.